MASTER THESIS

A study towards the optimization of pultrusion processes: Process - Microstructure - Property correlation

Author

BOLAR VANISHREE RAO

MSc. Sustainable Energy Technology

S2181304

Engineering technology

Faculty of Production Technology

Prof. Remko Akkerman

EXAMINATION COMMITTEE

Chairperson: Dr. Ir. Ton Bor

Internal examiner: Dr. Ismet Baran

Internal examiner: Onur Yuksel, MSc.

External examiner: Dr. Jamal Seyyed Monfared Zanjani

Enschede

28/01/2021

UNIVERSITY OF TWENTE.

MASTER DISSERTATION

A study towards the optimization of pultrusion processes: Process – Microstructure – Property correlation

by

Bolar Vanishree Rao

MSc. Sustainable Energy Technology

Faculty of Engineering technology

Department of Production technology

University of Twente

GRADUATION COMMITTEE

Chairperson : Dr. Ir. Ton Bor

Internal examiner : Dr. Ismet Baran

Internal examiner : Onur Yuksel, MSc.

External examiner : Dr. Jamal Seyyed Monfared Zanjani

Enschede

28-01-2021

Summary

Several problems have resulted in a negative impact on human civilization, which may eventually lead us into the brink of human existence. To eliminate the threat posed due to irregular and changing climate patterns it is necessary to safeguard the future. The mutual coexistence and inhabitation with our surrounding ecosystem and the different lifeforms are deteriorating eventually, which is not in our best interest. To avoid further destruction and calamities caused due to fossil fuel consumption, pollution, global warming, rise in the sea level etc., it is necessary to switch to a sustainable lifestyle. Several countries have agreed and are willing to contribute to this aspect by the development of sustainable goals in the form of Paris climate agreement, Kyoto protocol etc. A smooth transition from conventional energy sources to a renewable energy mix must be ensured. Rising population requires a more stable, energy-efficient source, which can balance the production and demand at all times.

Wind energy plays a significant and crucial role in the production of clean energy. To cater to the demand and increase the energy production share, longer blades are developed which can withstand the loads and reduce the cost. One of the essential components in the wind turbine blade is the spar cap. Spar cap contributes to the additional stiffness and strength, homogeneity and weight reduction which eventually leads to lower material usage and labour. Spar caps that are developed with a mold can be eliminated to create more space for manufacturing other components. According to an article [1], the reduction of spar cap moulds would increase the overall productivity due to the addition of blade moulds. Pultrusion is a suitable process, which not only reduces the weight but also helps to scale down the use of other components. Pultrusion is a continuous process and one of the oldest manufacturing techniques for composite materials. Pultrusion is an energy-efficient process if the process is continually optimized and controlled.

To ensure the continuity of the process and avoid the down-time due to die-jamming, pulling force is investigated in this study. Temperature and pulling force are measured continuously and monitored, to optimize the process, improve the quality of the product and the mechanical performance. To ensure a smooth operation, a stable pulling force is desired. The influencing conditions such as pulling speed, fibre volume content, fibre volume configuration and resin composition are investigated, as it may change the process and affect the pulling force differently. A pultrusion die is classified into different regions based on their contribution to the pulling force. This study tries to explore the possible effects of the length of different regions in the die on the pulling force. Cut-end tests are performed and compared with cure degree evolution, so as to predict this phenomena. A good quality product would have to adhere to the dimensions with minimal deviations. In this study, void content analysis is employed so as to check its affect on the mechanical performance. In addition to this, the strength of the material is assessed so as to quantify the type of product produced under different process settings. In conclusion, a correlation is established between the properties, structure and process is made, so as to improve the pultrusion process.

Acknowledgement

I am thankful to my supervisor Ismet Baran at the University of Twente, Netherlands for encouraging me to do this project. I am glad that he helped me pick the necessary Capita Selecta specialization courses which proved to be helpful for my thesis. I am grateful to him for providing weekly assistance and guiding me on the right path. I am grateful for his guidance, and all the interesting discussions we had at every stage of the research. Despite the COVID situation, he helped and backed me up, when I needed his guidance the most.

My sincere thanks to my daily supervisor Onur Yuksel, who has helped in conducting fabrication and microscopy experiments. Your knowledge and insight into the subject helped me to shape my project well. I'm happy that I got an opportunity to discuss the results and concepts with you. This helped me to organize my thoughts well during this thesis.

I would like to extend my special thanks to Nick and Bert for providing me with a timely assistance for booking the lab slots during these tough times. I deeply appreciate the help you rendered me, to organize my tests well. This project is carried forward using the lab-scale pultrusion line developed by Jasper at the University of Twente. I would also like to thank Jasper and Sakthi for providing me with valuable information. It was crucial in understanding the drawbacks of the process and the important parameters that affect the process.

I am happy to have earned a family of friends here at UT. I want to thank them for their friendship and continuous moral support throughout my stay in the Netherlands. Most importantly, I thank my mom and dad who stood by me at every phase of my life and all the love to them.
I must also thank my housemates - Chris, Hema, and Noor for supporting me and providing me with a study environment to work in, during this pandemic.

Table of contents

List of figures

List of tabulations

List of symbols

Symbol	Description	Unit
ρ	Density of air	kg/m^3
C_p	Coefficient of performance	
A_1	Swept area of the rotor	m^2
V_w	Wind velocity	m/s
η	Efficiency of generator and gear box	
ε'	Strain rate	
L	Support span length	mm
t	Thickness of the specimen	mm
σ	Stress	N/mm^2
F	Load on the sample	N
b	Width of the sample	mm
m	Slope of force-displacement curve in the linear region	
ρ_{tc}	Theoretical density of the composite	g/cm^3
ρ_{ac}	Actual density of the composite	g/cm^3
ρe	Density of ethanol	g/cm^3
m_a	Mass of the specimen in air	g
m_e	Mass of the specimen in ethanol	g
R	Percentage weight of resin in composite	
D	Density of resin	g/cm^3
r	Percentage weight of fibre in composite	
d	Density of fibre	g/cm^3
W_r	Total weight of the resin bath	g
V_r	Total volume of the resin bath	cm^3
W_f	Total weight of the fibres	g
V_f	Total volume of the fibres	cm^3
α	Degree of cure	
E_a	Activation energy	kJ/mol
R	Universal gas constant	kJ/K/mol
T	Temperature	K
n, o	Exponential constants	
A	Exponential factor	s^{-1}

N	Number of rovings	
l	Length of fibres	m

List of abbreviations and acronyms

Acronym	Description	Unit
PF	Pulling force	N
PS	Pulling speed	mm/min
FVF	Fibre volume fraction	
CAPEX	Capital expenditure	$
OPEX	Operational expenditure	$
RIP	Resin injection pultrusion	
IP	Injection pultrusion	
HP die	High pressure die	
LP die	Low pressure die	
LFF	Linear frictional force	N
ISO	International Organisation for Standardisation	
ASTM	American Society for Testing and Materials	
DSC	Differential scanning calorimetry	
TGA	Thermo-gravimetric analysis	
DOC	Degree of cure	
C	Configuration	
R	Roving	

A processing condition represents a certain combination of temperature, pulling speed, configuration type and fibre volume fraction.

TEX number represents the linear density of the composite and is measured as kg/km.

A sample is a composite material produced as a result of pultrusion. A sample is cut into several pieces which as referred to as specimens.

Chapter 1. Introduction

To note the obvious, the changes in the global climate pattern has greatly influenced our livelihood. Many disasters are witnessed due to the changes in the temperature, rise in sea levels, global warming etc. Human beings have encroached on the wildlife habitat, causing depletion in the quality of life. Biodiversity plays a crucial role in balancing and rejuvenating the ecosystem. With the rising human population and the disappearance of the species, it is necessary to rid the civilization from the harmful fossil fuels. Currently, many countries and organizations are working in unison to develop and implement several policies and reforms, to transform the world into a better place. To cut down the harmful emissions and to sustain the need of several billion people in the world, it is necessary to shift into cleaner and non-depleting energy source, like renewable energy. According to Sir David Attenborough's predictions, it is said that renewable energy would be a dominant source of energy in the next 20 years [2]. One of the prominent sources is wind energy in the renewable energy sector.

The key to developing a far more effective and efficient wind turbine relies on several factors such as the height of the wind turbine, diameter of the blades, the span length, aerodynamic structure of the blade, transportation of energy, storage mechanisms and so on. The weight of the wind turbine blade affects the mechanical performance. Currently, most of the wind turbine blades are made up of composite materials, due to better functionality in terms of recyclability, performance etc. Spar caps provide additional strength for the wind turbine blades, which are fabricated using several manufacturing techniques such as vacuum infusion, pultrusion etc.

The quality of the pultruded product is influenced by the processing conditions, such as the pulling speed, temperature, fibre volume content. The die dimensions, material, location of heating zones and the heat transfer rate are the extrinsic parameters that impact the pultruded composite. Pulling force measurement is used to evaluate the quality of the product. The liquid and the gel zone along the pultrusion line contribute to the pulling force, which is inter-dependent on the pulling speed, inlet and exit die temperature, the degree of cure, the configuration of fibre rovings, tension on the fibre rovings and the material characteristics of different components in the composite material. The other salient feature that is crucial for the pultrusion technique is to identify the contribution of different zones to the overall pulling force. Several studies in literature explain the influence of these parameters for different kinds of material and die dimensions, but only a few papers provide meaningful information in terms of trends for mechanical tests.

In this research, the pulling force and contribution of different zones to the pulling force are touched upon. The trends for the variation in the pulling force concerning temperature, fibre roving configuration and pulling speed are explained. The distinction between an acceptable product with higher tolerance can be explained with the void estimations and mechanical performance. The flexural modulus and strength in combination with their failure modes are reported. The estimations of the void content are interpreted with the microscopic image analysis software - Image-J analysis technique. The location or topography of the voids is noticed with Image-J analysis. The void percentage is verified with the density measurement since they accurately predicted the overall void content for the entire composite.

1.1. Outline of the report

In this section, the overall structure of the report is discussed. The first chapter introduces the subject or topic in a broader perspective and provides the technical knowledge, concepts and the different manufacturing techniques used, for the current scope of research. In addition to this, the first chapter constitutes and describes the various studies that were published, related to the current problem, and summarises their conclusions in the form of a literature survey. The purpose of this study is outlined and explained in the same section. The experimental set-up and methodology are expressed in the second chapter. The results and discussions of the research are given in further sections, which is followed by a summary of the main conclusions and recommendations. The supporting information and graphs are shown in the appendix.

1.2. Theoretical background

This chapter gives a vivid description of the different renewable energy sources and their current stand in the energy market. The fundamental working principle of the wind turbine and the importance of the different components and the manufacturing processes involved in their fabrication are briefly discussed.

1.2.1. Renewable energy resources and depletion of fossil fuels

As witnessed by many climate activists and scientists, it is well known that many devastations of land and ecosystem are affected by the global climate pattern. The CO_2 and the greenhouse gas emissions play a vital role in balancing the flora and fauna, which in turn affect the biodiversity of the planet. To stabilise and prevent further adversity, it is important to switch to 'cleaner' energy sources. The emissions from fossil fuels are depleting and harmful to the environment. According to the stats, the share of the renewables accounted for 10.8% in 2018 out of the total primary energy supply in the world [3]. The energy consumption from different energy sources is shown in *Figure 1*. After the COVID outbreak at the end of 2019, the renewable energy market forecasted a decline of 13% in 2020, in comparison to 2019 [4].

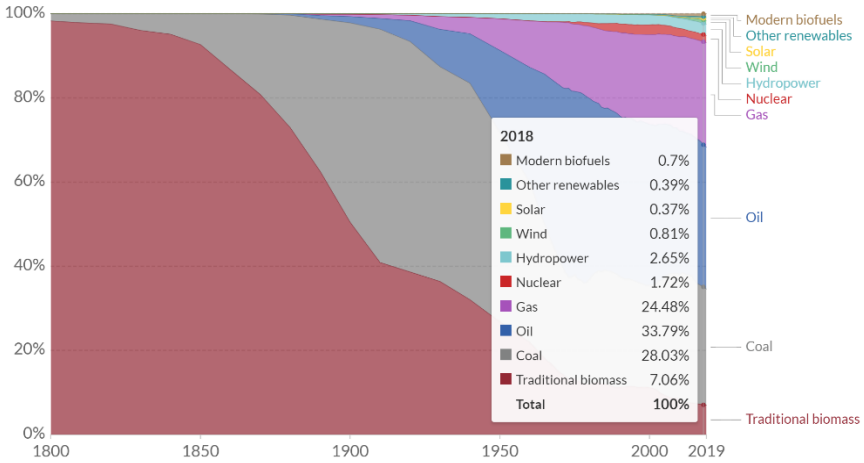

Figure 1: Share of different energy sources in 2018 [5]

1.2.2. Why wind energy?

Several policies and regulations such as the Kyoto Protocol, the Paris climate agreement and the sustainable development goals are introduced to promote sustainability. The three leading renewable energy technologies in power production are the hydro-power, wind and solar energy [6]. The annual growth rate is the second-highest for wind energy. In 2019, it accounted for 2% of the total energy produced in the world [7]. Albeit the promising trend, one of the major drawbacks is the slower pace of development in terms of technological improvement and their implementation in countries that do not actively support sustainability. Due to the current situation, transportation and manufacturing are greatly affected, which thereby predicts a slower growth rate in 2021 as compared to 2019 [8].

Waste management is also one of the important processes during the salvage process of wind turbine parts. Therefore, it is necessary to use easily recyclable material. The newer wind turbine installations have implemented new methods and techniques to cater to these needs, paving the way to a renewable future.

1.2.3. Components of a wind turbine

The energy captured by the wind turbine is dependent on the height, material of the tower, blade length etc. The energy produced by the wind turbine is given by,

$$Wind\ power, P = \frac{1}{2}\rho C_P A_1 {V_w}^3 \eta \quad (1)$$

Where,
ρ = *Density of air in* kg/m^3*, which decreases with the height*
C_p = *Coefficient of performance*
A_1 = *Swept area of the rotor in* m^2
V_w = *Wind velocity in* m/s
η = *Overall efficiency of the generator and the gearbox*

The wind velocity is proportional to the height of the wind turbine and can be calculated with the following formula's,

1. Power law velocity profile equation – velocity is proportional to the height of the tower raised to the power 'x', which can be determined is the velocities at two different heights are known.
2. Logarithmic velocity profile – velocity is proportional to the log(height/surface roughness). This formula takes into account, the type of land used for wind turbine installation.

Due to restrictions in the air space, other air turbulences and swaying of the towers, it is quite inconvenient to have longer towers. However, if the blades have to be mounted at higher altitudes, a lower weight blade with more strength is preferred. Another way to improve the performance is to have longer blades that are intended to capture more energy, due to a larger swept area. Therefore, this is a major concern and a golden opportunity for blade manufacturers.

1.2.4. Spar caps

To overcome bulky material that causes structural instability, it is better to have a lightweight structure on top of the tower. This also helps in cost reduction and waste minimisation. Wind turbine blades are fabricated in two parts, with the top and bottom outer shell that acts as a backbone for the blades, which connect the leading and the trailing edge of the blades. Shear webs are structurally integrated components that provide shear strength to the outer shell. Spar caps are long strips that stretch along the length of the blades. They constitute of composite materials. The different functions of spar caps include weight reduction with better blade stiffness, better resistance to tensile and compressive stress and the bending moment, superior rotor strength and lower cost to weight reduction ratio. The bonding strength of the adhesives and the material compatibility has to be considered carefully during the selection of materials for the spar caps.

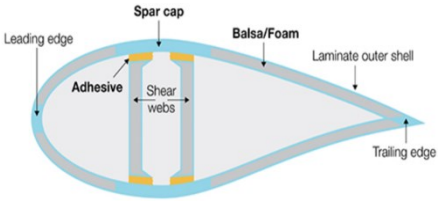

Figure 2: Structure of wind turbine blades [9]

.

Figure 3: I-Spar (left) and box spar (right)

The two notable spar cap designs are the box spar and the I-spar [10] as shown in *Figure 2 and Figure 3.*

The differences of I-shaped spar caps as compared to box spar caps [11] are enlisted below,

1. I-shaped spar caps can withstand larger loads due to their structural stability and they require lesser material than box spar cap.
2. I-shaped spars are difficult to fabricate.

The dominant manufacturing techniques used to fabricate the spar caps are infusion (90%), prepreg (5%) and pultrusion (5%). Prepreg is the primary or base material, which is further processed by other manufacturing processes. Several fibres are passed through the rollers which contain resin as shown in *Figure 4.* Due to the compaction pressure, the resin is mixed with the fibres. Multiple layers are layered on top of each other on the mould.

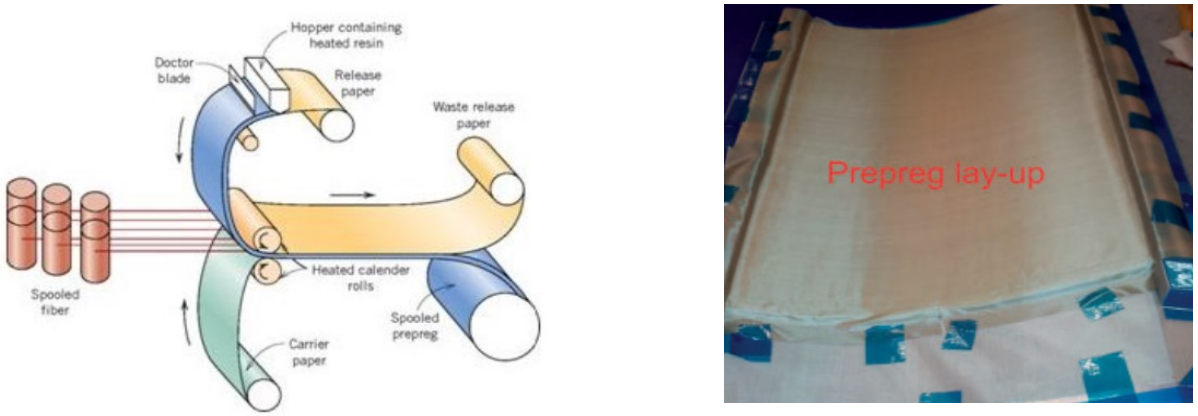

Figure 4: Prepreg manufacturing process (left) [12] *and the lay-up for spar cap (right)* [13]

Infusion process draws the resin into the mould in which the fibres are laid up, using a vacuum bag. The applied pressure determines the quality of the composite material. A schematic representation is as shown in *Figure 5*.

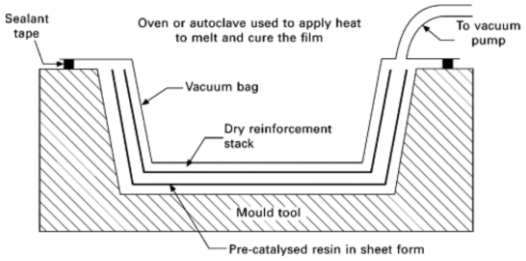

Figure 5: Schematic diagram for the infusion process [14]

Pultrusion is classified into a resin bath and resin injection pultrusion. The fibre rovings are pulled from the creel or bobbins which are impregnated in the resin bath with a pulling unit. The process undergoes a transformation from liquid (uncured) to gel to solid (cured composite part). Pultrusion is an energy-efficient method. A general schematic diagram is shown in *Figure 6*.

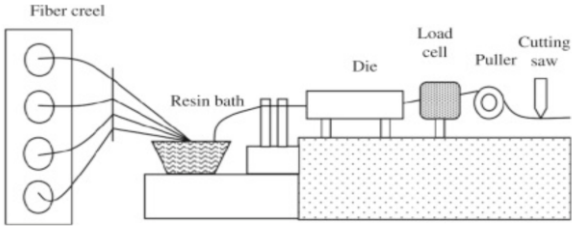

Figure 6: Schematic representation of a commonly used pultrusion line [15]

The features of different processes used in making a spar cap, the advantages and drawbacks along with a case study are discussed in subsequent sections.

1.2.5. Why pultrusion?

Following observations were noted based on the different case studies which are cited below,

1. *Pullwind solution* - 80m blade with pultruded spar caps, had the following features [16],
    - Overall cost savings of 9-12%
    - Reduction in CAPEX by 10% and a reduction in blade weight between 3-7%.
2. "*Gurit*" gave a comparison of infused v/s prepreg spar caps as follows [17],
    - Total processing time is 22.9 hours and 17.2 hours respectively.
    - Manufacturing cost for prepreg is $1500 cheaper than for infused spar caps
    - Prepreg spar caps are lighter in weight.
3. "*Structeam*" compared infusion and pultrusion. Pultruded spar caps had the following advantages [18],
    - Weight reduction of spar caps by 20%, thereby reducing the cost.
    - Blade weight reduction by 3%.
    - CAPEX and OPEX cost reduction by 11% and 28% respectively.

In general, the salient features of different manufacturing techniques are noted below in comparison with the other processes used in spar cap production,

1. *Infusion*
    - Large, complex parts can be manufactured in a single mould, once the main mould is prepared. Since the curing and final mechanical properties depend on the final degree of cure, longer cycle time is required for better curing.
    - As the process occurs in an enclosed/sealed mould, the styrene emissions are lower.
    - The void content may be higher as the material may have undergone non-uniform curing. Therefore, the process has to be well controlled for better quality products.
    - The material properties could be lower since the basic materials are not pre-processed to attain better properties.
2. *Prepreg*
    - The material properties are better than infusion since the fibres are pre-aligned.
    - Variable shapes with better mechanical properties (voids, strength, porosity etc) can be formed since the base material has higher uniformity and homogeneity.
    - Wastage of resin is lesser, due to pre-impregnation.
    - As the foundation material has to be fabricated separately, additional costs for logistics, manufacturing, labour, tool, equipment cost etc are incurred. The manufacturing lead time is also affected by the delivery time of these materials.
3. *Pultrusion*
    - Higher fibre volume to weight content, due to lower scrap rate.
    - Better fibre configuration, homogeneity and uniform weight distribution.
    - The process is applicable to produce unidirectional composites with a uniform cross-section.
    - Manufacturing time is less due to the quick curing process. The equipment set-up time is dependent on the product size and shape. Maintenance or down-time could be higher if the process is not well-controlled.
    - Material defects are largely eliminated due to superior mechanical properties in the fibre direction.
    - The process can be automated with a minimal workforce, thereby reducing labour cost.
    - Investment costs are higher since high-end equipment is used.

The primary objective of a spar cap design is to have better quality and lower weight. Since pultrusion caters to these requirements, it is noteworthy to adopt this process for the production of spar caps. Pultrusion process will be explained in detail in the upcoming sections.

1.3. Literature review

The variations caused due to different processing conditions with their different underlying mechanisms are briefly explained in the literature review. This chapter includes the studies that are associated with the die geometry and dimensions and their influence on the pulling force, the importance of different zones in the die, the relationship between the different process parameters with the pulling force and the strength, effect of different resin systems on the pulling force, a brief overview of the different computational techniques used for simulation of pultrusion and a review of different methods used to determine the voids.

Table 1 provides a brief overview of the different materials and the type of literature study carried out.

Research paper	Literature topic + analysis	Experimental details		
		Material and set-up	Die geometry	Cross-section shape
[19]	Experiment – RIP (resin injection pultrusion)	Vinyl ester + glass fibre	LP die HP die Conventional die	Rectangular - Thickness (4 or 6 mm) Width (90 or 180 mm)
[20]	Model + experiments - RIP	Vinyl ester + glass fibre Two out of three heating zones had a similar power rating.	Similar to set-up in [19]	
[21]		Epoxy + glass fibre		Circular
[22]	Experiments	Epoxy + graphite		
[23]	Model + experiments	Unsaturated polyester + glass fibre		Cylindrical and Rectangular
[24]	Model + validation from experiments used in literature	Epoxy + glass/ Kevlar/carbon fibres		
[25]	Models + experiments - RIP	Power drawn by 3 heating zones of different length are 40W, 10W and 40W respectively.	Triangular or square arrangement of fibres	
[26]	Model and experiments (bench-scale pultrusion)	Vinyl ester (Derakane 441-400) + carbon fibre		
[27]	Model + validation from literature.	Epoxy + graphite		Circular (9 different radii)
[28]	Models for PF	Epoxy + graphite		Circular

[29]	analytical and numerical results + experiments	Vinyl ester (Derakane) + glass fibre (U750)		
[30]		Epoxy + carbon fibre		
[31]	Model + experiments	Epoxy (Korea IPCO) • Temperature (170 or 190°C) • PS (varying 0.16 - 0.36 m/min).		Circular profile of 8mm with 50% FVF. rectangular composite of (6 x 12mm) with 55% FVF.
		Vinyl ester (Korea national plastic) • Temperature (160°C) • PS (0.20 - 0.47 m/min). Constant temperature was maintained during the tests.		
[32]	Simulation + experiments.	DARON resin + glass or carbon fibre	Conical (LP) Tear (HP) by [19]	
[33]	Models	Epoxy + graphite fibre		Cylindrical
[34]	Void content (micro-CT + Image-J)	Polyester + (4800 TEX) glass fibre		L-shaped
[35]	Void content and mechanical properties	Polyurethane and Epoxy (60 rovings of 2400 TEX) E-glass fibre • Temperature = 160°C , • PS = 300, 400 and 500 mm/min.		

Table 1: Overview of the different die shape, material and type of analysis in literature

Table 2 provides a review and the conclusions drawn for the current study. The justification for the conclusions drawn by the respective authors is also included in the table.

Paper	Conclusions	Reasons
[19]	1. PF is higher for the dry fibres. 2. Filler + resin mixture had higher a PF than resin mixture. 3. For the HP die, the PF decreased towards the end of the die. 4. PS increases with the PF, for the die of the same length. As the PS increases, the contribution to the PF from the rear end of the die becomes lesser. 5. For the LP die, the part shrinks away from the die. The PF is nearly constant after compaction. 6. PF of conventional die < PF of HP die < PF of LP die	1. Dry fibre friction and lubrication. 3. Less viscous drag and compaction. 4. PF constant at different PS for a non-activated mixture of resin and fibre.

	7. The highest contribution towards the PF arises from the gel zone. Viscous drag has the least significant effect on the PF. 8. Longer dies doesn't greatly affect the PF. 9. PF decreases with the increasing temperature. 10. Friction coefficient changes only at lower temperatures and effects the cure degree. 11. Pulling force is only affected by the shape of the HP die.	
[20]	1. Friction force > compaction force > viscous force. 2. PS increases with PF. 3. The temperature at the centre is lower than at the surface, at the start of the process and eventually, the trend reverses. 4. The final degree of cure at the centre more than the surface.	2. Large gel zone. 3. Conduction
[21]	1. A lower degree of cure is attained at higher speeds, with a slower curing rate. 2. Higher the amount of resin, higher is the degree of cure. 3. At higher die inlet and outlet temperatures, higher is the degree of cure. 4. The gradient of the centreline temperature is lower for larger cross-sectional dimensions and higher FVF. 5. Degree of cure decreases with the increase in the die size.	
[22]	1.The peak centreline temperature is higher and it takes longer to reach it for the largest pulling speed. 2.Lower degree of cure is seen at higher pulling speeds. 3.The length of gel zone increases with the increase in the pulling speed.	
[23]	The highest contribution to the PF comes from the gel region and thereafter from the viscous drag.	
[24]	1. Volumetric shrinkage decreases with the increase in filler + reinforcement ratio. 2. Lower FVF leads to higher cure degree. 3. Maximum temperature attained followed the trend: Glass > Carbon > Kevlar. The highest PF was obtained for carbon fibre. 4. PF increases with the PS. PF for carbon fibre > Kevlar > glass fibre. 5.Point 1 by [7] is also observed.	1. Lower FVF means that the time required to reach the gelling temperature is higher due to larger resin barrier. 2. Peak temperature attained is higher due to more heat released during the exothermic reaction. 3. Thermal conductivity
[25]	1. Smaller dies had a higher tendency to die seizure and sloughing due to lower force value corresponding to the detachment phenomena. 2. The shear force is higher for composites with high FVF. 3. Frictional force and the shrinkage of the resin was negligible compared to the viscous force.	1.Viscous force contribution through modelling.
[26]	1. Die seizure problem could be temporarily prevented by increasing pulling speed or reducing the temperature, before process termination. 2. PF increases with decrease in PS and increase in the FVF. 3. The PF increased gradually, which eventually caused die seizure.	

[27]	1. As the part thickness increases, a higher temperature peak is attained at a much slower rate. A similar trend is observed for the degree of cure profile. The temperature drops to nearly room temperature after the die exit for a smaller thickness. For parts with larger thickness, the temperature increases after the exit and then the part cools down. 2. The viscous force increases with the part diameter and is unaffected by the liquid zone. The frictional force increases with the part thickness. 3. The overall PF increases with the size.	1. This is due to the higher heat release rate. 2. The detachment point shift is more prominent for parts with larger thickness.
[28]	1. Viscous drag > Frictional force > Compaction force 2. The centre of the profile is cured after the die walls and at a much faster rate.	
[29]	1. Higher the temperature, larger is the variation in dimension. 2. At higher PS, the detachment point is closer to the die exit and the PF increases. 3.Frictional force after the gel zone has the highest resistance to the PF. 4. The factors that influence blister formation are initiator or hardener type, constituents, concentration, resin viscosity, die temperature, fibre stacking, geometry, FVF etc.	4. Higher PS lower contact pressure, lower impregnation and lower final cure degree
[30]	1. PF increases gradually with the volume of the material at constant temperature and PS. 2. Superior quality material has the highest PF at a constant temperature and PS. 3. Highest PF at moderate speed and lowest PF occurs at highest PS.	
[31]	PF decreases with the decrease in PS and increase in die temperature.	
[32]	Observations by experiments: 1. Constant PS and temperature for glass fibres, the PF increased with the increase in FVF. For the tear-drop die: 2. PF decreased with the decrease in temperature at constant FVF and PS condition 3. PF increases with the decrease in PS at stable temperature and FVF.	
[33]	1. Viscous drag was the largest resistive force. 2. In the presence of fillers, PF reduced with the increase in shrinkage.	
[34]	Fibre misalignment (especially the fibres in the in-plane direction) and resin-rich area reduced the stiffness of the composite in the fibre pulling direction by 20%.	
[35]	Void content decreased with the increase in the PS and an increase in flexural strength. Similar results were found by other researchers [36] for carbon + epoxy composites and other composite types [37].	

Table 2: Main pointers and the reasons

The details of the experiments carried out by [19] are mat tracer method and short die length method. Further details of these methods are given in the *appendix A1*.

The following negative remarks could be drawn from the literature survey:

1. The highest contribution of different parts of the die on the pulling force varied for different experiments. Several experiments were conducted to prove the overall effect of different regions on the PF, however different studies show a different trend for the effect of die zone length on the PF. This could be due to different die shapes and the material used for the study. The stability and variation of different process parameters such as temperature and line speed are not accounted for.
2. The largest influence on the PF due to the components such as additives and mold release agents are not established.
3. The PF trends may vary for different processing conditions and are time-dependent.
4. Several discrepancies are observed in the concluding remarks for parameters such as die length, variation of PF with respect to PS etc.
5. It could be noted that fibre stacking arrangement may affect the void content, but no experiments are conducted to prove this hypothesis.

Due to the ambiguity in the results from different literature studies, it is important to identify the major contributing process parameters that affect the process reliability, yield and efficiency.

1.4. Research objectives

From literature study the following observations are made:

1. The surface roughness of the product or in other words, the dimensions of the product and the resulting composite material are dependent on the processing conditions – temperature, pressure, time and the chemo-rheology of the material.
2. The product dimensions are vulnerable and are affected by pulling force or in other words, the product quality varies. Variations in the line speed and temperature are the notable parameters which affect the pulling force (PF). Pultruded products are prone to reduced quality as a result of variable void content, resin-rich areas, uneven surfaces with unacceptable tolerances and non-uniform fibre distribution.
3. In theory, the pultrusion process during a steady-state condition would be subjected to uniform processing conditions and material configuration which would give rise to a non-fluctuating pulling force.

The gaps and loopholes in literature study due to topic irrelevance, partial or incomplete study and reasoning have to be eliminated, to understand the pultrusion process. The following questions are either unanswered or are ambiguously answered in the literature study, and therefore a discussion is made around the topics which are listed below,

1. Die seizure/die jamming arises under stable conditions. Why does this occur?
2. Resin bath composition and the proportions used during the tests may influence the pulling force. Does this effect occur in our study pertaining to the resin-reinforcement system used?
3. What is the contribution of different regions of the die on the PF?
4. Does fibre stacking pattern affect product quality?

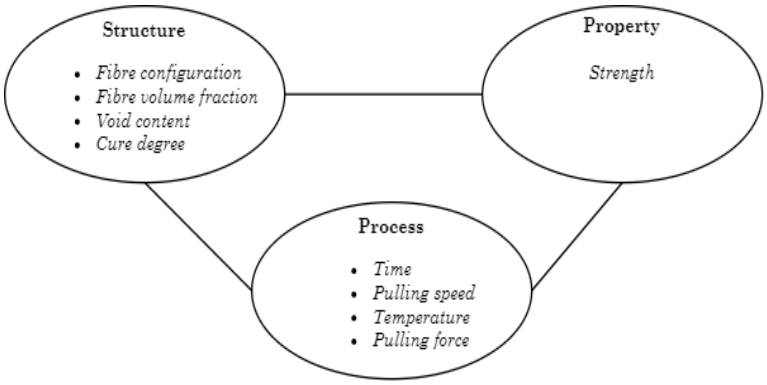

Figure 7: Primary objective of this research [38]

To implement and charter the best possible outcome for the pultrusion process, several parameters have to be analysed and the mutual relationships need to be established. The main objective of this research is to find the correlation between the process, structure and the property, to find the resultant outcomes for the pultrusion process as shown in *Figure 7*. The process includes all the parameters which can be changed during the fabrication process and the parameters that are influenced by these changes. The structure represents the parameters which cannot be changed during the process and also the values which are predicted as a result of these processes. Properties are material-specific, such as dielectric constant, thermal conductivity as so on.

To cater to the main goal of the project, the following sub-research questions were formulated:

1. What is the effect of fibre roving configuration, temperature, pulling speed and number of rovings on the pulling force?
2. What is the effect of voids in the microstructure on the overall product quality for different processing conditions?
3. What methods are used to quantify the failure mechanisms of the fabricated composites and how do the different processing conditions relate to determining the best suitable component?

Chapter 2. Research methodology

In this section, all the equipment's and the different components are explained in detail. In addition to this, all the tools used for the analysis and the procedure for the determination of the important parameters used in calculations are also elucidated. The different set-up's used for the fabrication and experimentation are as shown in the figure below.

The flowchart represents the values measured during the fabrication process and the different tests conducted. The experiments conducted during the thesis are mentioned briefly in the flowchart.

For this thesis, fabrication of the composite, experimentation and analysis was carried out to understand the pultrusion process. The experiments conducted were used as tools to optimize the process. Three-point bending test was used to determine the flexural strength and modulus of the material. During this test, the material undergoes a combination of tension, compression and shear stress. Tensile and compressive tests were not conducted for this study due to insufficient time and limited product availability. Due to insufficient time, only a few images were obtained by microscopy that was further analysed with Image-J software. Since the results were confined to users point of view, other tests were conducted. Therefore, to determine the exact void content, Archimedes test was used. An attempt was made to find the exact void content through a burn-out test, but the tests were unsuccessful. Thickness and width were measured to check the influence on the flexural test.

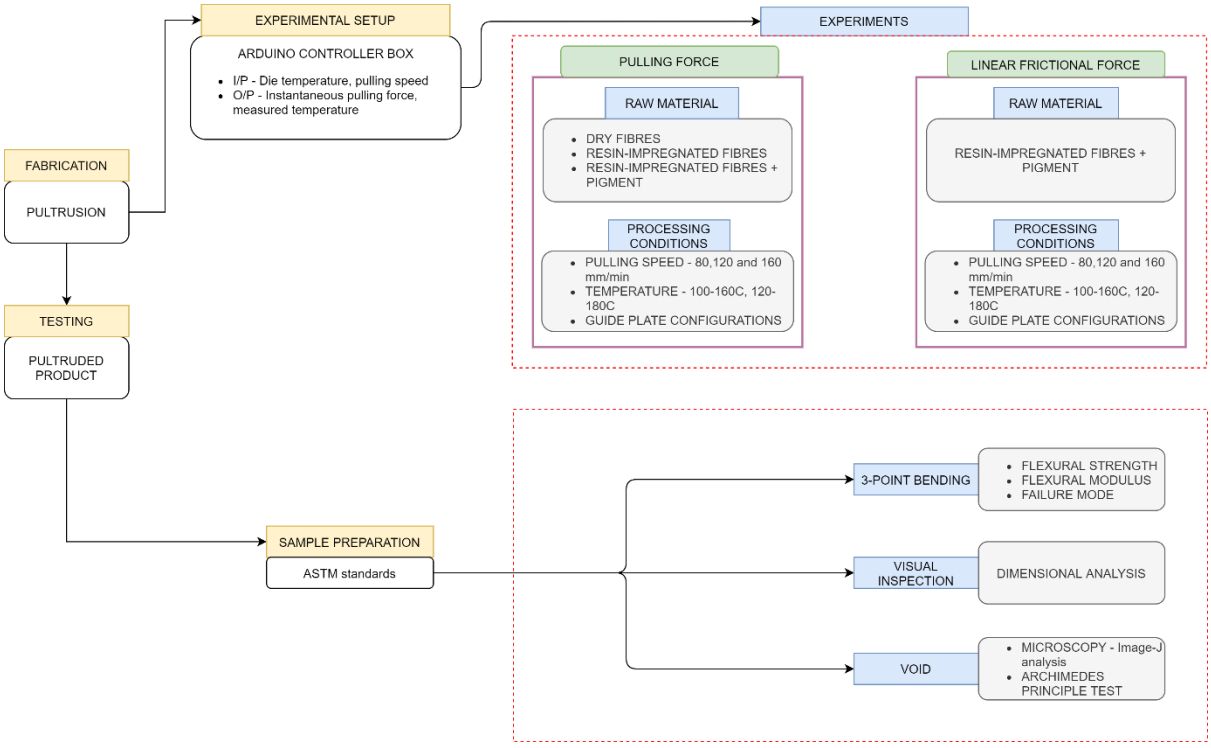

Figure 8: Flowchart representing the fabrication equipment and different experimental set-up

2.1. Experimental setup

In this section, the reasons for the material selection, the components used for the fabrication equipment and experimental set-up used for different mechanical tests are discussed. In addition to this, the type of experiments conducted is touched upon. The calculations used to process the results from these experiments are given in this section.

2.1.1. Material selection

Material selection is one of the crucial and essential parts in the process as it influences the strength, durability and stability of the structure. Composite materials are light in weight, have better strength to weight ratio and have a better response to static and dynamic loads.
Several types of composite materials are used in the production of spar caps, which are described below. Commonly used reinforcing materials in spar caps are [39],

1. *Glass fibres*
   It is one of the most commonly used materials for wind turbine blades. It is easily available and easy to process. Most commonly used glass fibres are S and E-glass fibres. The defining factors for this material – low cost, better damage resistance over longer operational periods.

2. *Carbon fibres*
   Carbon fibres have better strength and stiffness due to stronger chemical bonds. It has low material weight, therefore less usage of material as compared to glass fibres. A negative coefficient of expansion of the carbon fibres enables to have better dimensional quality, for thermosetting polymers. The exorbitant price of this material makes it less worthy to be used in processes that do not require extreme dimensional tolerances. Therefore, it can be used in the aerospace industry that requires high precision parts. Carbon is a good conductor of electricity and it can be subjected to galvanic corrosion if additional metals are added to improve its properties.

3. *Aramid fibres*
   The most commonly used aramid fibres are Kevlar. Aramid fibres have higher strength, better resistance to water absorption and heat [40]. Kevlar fibres have comparable strength to carbon fibres and have a moderate modulus of elasticity with respect to carbon and glass fibres [41]. They are sensitive to UV radiation and are expensive, therefore may not be suitable for wind turbine applications.
   In the current market, hybrid fibres with a combination of carbon and glass fibres are generally used to achieve the best of both the worlds. In the current research, E-glass fibres are used as they have a good balance between strength and cost.

Pultrusion requires a matrix material that can cure quickly so that the process can be completed inside the die. A few pointers describing the characteristics of the commonly used matrix materials are discussed below [41].

1. Polyester resin – It has a market share accounts for 75%. It is versatile and cheap. It can be easily produced. It is less durable than vinyl ester resin. Since the wind turbines can be installed in a humid environment, it's not suitable for this application. Also, it has an unpleasant odour.
2. Epoxy resin - Due to low shrinkage rate, it cannot be used for high-quality products. Addition of hardener or initiator helps in better control over curing. It functions well in high temperatures, but this is not essential for better performance of the blades. It

offers excellent corrosion resistance. It is not favourable due to high viscosity which leads to a post-curing process, which increases the cycle time.

3. Vinyl ester resin - One of the major problems is the production rate. This resin has a faster cure rate. Other properties that favour this resin are moisture resistance, corrosion resistance, better strength and chemical resistance at high temperature.

Vinyl ester resin and glass fibres are used for this research.

2.1.2. Pultrusion line

The experiments were conducted in the lab-scale pultrusion line was constructed by Jasper Van Meurs, for the Master study. The schematic diagram representing the top view of the pultrusion line is as shown in *Figure 9*. The image of the pultrusion set-up used for the fabrication is shown in *appendix A2*.

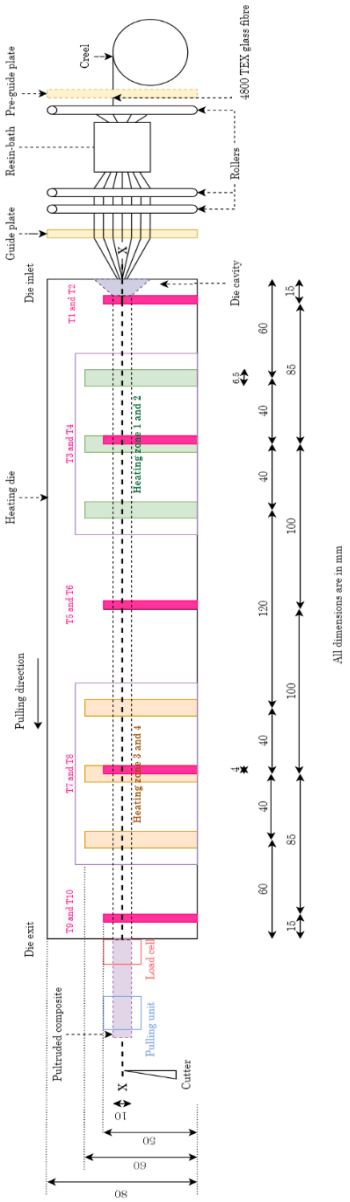

Figure 9: Schematic diagram for pultrusion set-up

The main parts of the conventional pultrusion line are explained below.

1. *Fibre guide-way and rollers*:
   The creels consist of 4800 TEX glass fibres and the fibres are drawn from the inner diameter of the creel.
   The glass fibres are drawn from the creel over the guideways. This enables the fibres to be separated from each other and prevents fibre entanglement to a greater extent. The rollers placed before the resin bath, help in the symmetrical distribution of fibres. The rollers are attached at different heights after the resin bath, to ensure removal of excess resin on the fibres.

2. *Resin bath*:
   The set-up resembles the open bath resin pultrusion or conventional pultrusion. The resin bath consists of vinyl ester resin (Atlac 430), peroxide initiator or hardener (Trigonox-C), lubricant (Zelec UN), degasifying agent (BYK-A 555). Polyester pigment PR-Tint (YT 100wi) from Resion resin technology was used in addition to the above components for certain experiments. The ratio of resin to the other components are 100:1.
   The sensitivity of the weighing scale is 1g. Fillers, such as chalk could be used for better dimension stability, without affecting the chemical process. Fillers are not used in the experiments.

3. *Pultrusion die*:
   It consists of top and bottom metallic blocks with heating cartridge inserts. The two heating zones consist of three heating cartridges each (40W). The top and bottom plate of the die hold five temperature sensors each, which controls the temperature switching circuit. Two shims are aligned symmetrical to the length of the die and are sandwiched in between the plates. Their combination prompts a uniform cross-sectional area. The excessive scratches on the surface of the plates may lead to resin leakage and resin adhesion in the pits.

4. *Load cell and control unit*:
   A load cell is used to measure the pulling force during the process. The load cell is connected to the control unit. The control unit magnifies the load readings from the set-up and sends it to the Arduino. Nevertheless, the sensitivity of the control unit is also dependent on the noise and vibrations. The Arduino displays the pre-set temperature and speed, measured temperature and pulling force. The orientation of the load cell determines if the component of the pulling force or the entire force value is measured. The readings for these components are measured for every second and the values are displayed for every five-second interval.

5. *Pulling unit*:
   The pulling speed is set using the pulling unit. The rollers are connected to the motor. The direction of rotation of the rollers can be reversed. The gap between the rollers was adjusted with four springs. The tacky tape is applied initially on the composite part to prevent slippage between the rollers, for 6 and 7 rovings. A hacksaw blade is used to cut the sample.

The overview of the different tests conducted with the pultrusion line is as shown in *Table 3*.

No.	Fibre configuration	Type of data analysis	Number of test runs	Speed (mm/min)	Temperature (°C)	Composition
C1 (7R)	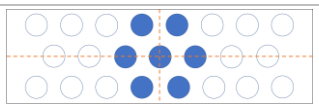 FVF – 68.12%	PF	2	80	100-140	No pigment
				120		
				160		
C2 (6R)	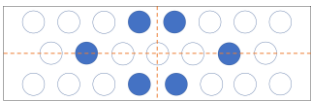 FVF – 54.96%	PF	1	80	100-160	No pigment
				120		
				160		
		LFF	1	160	100-160	No pigment
		Dry	1	80	100-160	-
				120		
				160		
		PF	1	80	100-160	Pigment
				120		
				160		
C3 (8R)	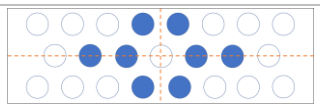 FVF – 73.28%	PF	1	80	100-160	No pigment
				120		
		Dry	1	80	100-160	-
		PF	5	80	100-160	Pigment
			4	120		
			3	160		
		LFF	1	80	100-160	Pigment
			1	120		
			2	160		
		PF	2	80	120-180	Pigment
				120		
				160		
		LFF	2	160	120-180	Pigment
C4 (7R)	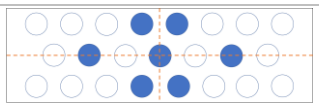 FVF – 73.28%	Dry	1	80	100-160	-
				120		
				160		
		PF	1	80	100-160	Pigment
				120		
C5 (7R)	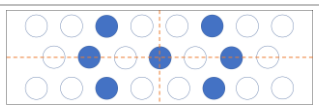 FVF – 73.28%	PF	1	80	100-160	Pigment
				120		
				160		
		LFF	1	160	100-160	Pigment
C6 (8R)	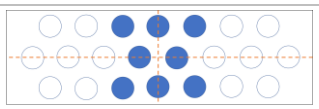 FVF – 73.28%	PF	5	80	100-160	Pigment
			5	120		
			4	160		
		LFF	2	160	100-160	Pigment
		LFF	1	80	100-160	Pigment
C7 (8R)	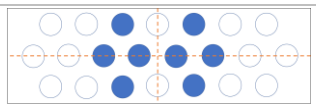 FVF – 73.28%	PF	1	80	100-160	Pigment
				120		
				160		
		LFF	1	160	100-160	Pigment
C8 (8R)	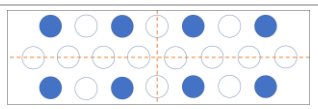 FVF – 73.28%	PF	1	80	100-160	Pigment
				120		
				160		
		LFF	1	160	100-160	Pigment

C9 (8R)	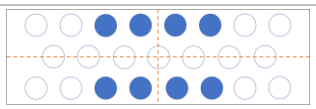 FVF – 73.28%	-	1	-	100-160	Pigment
C10 (9R)	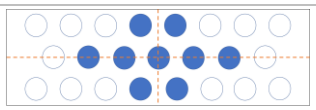 FVF – 82.44%	-	1	160	100-160	Pigment

Table 3: Overview of the fabrication experiments and measurements taken

2.1.2.1. Force analysis:

In this section, the details of the experiments conducted and the data skimming process is explained.

Pulling force is affected by the die material and cross-section, placement of heaters, load cell placement and fixtures, fibre stacking mechanisms and the number of fibre rovings, temperature, resin components, line speed etc. The errors in readings may arise due to vibrations and noise owing to system disturbance. The repeatability of the results are measured for the different process settings and the scenarios when the pigment was added to the resin mixture are shown in *Table 3*. Load-cell was calibrated using known weights to check the output readings of the PF. The response of the load cell was good since a linear graph of force vs weights was plotted. During the process for 8R, the fibres were initially pulled manually, until the point where the last part of the dry fibres enters the die or in other words, the point until which the resin-impregnated fibre reaches the die inlet. The tacky tape was used in certain cases, to avoid the slipping of the fibres between the rollers to maintain the tension. In other cases, the tacky tape dint work, as the material slipped.

Linear frictional force (LFF) analysis is used to calculate the force correlating to different regions of the die for different settings. During this process, the resin-impregnated glass fibres are cut and allowed to enter the die and the force values are noted until the cut material reaches the end of the die. The initial temperature and time are noted when the final part of the cut resin-impregnated fibres enters the die.

The data analysis process can be realised after data skimming process. The datapoint collection begins after the controller is connected to the computer. Invalid data points were eliminated using the following procedure.

1. Datapoints with temperature and pulling speed readings, lower than the pre-set process conditions are eliminated.
2. During the test run, the pulling speed is upped, to find the new data points. Material inside the die is processed at previously set lower PS, PS between the newly set speed and the previous speed, PS at the newly set speed.
   In such a scenario, the data points during the change in the process are eliminated, i.e., the data points showing a predecessor PS or a PS between the old and new set PS, are eliminated. In addition to this, due to material clean-up time (time required for the material produced at previous PS to come out of the die), the data points corresponding to transition(from 80 to 120 mm/min or, 120 to 159 mm/min) are eliminated. This accounts for 200, 150 secs after the transition phase.
3. The average force values were calculated until the process conditions were changed or till the die jamming problem occurred.

4. The average inlet and outlet temperature are calculated for thermocouples T1, T2 and T9, T10 respectively.
5. The data points which measured faulty temperature readings are not considered inlet or outlet mean temperature calculation. If the temperature readings are not measured correctly for the entire experiment, due to misconnection then the average temperature is noted for one thermocouple.
6. PF and temperature data points corresponding to manual fibre pulling and until the tacky tape crosses the pulling unit are eliminated.
7. The measurement of PF for dry fibres for stable PS is used. During the process, the rovings are cut to conduct a new experiment. In such a scenario, PF corresponds to the data points until which the speed is measured for the fibres until they exit die.
8. For the LFF analysis, resin-impregnated fibres are most likely cut after the process is steady and stable in terms of PF. However, this is not always the case. The exact time duration between data points is used for the DOC and PF plots, instead of the standard 5s interval.

2.1.3. Testing methods

A brief description of the different tests used in this study and the procedure of how the tests were carried out are described. The assumptions made during the calculations are provided.

2.1.3.1. Three-point bending test:

During the flexure test, the material undergoes a combination of tensile stress (on the outer layer), compressive stress (on the inner layer) and shear stress. The mode of failure for each material is reported in *appendix G2*. The type of failure of the material provides an insight about the weak parts in the composite, such as bonding strength between layers etc.

The fabricated samples are cut using a hacksaw blade. Every sample is cut into smaller pieces (referred to as the "specimen") as per the required ASTM standard dimension for the test. The specimens were cut using a diamond saw cutter. Eight to ten specimens were used for the test, for every dataset or processing condition. The following steps were taken during cutting and placement of specimen.

1. The initial part of the specimen having uneven roughness and irregularities are eliminated.
2. The left cross-section of the specimen corresponds to the left cross-section of the die.
3. Half of the tests were conducted with the top of the specimen corresponding to the top surface of the sample. For the other experiments, the top surface of the product as obtained after fabrication, become the bottom layer of the specimen. Repeatability was checked to identify the differences in bonding and the distribution of fibres.

Test set-up:

The three-point bending test set-up consists of two bottom rollers with a diameter of 1.5mm and a top roller with a diameter of 3mm. The sample is placed between the rollers and a load is applied, as seen in *Figure 10*. The nominal specimen thickness (t) and width (b) are 2mm*10mm.

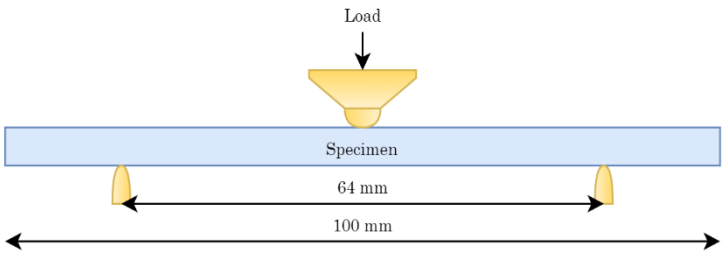

Figure 10: Three-point bending test set-up

The ratio of support span length to the thickness of the specimen is 32:1 [42]. According to the standard, the span length ratio to the thickness for class IV material is 50:1. The speed of testing is given by,

$$V = \frac{\varepsilon' L^2}{6t} \tag{1}$$

Where,
L *= support span length (mm)*
t *= thickness of the specimen (mm)*
ε' *= strain rate = 0.01*

Least thickness of the sample was found to be 1.94mm, with the support span length of 64mm. Based on the speed tolerance (as per the ISO standard), the speed must lie between 2.8 mm/min and 4.2 mm/min. The set test speed is 4 mm/min. The different modes of failure are also elaborated in the standards.[43]

The flexural strength corresponds to the maximum stress or force the material can withstand, before undergoing complete permanent deformation. The maximum flexural strength is found for with the maxima function for every point. Flexural strength is given by,

$$\sigma\ (N/mm^2) = \frac{3FL}{bt^2} \tag{2}$$

Where,
F *= load applied on the specimen (N)*
b *= width of the specimen (mm)*

To reduce the deformation of the wind turbine blades, it is necessary to have stiffer blades. The flexural modulus is the material property and signifies the stiffness of the material.

$$\sigma\ (N/mm^2) = \frac{mL^3}{4bt^3} \tag{3}$$

Where,
m *= slope of the linear region on the force-displacement curve*

The slope is found for the displacement of 2mm and 1mm, using the corresponding force values at these points. The specimen width and thickness is different for every specimen and it is measured using a digital vernier calliper.

The modulus and strength are calculated for every specimen and the variations within the sample are reported in *appendix G1*. The variation of flexural modulus and strength for different processing conditions and their results are discussed in further sections.

2.1.3.2. Testing for void content

Void content is essential to determine the quality of the product. The lower the void content, better is the mechanical properties. Void content is estimated using 2 methods:

a. A combination of microscopy and image analysis
b. Archimedes principle test – experimental void content

Image and microscopy analysis

Microscopy experiment is carried out to familiarise with the material defects or imperfections such as voids, resin-rich areas, distribution of fibres and the location. This analysis could provide a discussion of the possible reasons for preventing defects. One of the steps taken to improve the image quality is the addition of the pigment due to the transparency of the pultruded composite. There are several steps taken during microscopy,

1. *Cutting*
   Up to four specimens were cut for each sample using a diamond saw cutter. The length of the specimen is 1cm.

2. *Embedding*
   The specimen is held in place with a copper or plastic specimen holder as shown in *Figure 11*. The specimen holder restrains the movement of the specimen when the solution is poured and it presses down the cross-section of the specimen to the horizontal surface. A solution of EpoFix Resin and EpoFix hardener is mixed in the ratio of 8.33:1 and poured into the mould containing the specimen. The resin-mould product is obtained by de-moulding it from the mould case, after curing the epoxy resin overnight.

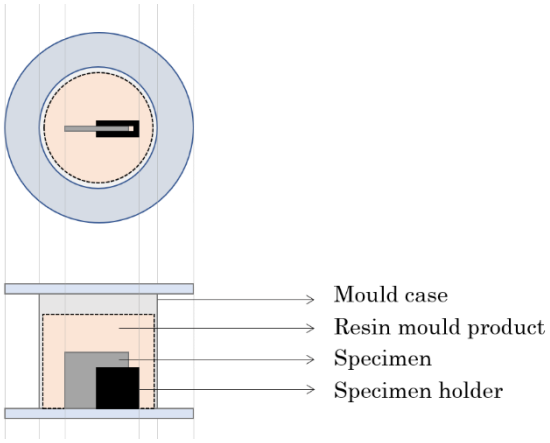

Figure 11: Sample embedding

3. *Polishing and cleaning*
   The purpose of polishing the sample is to improve the image quality, by eliminating small dents, surface protrusions and so on. Polishing comprises of 6 stages that include the use of SiC foil (500, 1000, 2000 and 4000), MD-Chem (OPS-dry) and SiC foil (4000) sanding with water. Ethanol was used to eliminate any suspended particles, dirt and moisture,

since it affects the image clarity, thereby giving the wrong perception about the resin content. Appropriate lighting is used to find the best suitable image for the analysis.

The microscopic images obtained from the Keyence microscope is uploaded into the Image-J software for image processing. The images were used to find the void content and the values were noted for each specimen and compared amongst themselves for every sample dataset or process combination. The results from the analysis are reported as theoretical/analytical results for void content. The following steps were taken during the image analysis,

1. The unwanted edges of the images are trimmed and saved for further use.
2. The image is converted into an 8-bit image.
3. Filters were used to remove the noise. The two filters were used separately and the results were compared. The size of the median filter was set at 15mp, 17mp and 23mp for 3, 2 and 22 images respectively. The sampling window width is set at 19,21 and 35. The sampling size of the filters depends on the ability to detect the fibres and eliminate the scratches and unpolished surface marks.
4. Different threshold limits were applied for the images. The threshold limiting value was set using naked eye vision by comparison with the original image. Certain greyish spots that appear black were not considered as voids, due to lighter colour contrast. Perfectly dark spots were considered as voids. The size and location of the voids were compared to the original image during thresholding.

The threshold values and the sampling width value for each specimen are listed as a tabulation in *appendix F1*. The results for void content are discussed in the subsequent section.

Archimedes principle test

Two methods used to obtain the accurate density measurement are the Archimedes test and the burn -out test. The details of the tests are explained in this section.

Archimedes test for density determination

Archimedes test was performed to identify the actual density of the specimen. The test is based on the principle of buoyancy. According to this principle, the volume of the displaced fluid when the specimen is completely immersed in the liquid is equal to the volume of the specimen. AT261 Delta Range by Mettler Toledo was used for the test. The equipment consists of a weighing machine with a sensitivity of 0.1mg. *Figure 12* represents the density measurement test set-up used for the experiments.

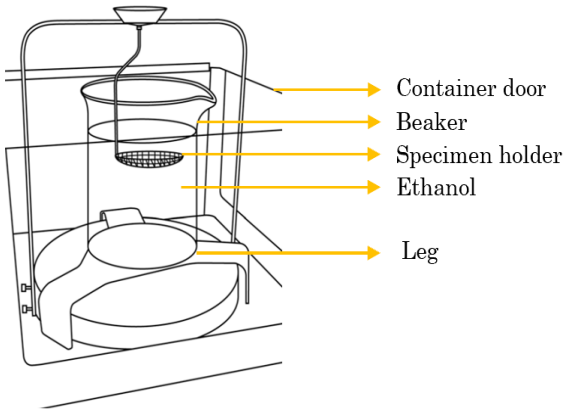

Figure 12: Density measurement set-up [44]

Procedure for the density measurement test is as follows,

1. 3 specimens per sample were used for the test. According to ASTM standards [44], the volume of the sample must be less than 2cm^3. The cross-sectional dimensions are fixed at 0.2cm*1cm. Since the beaker diameter is 8cm, therefore a sample with the length of 10cm is not feasible. Three specimens each spanning 3cm in length, were used for the tests.
2. To measure low-density substances, ethanol is prominently used as opposed to water. In this test, ethanol was used. Ethanol is poured into the beaker, such that it surpasses the level of the cup. The cup is installed to hold the specimen.
   The 'weight of ethanol' (A) is measured before every test is conducted. The measurement is taken by closing the container door. Due to vaporization of ethanol over time, therefore weights are measured after subsequent trials.
3. The specimen is then placed on one of the three legs at the bottom of the beaker. The container is closed, to avoid the fluctuation in weight due to air disturbance. The sample is kept for half a minute and the reading is noted for 'weight of the specimen in air'(B). Meanwhile, the temperature's are also noted, due to its effect on the density.
4. The specimen is placed on the cup, that is submerged in ethanol and the container door is closed. The weight readings correspond to the 'weight of the specimen + ethanol' (C).

It should be noted that the ethanol sample turned to a light blue shade due to the presence of blue ink on the sample. Since the ink used is negligible, it is assumed that the sample weight is not affected.

The procedure to calculate the actual void content is as follows,

1. The actual density of the composite for each specimen (ρ_{ac}) is given by,

$$\rho_{ac} = \rho_e \left(\frac{m_a}{m_a - m_e}\right) \tag{4}$$

Where,
ρ_e *= Density of ethanol = 0.78691 g/cm³* [45]
m_a *= Weight of the specimen in air = B – A (g)*
m_e *= Weight of the specimen in ethanol = C – A (g)*

2. The theoretical density of the composite (ρ_{tc}) is computed using,

$$\rho_{tc} = \frac{100}{\left(\frac{R}{D} + \frac{r}{d}\right)} \tag{5}$$

Where,
R *= % resin in composite with respect to weight*
D *= density of the resin = 1.062 g/cm³*
r *= % fibres in composite by weight*
d *= density of reinforcement = 2.64 g/cm³* [46]

Note that, the density of reinforcement is assumed to be 2.64 g/cm^3, since the exact type of E-glass is not known. Therefore, a mid-value between 2.62 and 2.66 g/cm^3 is considered.

The resin bath composition comprises of different substances. Before the fabrication of the composite, the weights of each component is noted as tabulated in the table below. Therefore, the density of the resin bath is calculated by,

$$D = \frac{W_r}{V_r} \tag{6}$$

Where,
W_r *= Total weight of the resin bath*
V_r *= Total volume of the resin bath*

Resin bath components	Weight (kg)	Density (kg/m^3)	Temperature at which density is measured (°C)	Volume (m^3)
Atlac 430 resin	0.5	1060	23	0.000471698
Peroxide	0.005	1060	20	4.71698E-06
De-gassing agent	0.005	880	20	5.68182E-06
Lubricant	0.005	980	25	5.10204E-06
Pigment	0.005	2200	-	2.27273E-06

Table 4: Resin bath composition and their density

The calculation for the volume fraction of the fibre is in *appendix A1*. The weight fraction of the resin (R) can be found as follows,

$$R = \frac{W_r}{W_r + W_f} \tag{7}$$

Where,

$$W_f = d.\, V_f \tag{8}$$

To calculate the volume of the fibre (V_f),

$$V_f = \frac{FVF\ .\ V_r}{1 - FVF} \tag{9}$$

Therefore, R = 12.79% and r = 87.21%. Substituting in equation (5), we get ρ_{tc} = 2.218 g/cm^3.

Void content is calculated with,

$$\%void\ by\ volume = 100\ .\left(\frac{\rho_{tc} - \rho_{ac}}{\rho_{tc}}\right) \tag{10}$$

The void content results are discussed in the upcoming sections. Since the burn-out test was only conducted and no useful results were obtained, therefore a brief overview of the test is given in *appendix C1.*

Chapter 3. Data analysis

The method followed for the calculation of cure degree is explained in this section.

3.1. Cure kinetics model

During the preparation of the resin mixture, additional components such as lubricant, hardener, de-gassing agent etc are added to improve the process. Addition of additives into the mixture in varied proportions could probably have a significant effect on the cure kinetics of the resin. Due to time constraints, DSC tests for the resin combination used in this study couldn't be conducted. Therefore, results published by Yaroslav et al. [47] were used for the cure kinetics model. Other relevant papers that used similar resin combination such as their study were not available. A combination of ATLAC 430 vinyl ester resin, Perkadox, Trigonox C, BYK agent and a few additives such as zinc stearate and $Al(OH)_3$ were used in their experiments.

It was found that if both additives were used simultaneously, then it did not have a significant effect on the cure degree as compared to the no additive case. The highest cure degree was found without the use of additives. A similarity in the resin composition and the experimental verification of the most suitable governing cure kinetics equation was best suited for this study. Resin characterisation using DSC test to find the glass transition temperature and the heat release rate was published. Four resin composition combinations were presented by Yaroslav et al. First resin composition was used for this study. Cure kinetics equations used for this study is,

n^{th} order autocatalytic reaction:

$$\frac{d\alpha}{dt} = Ae^{\frac{-E_a}{RT}}(1-\alpha)^o(1+K_{cat}\alpha) \quad (11)$$

Where,

α = *degree of cure*
E_a = *activation energy* = *108.49 kJ/mol*
R = *universal gas constant* = *0.008314 kJ/K/mol*
T = *temperature (K)*
o = *experimental constants, o = 1.71*
A = *exponential factor* = $1.23 * 10^{12}/s$

This equation was chosen as it best represents the cure kinetics behaviour for this particular combination of resin mixture based on the research paper. The key point in this study is that the cure kinetics behaviour varies with the ratio of different components mixed with the resin, thereby providing sufficient information for process optimisation.

Procedure to plot the predicted degree of cure profile:

1. The top thermocouples (T1, T3, T5, T7 and T9) and the bottom thermocouples (T2, T4, T6, T8 and T10) measure the temperature readings after every 5-second interval. The top and the bottom thermocouples are placed at the same distance from the die entrance and are symmetrical about the horizontal axis and are henceforth mentioned as identical thermocouples. The thermocouples are located at 15, 100, 200, 300 and 385mm respectively.
2. For the linear frictional force analysis (LFF), the temperature average for all the thermocouples is taken. Mean temperature is calculated for the pulling force analysis used

steady-state condition for a set temperature range (± 10% difference in temperature and 5% in PS, is considered as an acceptable steady-state condition).

3. During the experiments, two thermocouples were used at both the inlet (T1 and T2) and outlet (T9 and T10) of the die to measure the temperature. Due to their non-functionality, some thermocouples had to be plugged out. But, for all the experiments, either T1 or T2 was plugged in at the inlet. In certain similar conditions, the same problem was encountered at the exit of the die during experimentation. If the thermocouple is plugged out, no temperature reading is taken. For instance, in such a scenario, if T1 is working and T2 isn't, then T2 would have the same value as T1. In other words, The location of different thermocouples (T1 to T10) is known. Therefore, the location of the thermocouple is translated into time dependence variation and is tabulated in *Table 5*.

Distance of thermocouple	PS = 80 mm/min	PS = 120 mm/min	PS = 159 mm/min
T1 or T2 at 15mm (limit)	11.27s	7.5s	5.66s
T3 or T4 at100mm	75.18s	50s	37.73s
T5 or T6 at 200mm	150.37s	100s	75.47s
T7 or T8 at 300mm	225.56s	150s	113.2s
T9 or T10 at 385mm (limit)	289.47s	192.5s	145.28s

Table 5: Distance travelled by the thermocouple for different speeds

4. The temperature and distance values for every 1s interval between the given limits in the table are interpolated using the forecast function. Forecast function in Microsoft excel simply interpolates or linearly extrapolates the value. The values of temperature and distance beyond the limits are extrapolated linearly based on the differences in the trends. The temperature at the ends of the die is lower due to convection losses. However, this may not always be the case, due to imbalance in the heaters.

5. Temperature (in K) and the boundary condition, $\alpha = 0$ at t = 0s, is plugged into (11) after 1s. The cure rate after 1s, $\frac{d\alpha}{dt}$ is obtained. The cure degree for the 1st second is the same as the cure rate. Numerical integration method is used. The subsequent new cure rate is calculated for each second, starting from 2s until the end limit with the cure rate obtained from the previous step and the new temperature. The new cure degree (α) for step 2 is calculated by multiplying the time difference between the two steps (=1s) and the new cure rate and adding it to the previous cure degree.

6. Cure degree vs distance is plotted for different process parameters.

The results for the different process settings are discussed in subsequent sections.

Chapter 4. Results

In this section, the trends of different results and the reasons are explained and the process is optimized to find the best possible outcome for the experiments performed. The dimension and degree of cure results are briefly explained for the different processing conditions and the comparison is made. Furthermore, the variation of process parameters that affect the process such as temperature, PS, fibre rovings and configuration are discussed.

4.1. Forces in the pultrusion die:

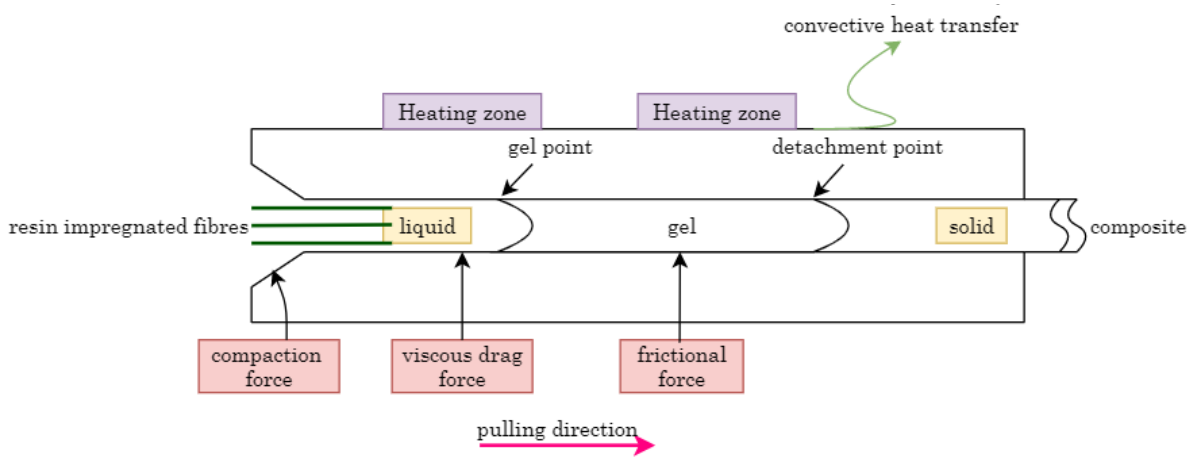

Figure 13: Forces acting on the pultrusion die

In thermoset pultrusion, resin-impregnated fibres upon entry into the die undergo 3 phase changes, from liquid to gel to solid. The pultrusion die is mainly classified into 4 regions based on the resistive forces generated during the phase change, as seen in *Figure 13*. Compaction force occurs due to pressure development as a result of reduced volume and size. In the beginning of the pultrusion process, the resin is in the liquid state. In the compaction zone, excess resin is squeezed out. A shear force between the thin resin film layer and the die surface walls results in a viscous force, caused due to skin friction. Heat source (also referred to as heating cartridges or heating zones) are located at the entrance to increase the die temperature. The resin layer thickness varies over time, due to the chemical changes. In the gel state, the cross-linking of polymers occurs and the viscosity reaches a constant peak value. A combination of thermal expansion of fibres and chemical shrinkage (a function of cure degree) causes sliding friction between the die wall and curing composite. After a certain cure degree, the material detaches from the die wall (detachment point) and transforms into a solid material. During the transformation from a partially solid state to a completely solid-state, friction develops along the contact surface. The coefficient of friction changes with the cure degree.

The findings from another study are cited by a researcher [25] and they concluded that the probability of die jamming is higher for lab or bench scale dies with a smaller cross-section. Moreover, incorrect placement of the heating cartridges in the commercial dies could be the reason for die jamming. The failure of the composite due to fibre breakage was more prominent in smaller dies and at the farther end of the die. Sloughing occurs due to non-detachment of the composite from the die wall or due to breakage of gel in the middle. A suitable mold release agent must be used for a smaller die to reduce the resin layer thickness near the die wall. The runaway tendency is defined as the point where the pulling force would not stabilise after steady-state condition is

reached. Part with large thickness would be subjected to a uniformly distributed pressure, due to lower shrinkage. PF largely depends on temperature and the resin conversion, pulling speed, fibre surface pattern and the materials. The PF for all the runs is shown in *appendix D*.

4.1.1. Pulling force results

Pulling force graphs for different configurations are as shown in *Figure 14*. The details of the trends are explained in the upcoming sections. The averages for the different trial runs are calculated together and reported as the average value of PF for each process setting. The average pulling force for all the process settings is represented by a bar graph with a bold outline. The notations used for average pulling force and the standard deviation is PF ± SD, for all the configurations. Configurations C1, C4 and C5 correspond to 7R, C2 corresponds to 6R and C3, C6, C7 and C8 correspond to 8R.

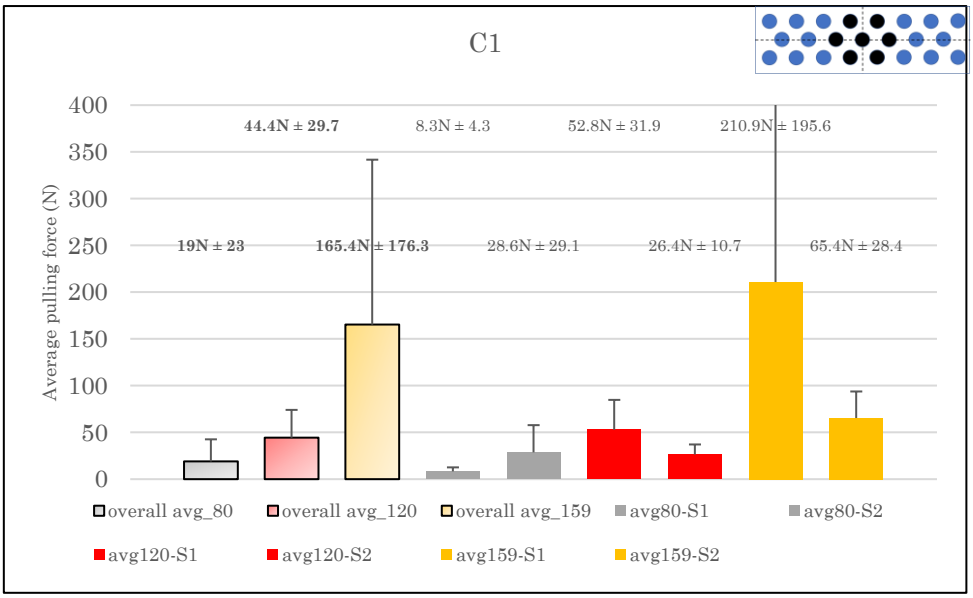

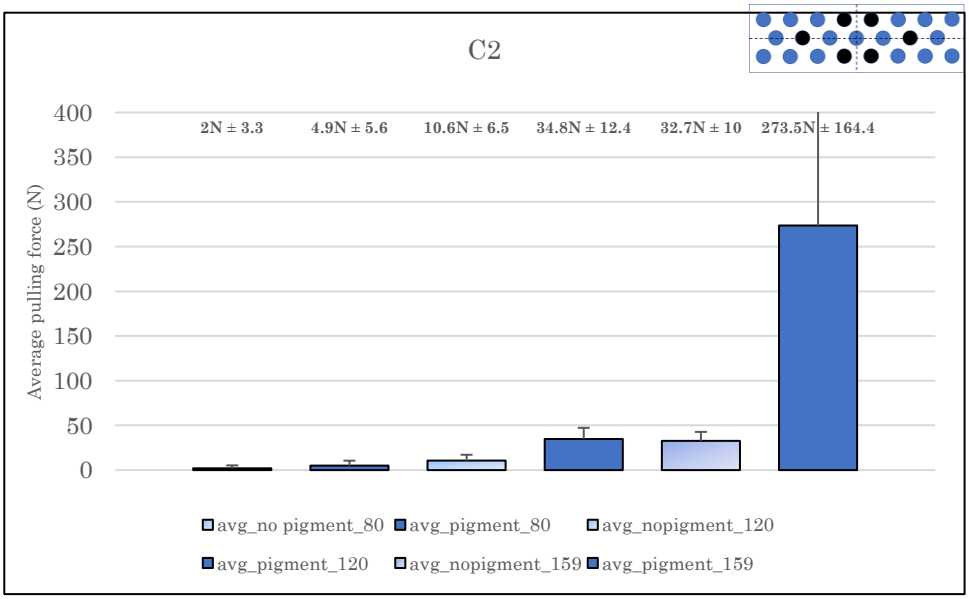

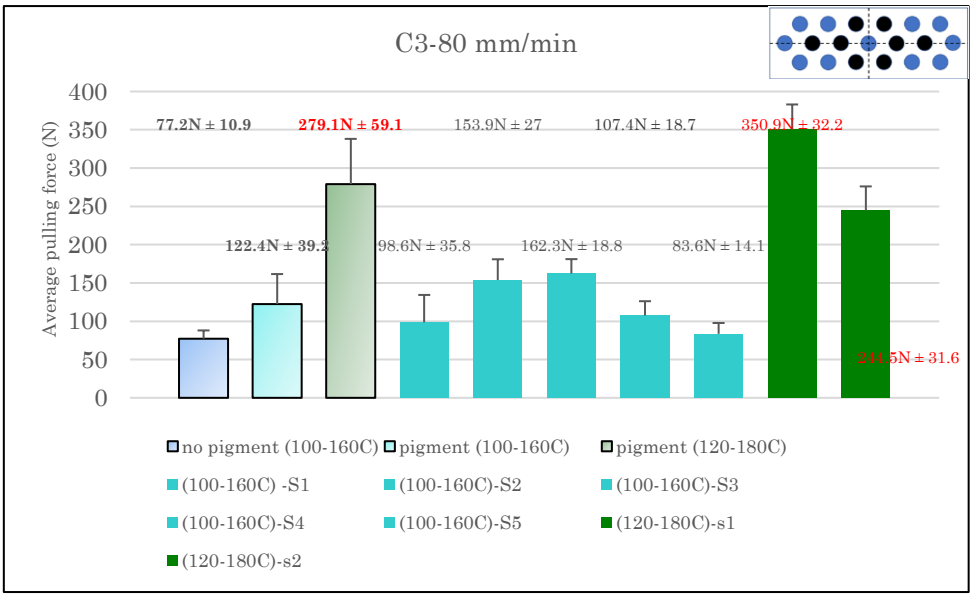
C3-80 mm/min
Average pulling force (N)
400
350
300
250
200
150
100
50
0
77.2N ± 10.9
279.1N ± 59.1
153.9N ± 27
107.4N ± 18.7
350.9N ± 32.2
122.4N ± 39.3
98.6N ± 35.8
162.3N ± 18.8
83.6N ± 14.1
244.5N ± 31.6
no pigment (100-160C)
pigment (100-160C)
pigment (120-180C)
(100-160C) -S1
(100-160C)-S2
(100-160C)-S3
(100-160C)-S4
(100-160C)-S5
(120-180C)-s1
(120-180C)-s2

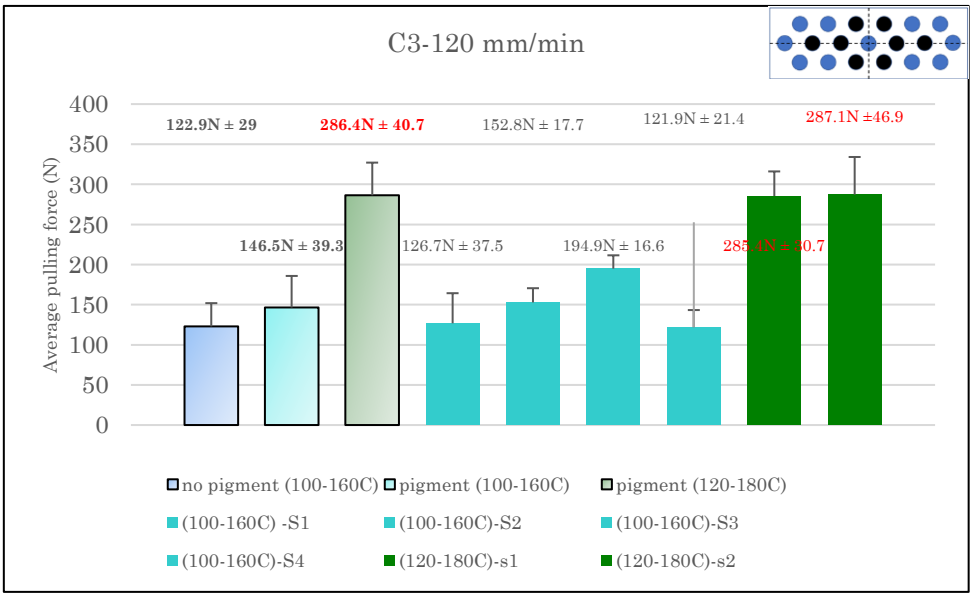
C3-120 mm/min
Average pulling force (N)
400
350
300
250
200
150
100
50
0
122.9N ± 29
286.4N ± 40.7
152.8N ± 17.7
121.9N ± 21.4
287.1N ±46.9
146.5N ± 39.3
126.7N ± 37.5
194.9N ± 16.6
285.4N ± 30.7
no pigment (100-160C)
pigment (100-160C)
pigment (120-180C)
(100-160C) -S1
(100-160C)-S2
(100-160C)-S3
(100-160C)-S4
(120-180C)-s1
(120-180C)-s2

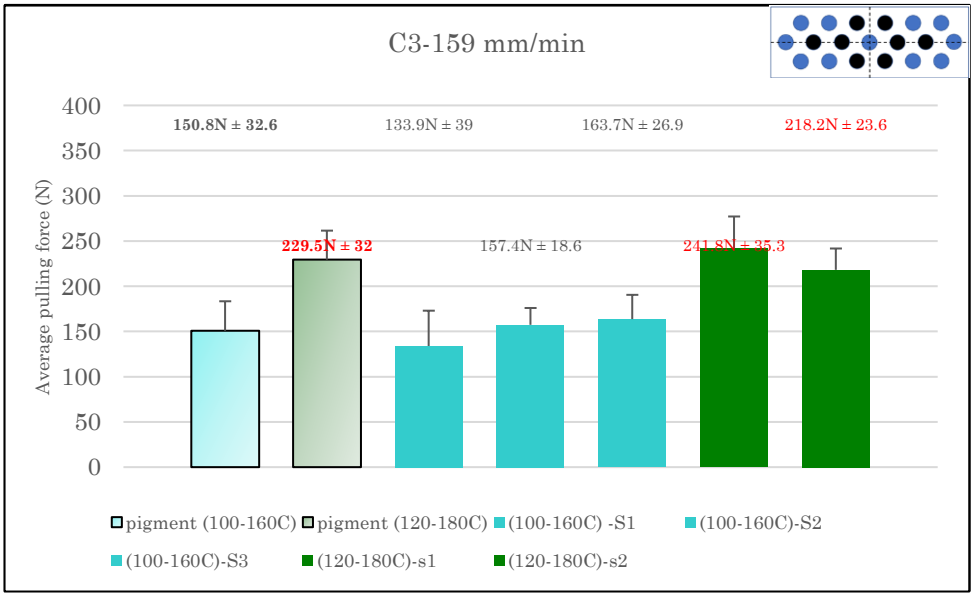
C3-159 mm/min
Average pulling force (N)
400
350
300
250
200
150
100
50
0
150.8N ± 32.6
133.9N ± 39
163.7N ± 26.9
218.2N ± 23.6
229.5N ± 32
157.4N ± 18.6
241.8N ± 35.3
pigment (100-160C)
pigment (120-180C)
(100-160C) -S1
(100-160C)-S2
(100-160C)-S3
(120-180C)-s1
(120-180C)-s2

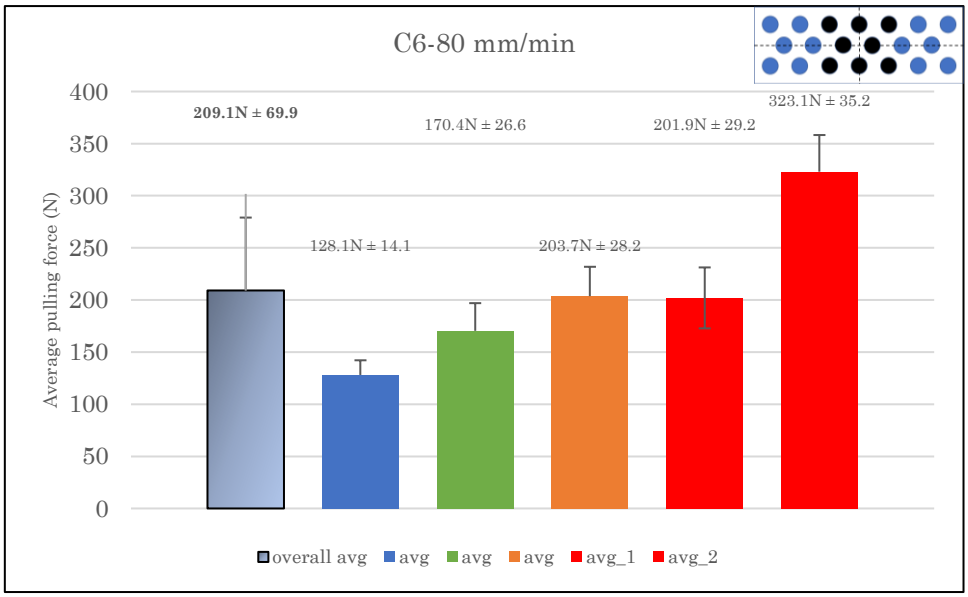
C6-80 mm/min
209.1N ± 69.9
128.1N ± 14.1
170.4N ± 26.6
203.7N ± 28.2
201.9N ± 29.2
323.1N ± 35.2
Average pulling force (N)
400
350
300
250
200
150
100
50
0
overall avg
avg
avg
avg
avg_1
avg_2

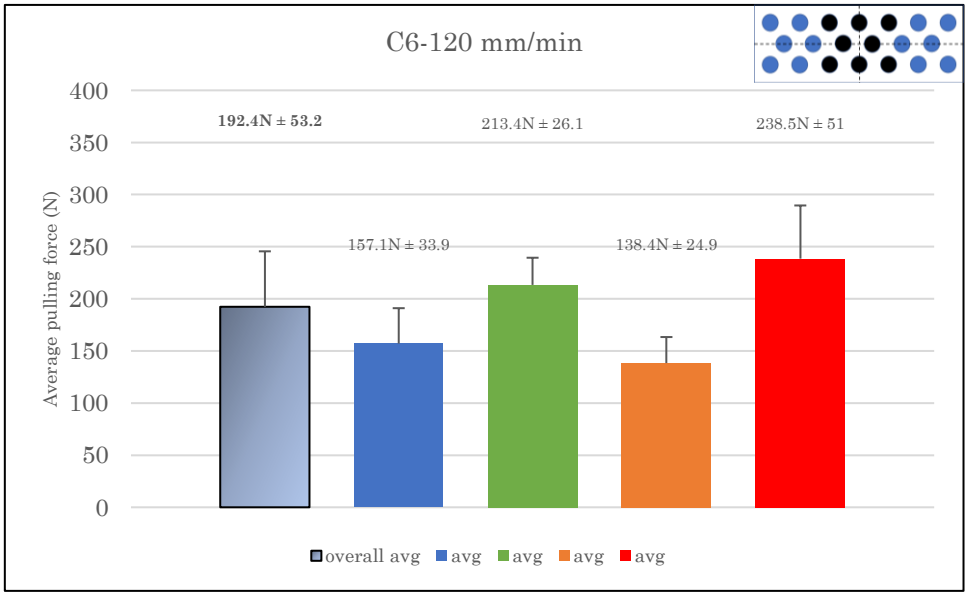
C6-120 mm/min
192.4N ± 53.2
157.1N ± 33.9
213.4N ± 26.1
138.4N ± 24.9
238.5N ± 51
Average pulling force (N)
400
350
300
250
200
150
100
50
0
overall avg
avg
avg
avg
avg

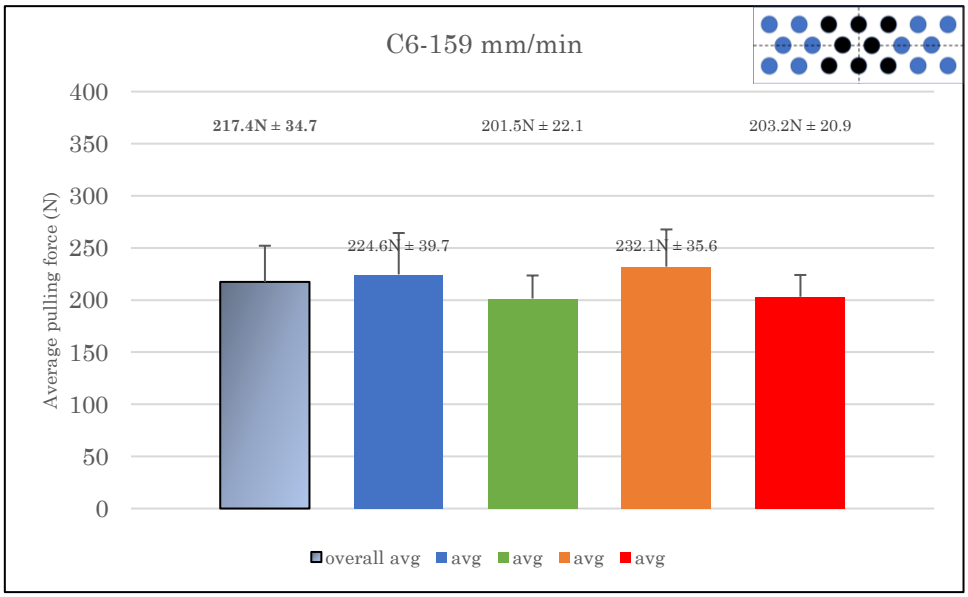
C6-159 mm/min
217.4N ± 34.7
224.6N ± 39.7
201.5N ± 22.1
232.1N ± 35.6
203.2N ± 20.9
Average pulling force (N)
400
350
300
250
200
150
100
50
0
overall avg
avg
avg
avg
avg

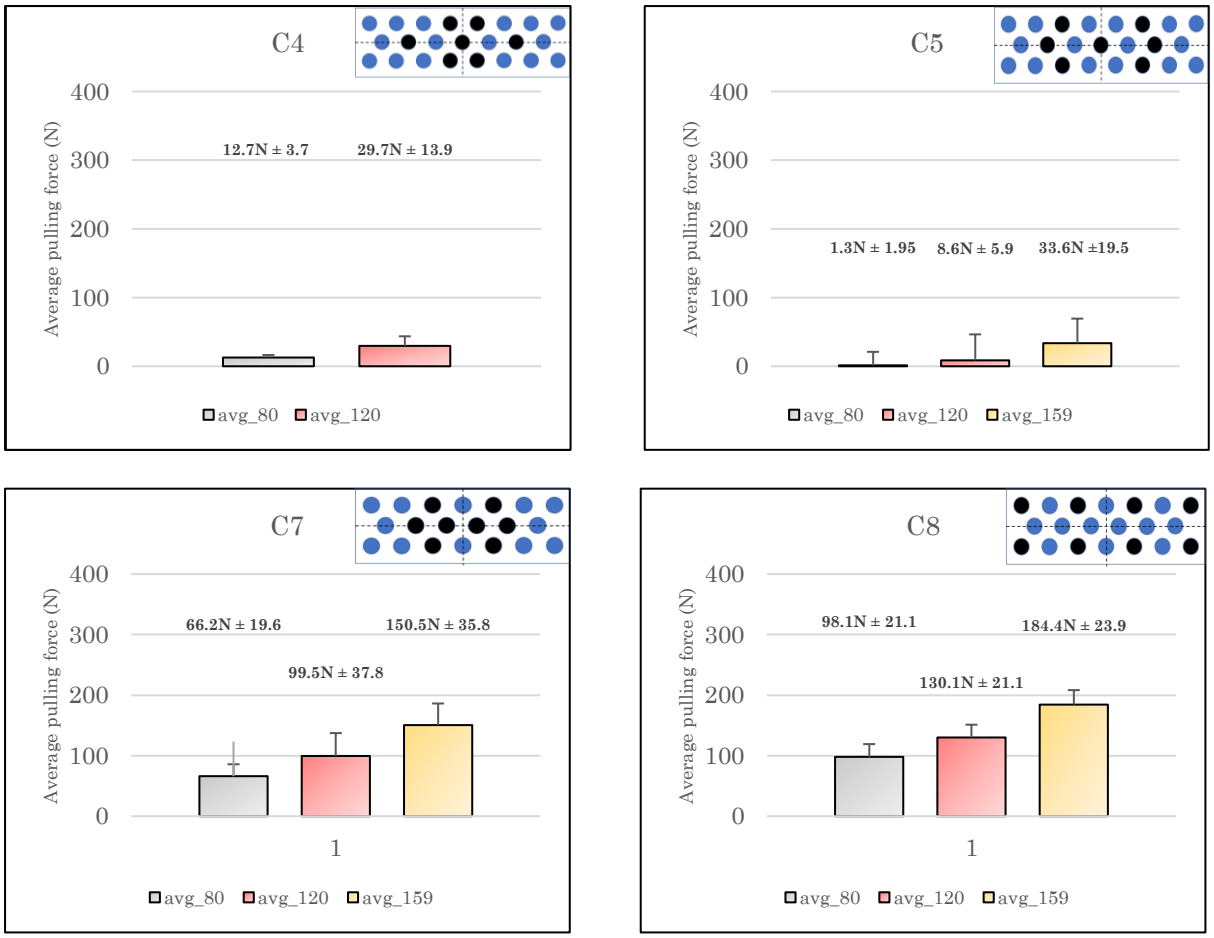

Figure 14: Pulling force for different configurations, speeds and temperature for individual trials and their averages

Configurations – C4, C5, C7 and C8 had one set of experiments for each process setting for a pigment-based resin system. Configuration – C2, had one set of experimental trials each, for with and without pigment-based resin combination. Configuration – C3, had one experimental trial for no-pigment resin bath scenario. Other configurations had more than one trial (for resin bath with pigment), which are represented in the graphs as "avg-speed-sample number" for C1, "(inlet-outlet temperature)-sample number" for C3 and, "avg" for C6. Configuration – C3, was used to fabricate the composite at 100-160°C and 120-180°C (represented as red text) processing condition. A test run was conducted with increasing speed setting (in mm/min) from 80 (avg_1) → 120 (avg) → 159 (avg) → 120 → 80 (avg_2), which is represented by red bar graph for C6. Speed was reduced in steps due to low resin content in the bath, despite the noticeable instability of PF. No plot is made for 120mm/min since the data points were eliminated during the transition phase from 120 to 80mm/min for C6 (The temperature for a data point, at PF = 221N, which wasn't eliminated during data skimming process is noted for the speed reduction trial).

All the experiments are conducted for 100-160°C unless otherwise mentioned or denoted in the graphs. Experiments are conducted for the same temperature set and configuration, but with the increasing or decreasing line speed. To depict this, the following notations were used to denote the differences between each trial - "avg-speed-S-trial number" for C1, "(temperatures)-S-trial number" for C3 and it is depicted as a colour code for C6. The different trial runs for all the process settings and the measured average temperature values are seen in *appendix C*.

For configuration C2, the average force and standard deviation for with and without pigment case at 80, 120 and 159 mm/min are 3.5N ± 4.9, 19.2 N± 14.7, 93.3N ± 133.4 respectively. Any adjustment in the load cell or the batch of resin used in portrayed in the temperature tabulations. The new batch of resin had lower viscosity then the old batch of resin.

Discussion for pulling force graphs based on experimental observations

1. *Speed*:
   For all the configuration, it is apparent that as the line speed increases, the PF increases, except for C3 at 120-180°C. A higher value for C6 at 80mm/min is due to the datapoint considered (due to process instability) in the speed-reduction test. As the line speed increases, the gel zone area becomes larger. As a result, PF increases.

2. *Pigment, load cell adjustment and resin batch used:*
   The average force values for configuration C5 (with pigment) are much lower than C1 (no pigments) for all the line speeds. This could be due to the addition of pigment or the use of new batch of resin for C5 and C2. The old batch of resin used for the experiments were expired. On the contrary, for a similar configuration (C2), PF was higher for with pigment case (new resin batch) than without pigment (old resin batch). These trends are different and can be observed only for a trial. This suggests that the FVF and fibre configuration affect the PF. Similar trends for PF were seen for C3 and C2, where the PF was lower for the no-pigment case, as compared to pigment. The effect of the load cell isn't clear, based on the comparison of different PF values in case of C6. In some cases, the PF decreased and for the others, it increased. The variation in the PF measured by the load cell may affect the values in certain cases (such as before the adjustment), as it measured only a component of the force instead of the entire force. Therefore, no trend was established for the additional use of pigment, load cell alignment for different tests and different resin batches used.

3. *Temperature*:
   The average value of PF for the 2nd run (C1) at 80 and 120 mm/min is much higher than the 1st run. This may be due to the higher outlet temperature. This suggests that the heat transfer rate from the bulk of the material to the die is higher. At higher outlet temperatures, a higher DOC could be achieved. This may be because the material would adhere or be in contact with the die wall surface for a longer period, due to the heat generation. However, a higher PF is reported for 159 mm/min due to die jamming. However, on the contrary, the different test runs for configuration C6 showed that the PF decreased with an increase in the average outlet temperature for all line speeds. The inlet temperature of the die inlet may have an adverse effect on the length of the zones (which contribute to the PF) and subsequently the final cure degree and therefore, the quality of the material. If the inlet temperature is relatively lower than the gelation temperature of vinyl ester resin (~100°C) at the die inlet, it could result in a larger viscous zone. The effect of variation of inlet temperatures couldn't be made, as the other processing conditions weren't kept constant.

4. *Fibre packing:*

   Different fibre configurations (fibre packing) affect the PF, as it is evident from the results. Comparison between configurations C4 and C5 showed that the PF decreased with an increase in temperature at nearly stable PS. This observation does not testify with the result published in literature by [31]. Configuration C8 has higher PF values as compared

to configuration C7 for all the test runs, even though C7 has a higher outlet temperature than C8.

The distance between the fibre rovings or in other words the fibre packing is more lumped towards the centre for C1. Each fibre roving has atleast 3 neighbouring fibre rovings for C1. So the fibre packing density is higher and more concentrated in the centre. On the other hand, for C5 the fibre packing density is not dense. This could mean that a large amount of resin may be squeezed out for C1 as compared to C5. Therefore, C1 may withstand lower PF at the beginning of the die (viscous drag), due to lower pressure. The alignment of the fibres could be also be affected, due to the resin content inside the die. Uniform pressure distribution and the lubricating effect of the resin are affected by the resin content and fibre alignment. PF for C5 is much lower than C1 could be as a result of the lubricating effect. Based on this theory, C5 should have lower dimensions compared to C1. C4 could have higher values of PF than C5 probably because most of the fibres are in contact with the top and the bottom part of the die, provided the alignment of the die is uniform throughout the cross-section. Therefore, the compaction rate may be different for C4 and C5. The lateral fibres of C4 are quite dispersed from the centre of the die, which may lead to some accumulation of resin as compared to C1.

For 8R, the average PF for different configurations in the ascending order for different speeds are as follows, C7 < C8 < C3 < C6 (80 and 120 mm/min) and C7 < C8 < C6 < C3. As mentioned previously, PF would change based on the resin volume. Therefore, if the same number of rovings are used then the variation in void content could cause a change in the properties. The packing density towards the centre is higher for C6 followed by C3, C7 and C8. The reasons for the difference in PF may be due to compaction pressure and resin entrapment between the fibres which may affect the size of gel zone. No clear explanation can be drawn for the differences in trends.

The exact reason for these changes are not easily identifiable and can be discussed further.

5. *Number of rovings:*
The average force of all the runs for 7R > 6R for all the speeds. At lower FVF, the resin content is much higher compared to higher FVF, since the compaction area is the same for any number of rovings. Lesser resin content maybe squeezed out at the initial stages, due to dispersion of the fibres for 6R as compared to 7R, thereby creating a lubricating effect. On the other hand, since the number of impregnated fibres carrying the layer of resin coat on their surface is lower for 6R as compared to 7R. Larger pressure exertion on the surface by 7R compared to 6R, involves eliminating most of the excess resin at the tapered inlet region of the die. In addition to this, the time required to transfer the heat from the surface to the resin impregnated fibres would also vary. PF is higher for 7R as compared to 6R, due to higher FVF (lesser lubricating effect). The average of all the forces for 8R is always higher than 7R, for with pigment case. For without pigment case (C3), the overall average PF for all the runs with 8R (C3) combination couldn't be compared with 7R (C1) combination for 159 mm/min. The overall PF trend for all the test runs corresponding to non-pigment case were 8R > 7R > 6R.

6. *Insufficient experiments and experimental drawback:*
Data couldn't be extracted for configuration C9, since the material was stuck in the die and couldn't be pulled manually or with the help of rollers. Nine rovings (C10) couldn't be pulled with resin and pigment combination. Therefore, further analysis with 9 rovings was not carried out for different configurations. Nevertheless, it is uncertain if other configurations could have been pulled through the die, possibly due to pressure variation. The possibility is that the 9 rovings cannot be fit into the die, though it is theoretically

possible. It can be seen from the micrographs that for any 8R configuration, the cross-section is pretty much packed. In other words, the resin volume inside the die (resin intake) could vary for different 9R configurations. It is quite ambiguous since the micrographs show a completely packed structure for different 8R configurations. Therefore, it may not be feasible to fabricate a composite with 9R in the corresponding die geometry used in this study.

7. *Repetition of tests:*
   At lower temperatures, the repetitive tests for C3 showed lower PF. The deviation of average PF reduces with line speed and the values are affected due to the number of tests conducted for each speed setting. The cleaning of set-up may have affected the results of C3. Three tests were conducted together with an increasing speed. The first test is represented as "(100-160°C)-S3", the second as "(100-160°C)-S4" and the third as "(100-160°C)-S5" for C3. The first test conducted has a higher PF value and subsequent tests show a lower PF value as compared to the previous test run for the same speed.
   For repetitive tests, the outlet temperature increases. It can be seen that at higher outlet temperatures, the PF increases. Nevertheless, at higher speed, this change in temperature doesn't have a significant effect on the PF. The load cell measurements before the re-assembly may have affected the values of PF.

Overall variation of pulling force and the explanation for the established trends

The variation of PF for different process settings are discussed below and the reasons for these variations are hypothesised.

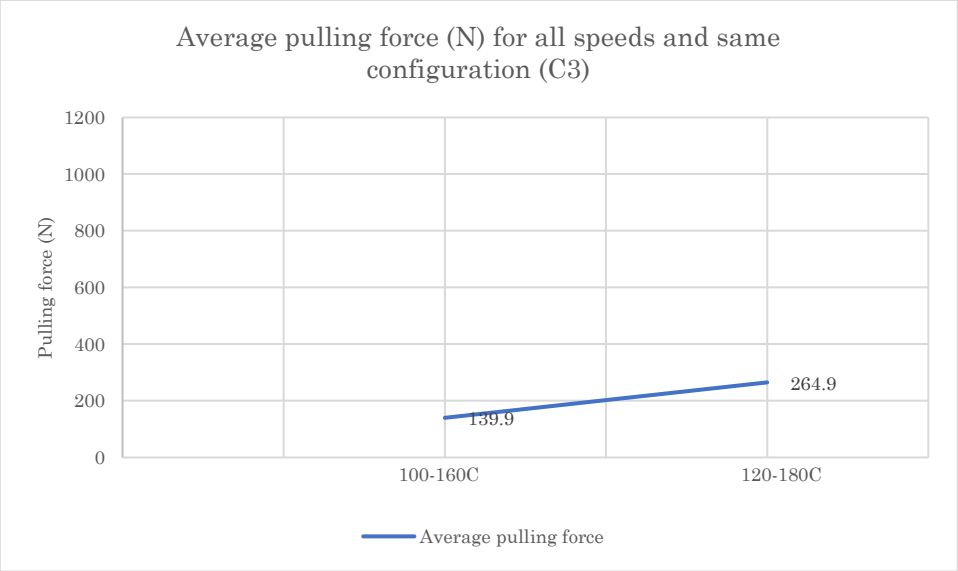

Figure 15: Average pulling force for increasing inlet and outlet temperatures with other uniform process settings

The average PF as shown in *Figure 15*, is calculated by using the value of PF for C3 at all speeds at a given entry and exit die temperature. PF is lower at lower inlet and exit temperature as compared to higher temperatures. The possible reason for this PF value is that at 100°C, the material starts to undergo curing at a much later point as compared to 120°C (maybe as a result of heat transfer rate) at a similar speed. The amount of material drawn and rejected may also vary, which has to be investigated. Additionally, to maintain a higher die exit temperature, more heat must be released at the die-product interface. This may take a longer time, as the material undergoes more curing (length of the zone affecting the PF becomes larger), thereby increasing the PF.

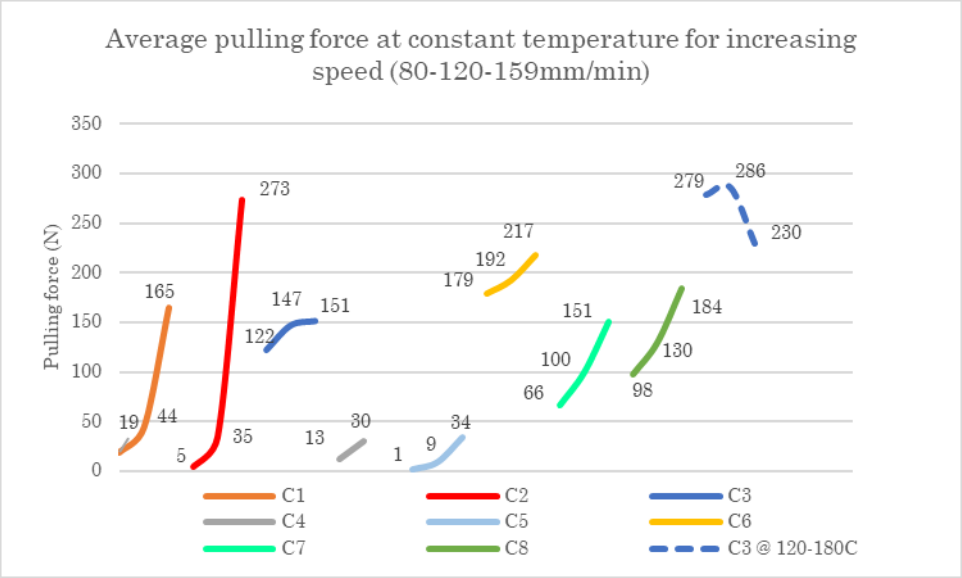

Figure 16: Average PF for different configurations with increasing speed and constant temperature

The average PF results which are reported in the previous sections are combined. In most of the cases, the PF increases, with the increasing PS (except C3 at 120-180C). In general, as the PS increases, a larger region of the die contributes to the PF. However, a small variation in PF for C3 could be due to a lower value of inlet temperature at 120mm/min and 159mm/min for the second trial. For C1 (at 159mm/min), PF is calculated for the data points which correspond to an unstable process and mostly all the data points corresponding to C2 had higher PF (unstable process). Therefore, these discrepancies are observed.

PF is lower for the combinations with lower FVF. The possible reason is that the resin uptake amount and the contact region between the die wall gets lower. This could be further verified with microstructure analysis. PF for different configurations with 7R (C1, C4 and C5) increases, based on the dispersion of fibre rovings from the centre. As the rovings get closer, there is a possibility of more resin being drawn into the fibre, due to the resin layer getting in contact with multiple fibre rovings (C1) as opposed to fewer rovings (C5). However, this may not be entirely true for 7R, as there is enough room for movement of rovings (7R) within the die. On the other hand, for a completely packed case (8R) the fibres may be compacted at the same rate, thereby squeezing out the same amount of resin. However, further investigation must be carried out, by checking the amount of resin being rejected for each scenario.

4.2. Linear frictional force (LFF) and cure degree evolution

The resin-impregnated fibres are cut at a certain distance from the die inlet and are referred to as cut-end tests. The measured values of PF just before the cut-end tests are shown in graph up to a distance of 6cm to the die inlet. The different LFF and DOC graphs for different process settings are shown below. For C6, 4 cut-end tests were done in total. Nevertheless, the results of 3 tests are tabulated, due to the faulty readings of average outlet temperature (146°C).

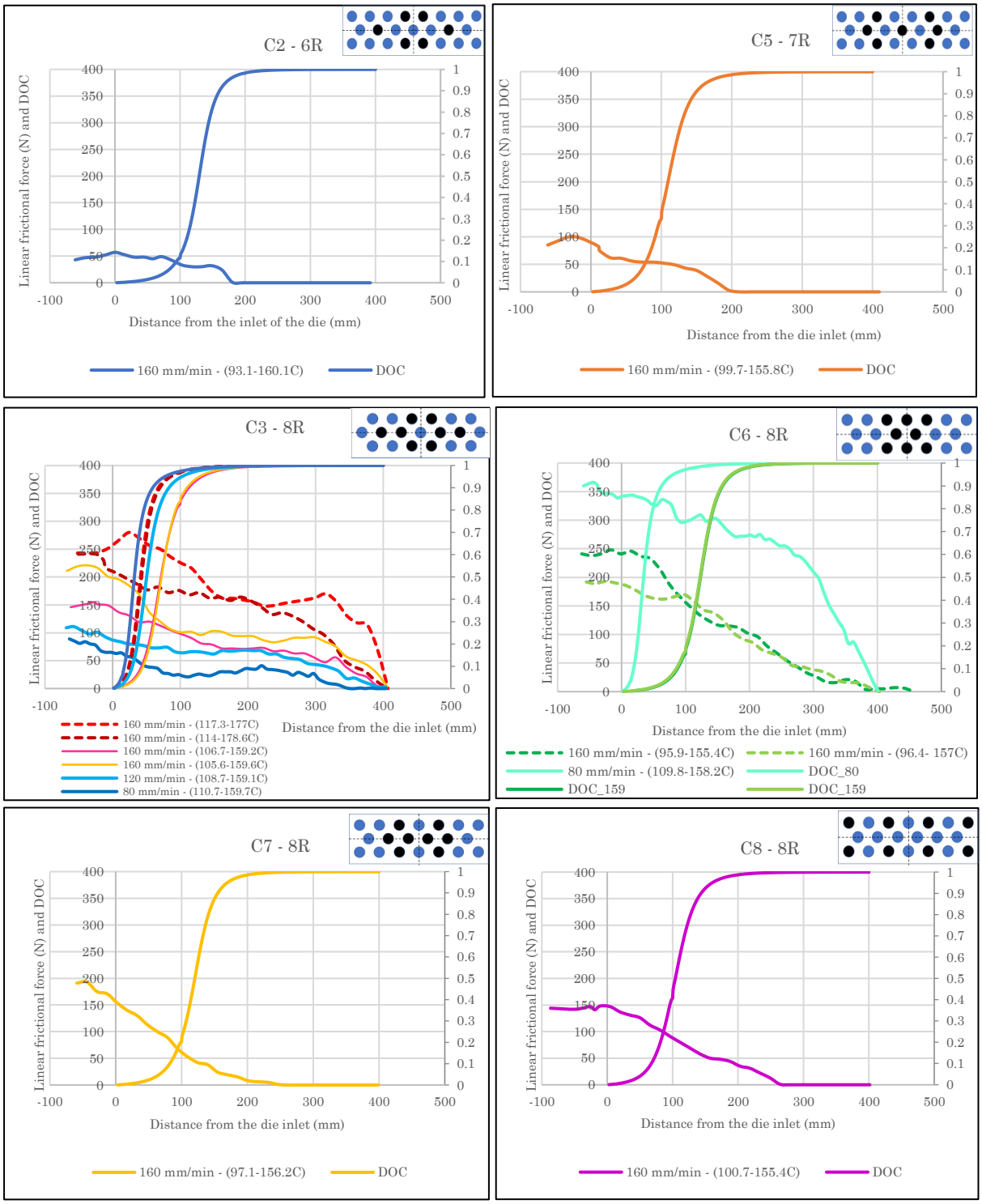

Figure 17: Linear frictional force values obtained by cut-end tests

The average of the measured temperatures at the inlet and outlet for different process settings are shown as legends in

Figure 17. The origin of the graph represents the point when the cut-end of the resin-impregnated fibres enters the die inlet. The negative x-axis shows the time or position-dependent PF with respect to the origin. For certain tests (such as C7), it can be seen that the force decreases, when the material enters the die. This may occur due to instability in force which can cause a difference in the zone length. Nevertheless, further tests must be conducted to verify this argument. Therefore, the results may not be concurrent for the test runs, with unstable PF before the start of the cut-end test. The DOC curve may not be accurate since the values are predicted for an average temperature for each process setting.

4.2.1. Prediction of zone length:

The method used to predict the start of the gel zone is as follows. An approximate of the gel point could be predicted based on the degree of cure profiles for the PF measurements. At the highest viscosity, the gelling starts. Therefore, if the temperature (resin transform from glassy to rubbery state) crosses the glass transition temperature, then this point corresponds to the end of gel zone. For the sake of simplicity, an arbitrary DOC value is defined for rubbery to glassy state transition to estimate the end of gel zone. The predicted DOC graphs can be used to determine the length of the gel zone which is shown in *Table 6*. The viscous zone starts from the tapered region of the die, which is located at 10mm from the die entrance until the point at which gelation starts.

The point where the gelation begins is estimated at 5 – 10% DOC. The PF, found by cut-end tests (shown by a drop in the value). This point is set based on the assumption that DOC would have a positively increasing slope, which means that the gelation has just sprung into action. The detachment point is estimated as the distance from the die inlet at which the pulling force becomes zero. As the end of the gel-zone cannot be easily determined, in theory, it can be assumed that the detachment point is the end of the gel zone. However, in this study, the end of the gel zone is noted as the point when the DOC reaches 90% to 95%, for these experiments. Certain test runs, do not have a detachment point and is marked as 'nil' in *Table 6*. Further reasoning can be discussed for determining the gel zone, as the understanding of the end of the gel zone is unexplored.

Configuration	Speed (mm/min)	Set inlet and outlet temperature	Run	Gel (start and end point based on distance from the die inlet) in mm	Detachment point (in mm)
C2 (6R)	159	100-160°C	1	79 – 161	180.2
C5 (7R)	159	100-160°C	1	72 – 151	195.6
C3 (8R)	159	120-180°C	1 – red dotted line	15 – 62	nil
	159	120-180°C	1 – maroon dotted line	15 – 65	nil
	159	100-160°C	1 – pink and yellow	47 – 116	nil
	120	100-160°C	1 – light blue	20 – 80	nil

	80	100-160°C	1 – dark blue	16 – 56	351
C6 (8R)	159	100-160°C	2 – light and dark green	88 – 165	nil
	80	100-160°C	1 – cyan	16 – 69	nil
C7 (8R)	159	100-160°C	1	82 – 161	246.7
C8 (8R)	159	100-160°C	1	69 – 161	264.1

Table 6: Prediction of gel zone region

The following conclusions are drawn for LFF and DOC based on the experimental observations,

1. *Effect of rovings and roving configuration*

The PF is initially high, as the entire composite is inside the die and it undergoes compaction. The distance of the detachment point starting from the closest to the farthest point with respect to die entry is 6R, 7R and 8R. For the different FVF and fibre configuration, a trend for the variation of gel zone length cannot be determined. The DOC for different 8R configurations is around 200mm, except for C3. The start of gelling (at 100-160°C and 159 mm/min) is in the order, C3 < C8 < C7 < C6.

2. *Effect of pulling speed*

PF is lower for lower speeds. PS decreases with the length of the gel zone.

3. *Effect of temperature*

Highest LFF is obtained for 120-180°C combination as compared to 100-160°C. The length of gel zone is closer to the die inlet for 120-180°C combination and smaller in length. This trend is based on C3. The exact trend cannot be commented on since the trials for different configurations are not conducted. The resin gets cured quickly at higher temperature as opposed to lower temperature settings due to the drop in viscosity.

Overall variation of detachment point and the explanation:

The results in graphs below show the detachment point for each process setting and results are interpreted with a possible hypothesis. The length of the die is 400mm. Therefore, the detachment point values which are higher than 400mm, means that the composite doesn't detach from the die.

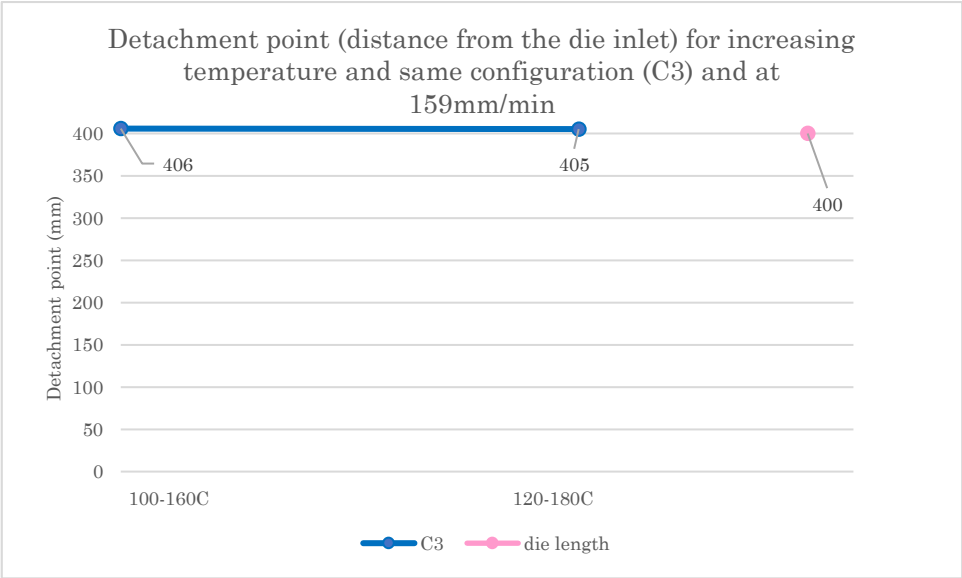

Figure 18: Detachment point for different die temperatures with constant settings for other processing conditions

The configurations which have trial runs for both 100-160°C and 120-180°C are considered, to establish a trend for increasing temperature. It can be observed that the detachment point doesn't exist for C3 and therefore no trend was observed.

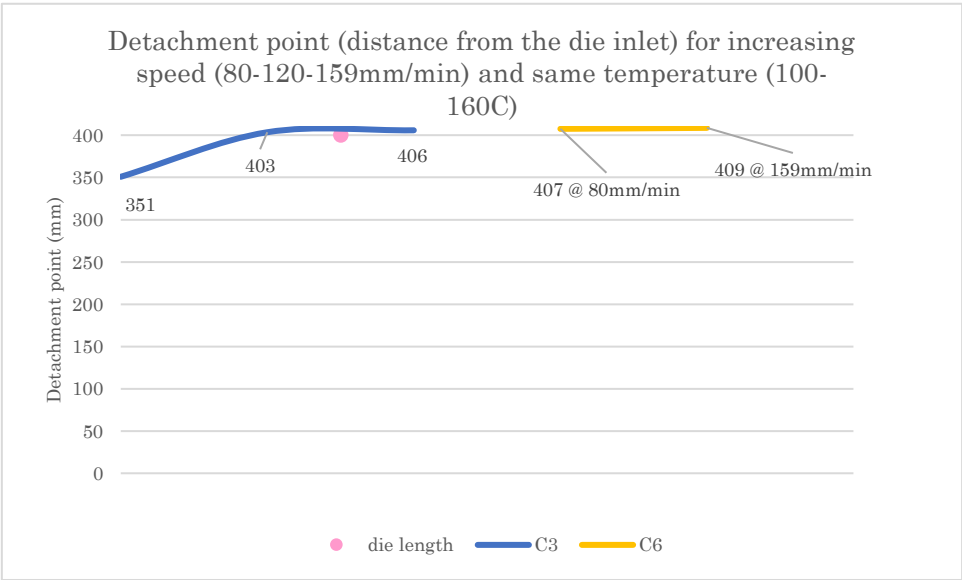

Figure 19: Detachment point for different speeds at the same temperature

The detachment point doesn't exist for different points, therefore no comments can be drawn for increasing speed, as shown in *Figure 19*. The data points without detachment are predicted. Based on these points, it can be noted that the detachment point gets farther from the die entrance, as the pulling speed increases. This could be due to larger gel zone lengths, therefore pushing the detachment points. However, these values may not be accurate and the explanations

may be vague and unreasonable. The predicted gel zone length increases for increasing speed (at constant temperature), as the material is drawn quickly at higher speeds.

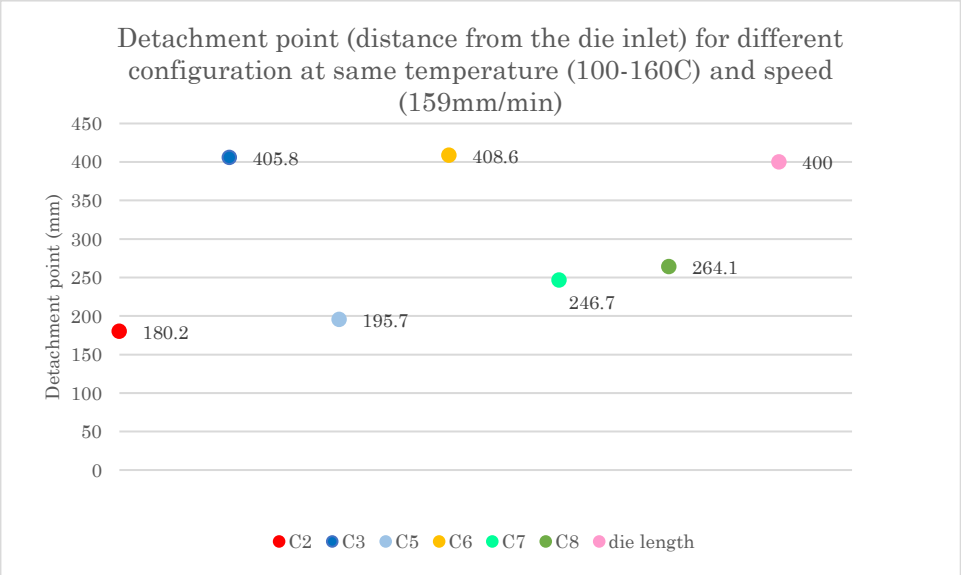

Figure 20: Detachment point for different configurations with the same processing conditions

Figure 20 represents the detachment point for different configurations at 100-160°C and 159mm/min. The detachment point increases with an increase in the fibre rovings, as the time required for the heat to transfer is affected. However, gelation starts at a much later stage for 6R (C2), possibly due to lower inlet temperature as compared to 7R (C5). Similar trends were observed for 8R, where the gelation starts earlier for C8 than C7. This may be due to temperature difference at the inlet since there is no room for movement of rovings within the die. In theory, the gel zone length must be larger as the number of rovings increases, due to the quantity of resin entering the die. This can be verified with experimental observations for similar processing conditions.

Drawbacks of the comparison made with regards to literature study:

The type of resin, the die geometry and the absence of the compaction zone due to tapered die inlet in their experiments [48] do not match our processing conditions. The length of different zones by comparison of PF profile gradient and plateau trend and the reported values in *Table 12* are not appropriate, since the plateaus and trends cannot be clearly distinguished from the minute changes in the PF graphs. A straight type die was used in their research which does not develop a compression zone. Compression zone would vary as it is affected by the pressure used to inject the resin. The position and alignment of the load cell and its sensitivity are a determining factor for the results published in their study. This needs to be verified and it may hinder the observations and therefore the results presented in this study.

4.3. Void content and flexure test results

4.3.1. Image-J analysis

The size of the voids cannot be determined by plain naked eyesight as it may vary from person to person. Smaller spots are sometimes represented as voids and this can be misleading. If the surface is not cleaned well with ethanol or if it's not polished well, then some stains would appear as voids, as they create a shadow-like effect after filters are applied. The void content, flexural modulus and flexural strength are given below.

The void content was determined using image analysis for 8R (C3, C6, C7 and C8). Median and Kuwahara filters were used for the Image-J analysis. The composite was fabricated at 100-160°C for all the results pertaining to Image-J analysis. Three samples were tested at 100-160°C and one sample was tested at 120-180°C using Archimedes principle test, which is denoted in the graph.

Overall average and the SD are denoted as "average value ± SD" for the different processing conditions are represented by blue graphs. The overall average for each process setting is calculated by considering both the Kuwahara and the median filter for all the test runs. Whereas, the void content for individual test runs are represented by median filter values based on Image-J analysis since these values matched better with the Archimedes test results. The number of specimens taken for each sample is shown as green bar graphs.

The graphs below represent the void content for different process settings.

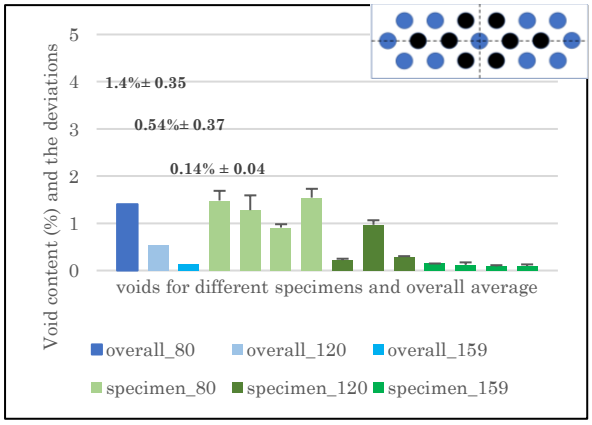

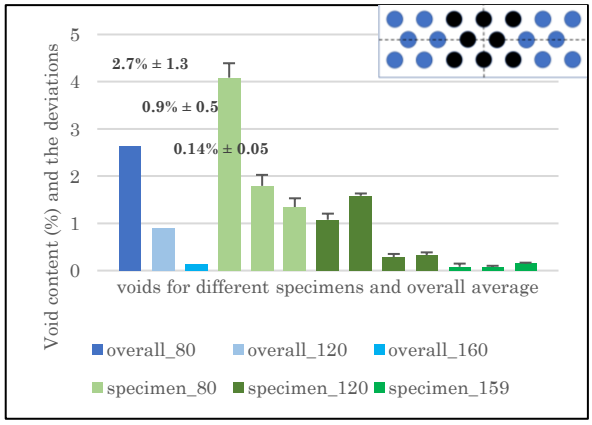

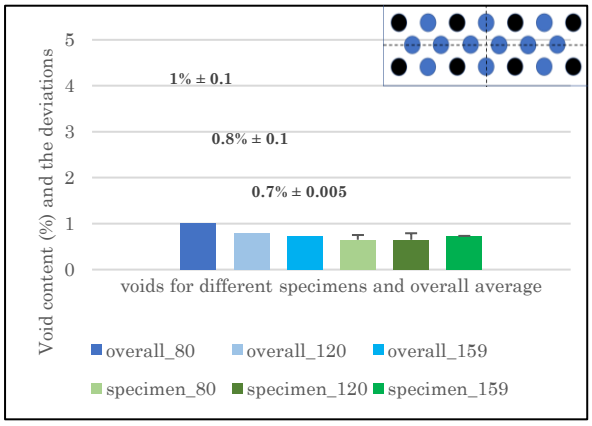

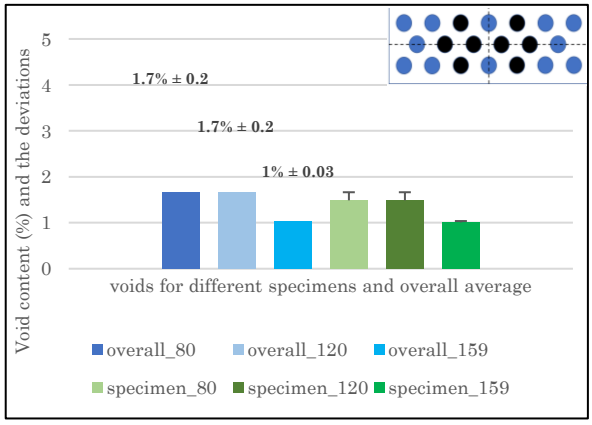

Figure 21: Void content based on Image-J analysis for 100-160℃ with top left (C3), top right (C6), bottom left (C8) and bottom right (C7)

For the Image-J analysis, it can be noted that the overall void content decreased with the increasing PS. Exact values of void content and the processed microscopy images are in *appendix F1.* For instance, to calculate the overall average for C6 – 80 from *appendix F1* , the average of the three specimens are taken, for both median and Kuwahara filter. But, this misinterpretation may cause a higher overall average for void content. Therefore, the readings from these trials could be eliminated.

Repetitive tests for different runs do not produce the same void content results. Possible reasons for not establishing a trend could be the variation of void content for different cross-sections taken from different parts of the composite, threshold limit and bad judgement about the size of voids during image processing, insufficient test runs, temperature variation, spots left due to polishing.

4.3.2. Archimedes test analysis

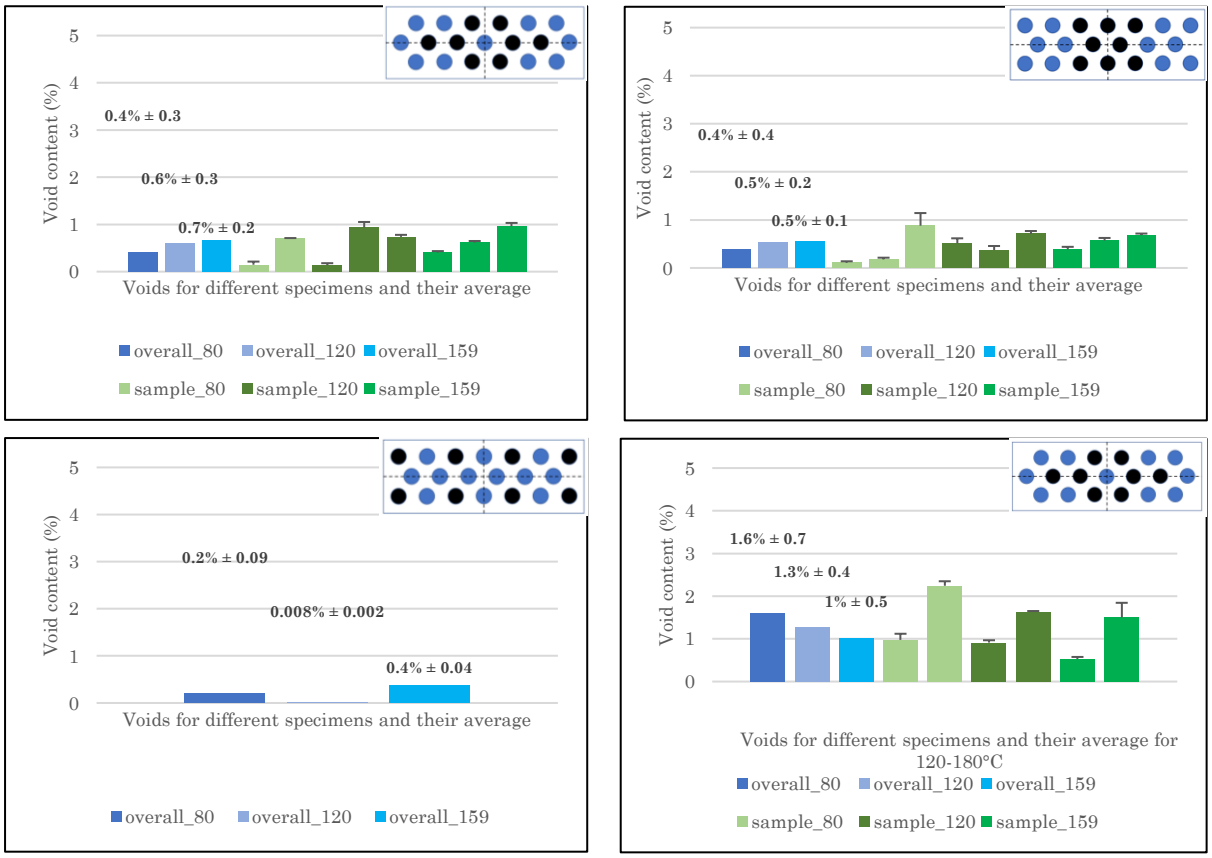

Figure 22: Void content based on Archimedes principle

Three specimens were used per sample set, for the Archimedes principle test. The overall average for each set is the average value of the all the sample sets for each PS, fibre roving configuration and temperature.

The overall void content increases for all the configurations at 100-160°C except for C8. At 120-180°C, the overall void content decreases with the increasing speed. Moreover, no trend can be established between several test runs which are represented by green plots. The void content of C3 > C6 > C8. The void content for C3 at 120-180°C is higher than at 100-160°C for all speeds.

There is no clear agreement between the values found theoretically with Image-J analysis and by Archimedes principle.

4.3.3. Flexure test

The number of tests for each configuration and the details of the test is given in *appendix G1*. The average values (represented as a blue graph) are calculated by using the values obtained for individual sample sets (represented as a green graph). The strength values are plotted on the left side and the modulus is plotted on the right side of the page for the same configurations. The temperature setting for all the configurations is 100-160°C unless otherwise mentioned in the graphs.

The variation of flexural strength and modulus between different configurations and different runs for each configuration is not significantly large. It can be seen that, since the thickness and width don't change much for different configurations, therefore the flexural strength and modulus have nearly the same effect for different configurations. These values may not be perfectly accurate as the values are based on a different number of test runs. Different failure modes were observed during the flexural test. The details of these failure modes are shown in *appendix G2*. In addition to this, the values of thickness and width for the composite are described in *appendix G3*.

.

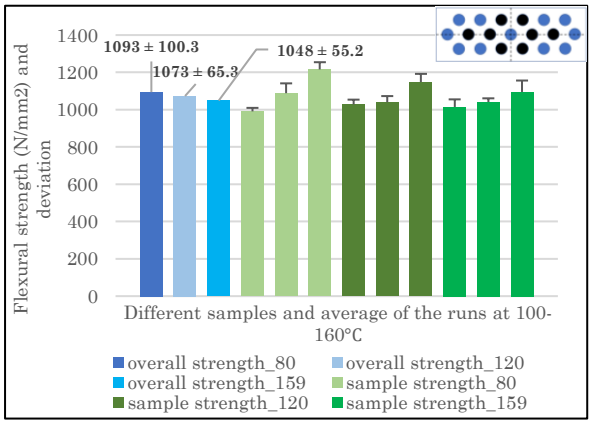

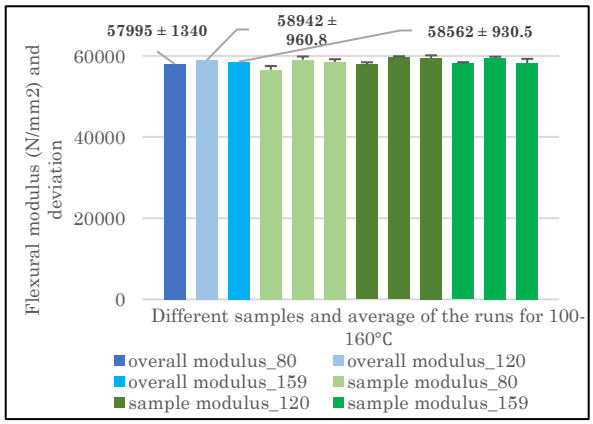

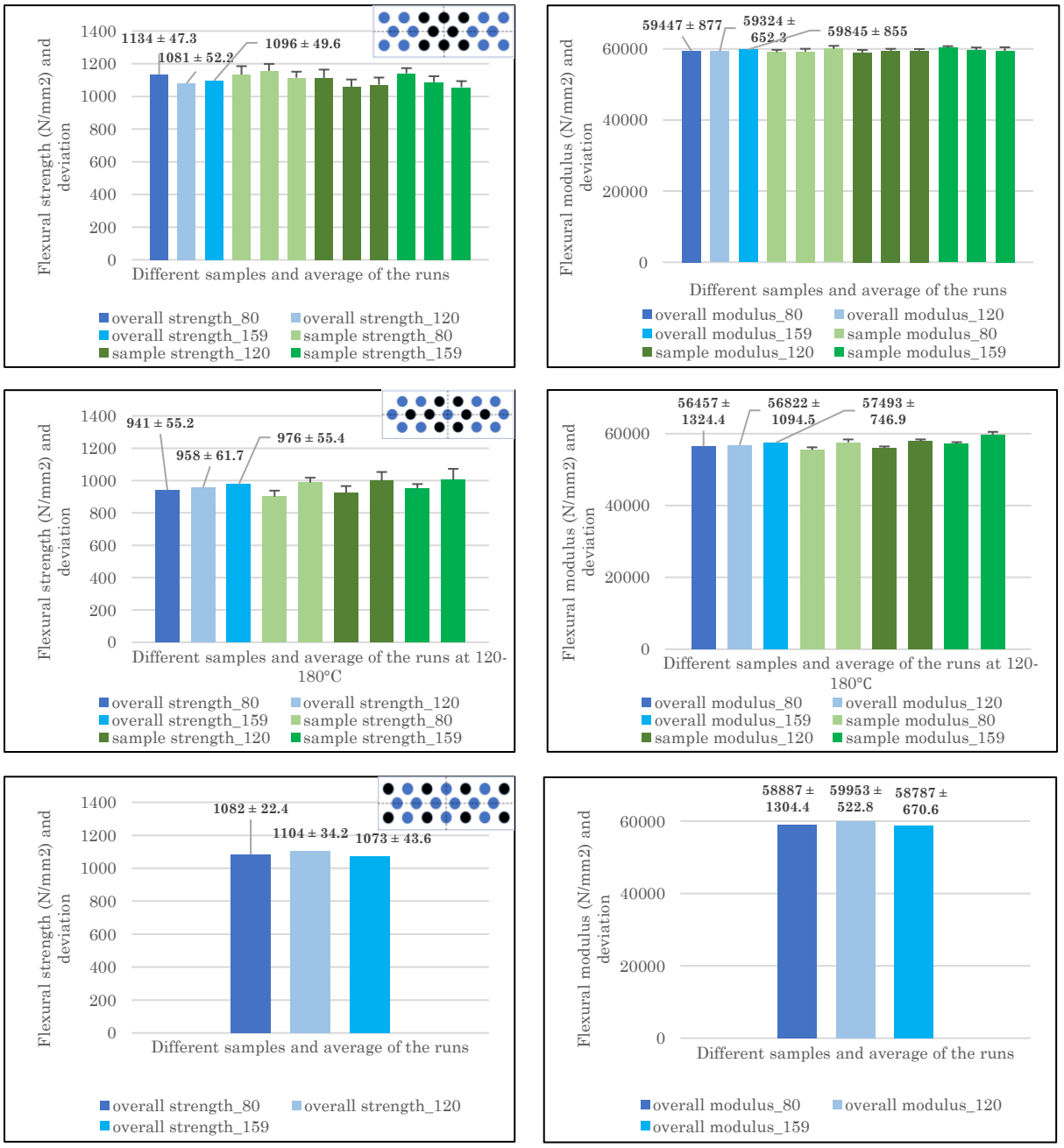

Figure 23: Flexural strength and modulus for different processes

The overall variation of strength and void content and the explanation

In this section, the overall trends corresponding to strength and void content for different configurations are explained.

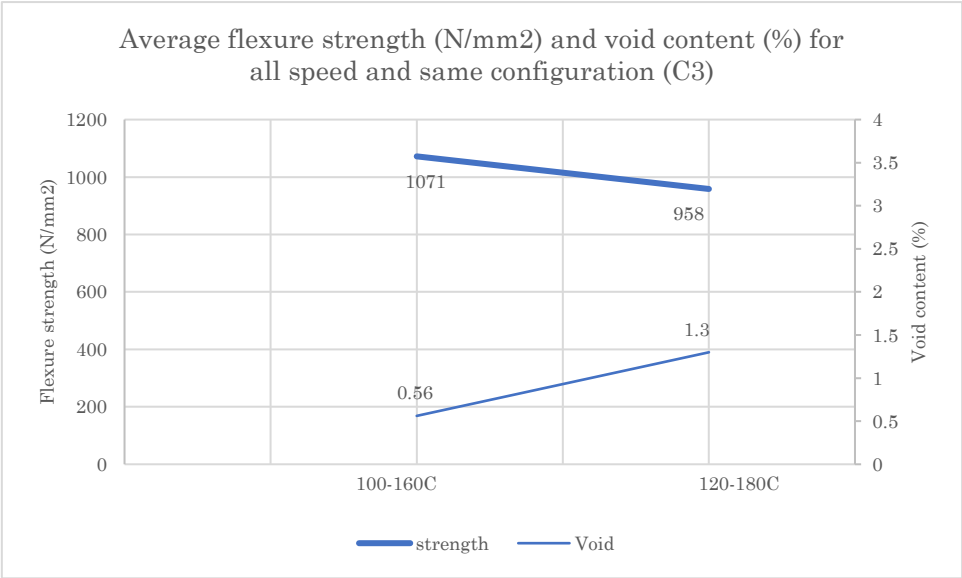

Figure 24: Flexure strength for increasing temperature

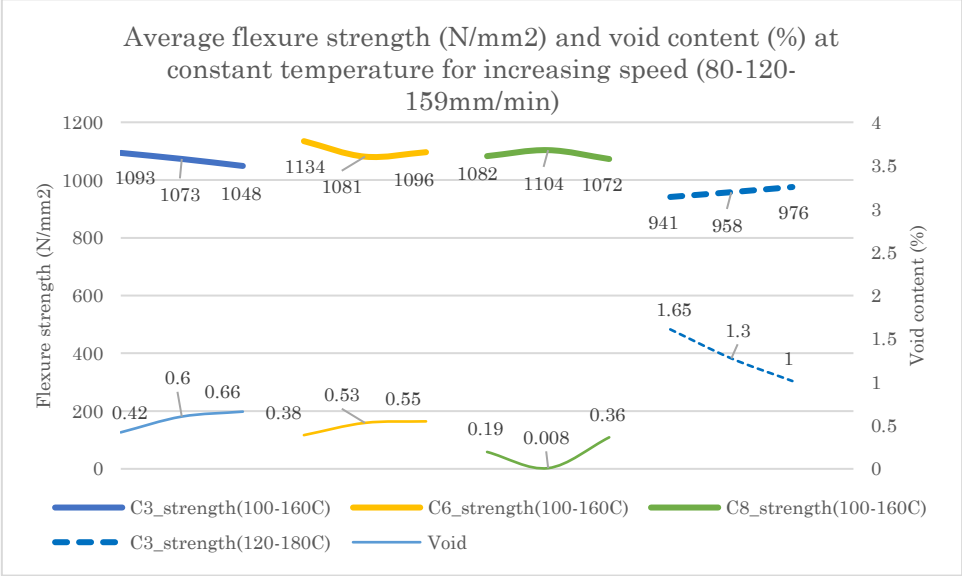

Figure 25: Flexure strength for increasing speed for different configurations

Flexure strength decreases due to an increase in the void content. From *Figure 24*, it can be observed that at lower temperatures, the flexure strength is higher. It is possible that when the temperature is higher, the viscosity drops faster and therefore the resin gets cured quicker. This means that the fibre rovings have lesser time for realignment and may therefore entrap more voids. In theory, if the rovings are pulled slowly (at lower PS) at higher temperature (120-180°C) there isn't enough time for the resin to penetrate and fill the fibre structure. Therefore, the void content is higher. On the other hand, at lower temperature (100-160°C) the void content is lower due to the vice versa effect. For the different fibre configuration, the relationship between the measured flexural strength is not directly proportional to the void content. This variation can be further analysed by having more trials for C8 and therefore the trends cannot be remarked upon. In addition to this the variation of void content for C3 > C6 > C8. However, this maybe due to

differences in the number of test samples or due to the permeability of the configuration, which in turn effects the void content in the sample.

Chapter 5. Conclusion and recommendation

In the pursuit of making wind turbines the most viable option, a major scientific breakthrough would be necessary. Several components of wind turbine blades need to be optimized, one of them being the wind turbine blades. To extract more energy, wind turbines are getting higher and a larger blade span length is desired. To ensure cost reduction, enhance the production capacity and to improve the stability of the tower, a lighter blade with higher strength is preferred. Spar caps are used to improve the stiffness of the blade and the dominant manufacturing technique owing to the current market share is the infusion process. The major drawbacks of this technique are the energy consumption, yield, quality of the product.

Pultrusion provides a better solution, which reduces the problem faced by other manufacturing techniques. Therefore, pultrusion process is researched extensively in the production of spar caps as it provides a high fibre volume content and a homogenous, lightweight end product which benefits the industry. Even though pultrusion is a continuous process, the fabrication process has to be controlled such that a stable and relatively lower pulling force is established. A material with large fibre content doesn't necessarily ensure a high-quality material. The deliverable of this project is to establish a connection between the three aspects – process, structure and property. In the current study, the strength and modulus of the material are considered to be properties. The fabrication process involves constant monitoring and control of the process as it measures the pulling force and the temperature. Void content is estimated using Image-J analysis to check the microstructure and the location of voids. Due to observation errors or polishing problems, the estimated void content may be faulty. Therefore, Archimedes test is implemented to give a clear idea of the void content. Strength and modulus of the material are evaluated by the three-point bending test. A cure degree evolution curve is predicted based on the models studied, to estimate the length of different regions in the die which contributes to the pulling force. Process-structure-property relation is a cycle of continual analysis to optimize the process.

Die jamming occurs as a result of an exponential increase in the PF. During the fabrication process, the pulling speed was increased to stabilize the process. This may occur due to the adhesive bonding force between the die wall and the resin-reinforcement mixture. An increase in the PS may try to break apart the bond formed and therefore may help to stabilize the process. This may be due to additional material entering the die inlet from room temperature (as a result of transport phenomena which occurs due to temperature gradient from the die inlet to the outlet), which will, in turn, reduce the temperature at the die inlet due to heat distribution.
Another method to reduce the exponentially rising PF independently of the previous technique could be re-adjustment of the set temperature value. It could be hypothesised that the die outlet temperature may mostly affect the final degree of cure and may not be able to change the exponential rise in the PF, as this value surpasses the gelation temperature. In addition to this, during the fabrication process, it was observed that the die was jammed mostly in between the die inlet and near the centre of the die. However, this method may not be convenient, as the die is not quite sensitive to the temperature change (due to the time taken to get adjusted to the new temperature settings).
Nevertheless, it is questionable if stability can be achieved, when the PF has already increased exponentially (as compared to stabilised PF). Further investigation must be carried out.

The resin bath contains different components as mentioned in previous sections. An addition of 1% of pigment did not affect the PF significantly. This may be due to the quantity of the pigment used and their chemical compatibility with the resin system used. Nevertheless, these results may not be perfect, due to the changes in the location of the load cell.

The results of the study partially match the conclusions made in the literature. However, these results are reliable due to the differences in the resin system and quantity, temperature differences, shape of the die inlet and the type of die used etc.

The explanations of the results are explained in the respective sub-sections of this study. The following conclusions were drawn from this study,

1. The deductions are made, based on the experimental readings of PF and temperature settings for configuration C3. The overall average pulling force increases with an increase in temperature.
   PF increases with the PS for all the configurations, except for C3 at 120-180°C. The overall average pulling force increases with the number of fibre rovings. The average PF for the different configurations in the increasing order for all speeds and 100-160°C is 196N (C6), 140N (C3), 137N (C8 - only one trial) and 106N (C7 - only one trial). These values may not be accurate, since the fabrication of C7 and C8 was measured with the old load cell arrangement.
2. The flexure strength increased when the void content decreased. Void content is lower for lower temperature (100-160°C) as compared to a higher temperature (120-180°C) for C3. The void content mostly decreases, with the decrease in PS for 100-160°C combination. However, at 120-180°C, the void content increases with a decrease in PS. The void content of the sample varies as C3 > C6 > C8 for 100-160°C at 159mm/min. The dimensions of the composite do not vary significantly for different process settings. This may have occurred due to smaller die dimensions, lesser shrinkage effect. In addition to this, the distance from the die exit and the rollers were also inconsistent during the process, which may have affected the results.
3. Several theories are explored in the literature to study the failure theory in composites. In this study, the different failure modes (for flexure test) experienced by different test conditions are mentioned in the *appendix G2*. A high-quality material intends to have a higher flexural modulus and strength with better product dimensions. For the experiments, the dimensions of 6R and 7R configurations weren't measured. However, the product dimensions are better for higher rovings, due to packing of fibres. To maintain the stability of the process, a lower average PF (implies lower PS) is preferred. On the contrast, to achieve higher productivity or yield (for industrial applications), a higher PS (implies higher PF) is preferred. Therefore, a balance between the PS and PF must be found to cater to both the needs. In addition to this, a material with lower die inlet and exit temperature (has lower PF) is preferred due to reduced void content and higher strength. The configurations used in this study shows that C8 has the least void content (and the second-lowest PF) and C7 has the least PF. Therefore, the optimal combination should be a combination of all the trends that are mentioned.

Recommendation for future work:

1. Resin characterisation must be implemented, to predict the exact cure kinetics model as additives such as pigments are added.
2. The distance between the rollers and the load cell must be fixed and not varied during the experiments, to maintain the repeatability. In addition to this, all the parts must be rigidly fixed to ensure that the vibrations don't affect the PF readings.
3. The peroxide used in the experiments were expired and the functionality of the activating agent is uncertain.
4. The mixing ratio, order of adding and mixing of different components must be maintained and a mechanical mixer can be used to ensure uniform and homogenous mixture. According to the spec sheet [49], the de-gassing agent must be added before adding the other components. During the experiments, these steps were always not followed.

5. The exact values of different physical properties such as density, used in the calculation must be accurate, to obtain accurate results.
6. A relation between the permeability, void content and configuration must be studied extensively to understand the behaviour. Additional tests must be conducted for all configurations to better understand the process.
7. Special attention must be given to the reactivity, curing rate and gel time of the activating agent or hardener (peroxide), even though it is considered inert at room temperatures. [50]
8. More tests must be carried out to ensure repeatability of results and a micro-CT scan could be carried out to improve the void analysis. Different 9R configurations could be tried to check the feasibility and limitations of the set-up.
9. Due to the small variation in PS, a technique must be used to measure the instantaneous speed. The distance of thermocouples placed inside the die must have uniform sensitivity and must be placed at the same length to maintain accuracy. Thermocouples can be sent into the pultrusion die with the resin-impregnated fibres, to measure the instantaneous values of temperature.
10. Cleaning of the metal shims must be carried out carefully, as the scratches may result in fibres getting stuck and may also cause small ridges on the surface of the workpiece.
11. The thermocouples which heat the die could be placed on both the sides of the die, to ensure uniform distribution of temperature. But this is recommendation, may not be accurate and therefore, a heat analysis model must be used to extensively simulate the heat transfer for the current set-up.
12. Load calibration must be made before the trails. The type of rollers used for the experiments may be changed according to convenience and to provide better tension on the composite.
13. All ten thermocouples which measure the temperature must be in working condition and calibrated. TGA test could be carried out, to calculate the exact value of void content for each sample, since the material decomposition temperature was unknown for the burn-out test.
14. The drawbacks seen in Capita Selecta courses are overcome in the experiments carried out for this study. The used resin that is squeezed out of the die is not mixed with the old resin, due to gelling. This step must be continued for further analysis to maintain a better quality product.
15. Analysis can be carried out for larger parts and an industrial scale pultrusion line, to compare if the results obtained from this study are predictable and practical and if they are in-line with the industrial standards.
16. A colouring agent may be used to replace the pigment which embedding the microscopy samples, to avoid interference with the material properties.

References

[1] M. Richardson, "Blowing in the wind," *Composites in Manufacturing*. https://www.composites.media/blowing-in-the-wind/.

[2] "Key Takeaways From David Attenborough's New Film, 'A Life on Our Planet' | Earth.Org - Past | Present | Future." https://earth.org/david-attenborough-new-film-a-life-on-our-planet/ (accessed Dec. 10, 2020).

[3] "Comprehensive historical review and current market trends in renewable energy," *IEA*. https://www.iea.org/reports/renewables-information-overview.

[4] "Renewables, including solar, wind, hydro, biofuels and others, are at the centre of the transition to a less carbon-intensive and more sustainable energy system.," *IEA*, 2020. https://www.iea.org/fuels-and-technologies/renewables.

[5] H. Ritchie and R. Max, "Energy." https://ourworldindata.org/energy.

[6] H. Ritchie and M. Roser, "Renewable Energy," *IEA*, 2020. https://ourworldindata.org/renewable-energy.

[7] H. Ritchie and M. Roser, "Renewable Energy," 2020. https://ourworldindata.org/renewable-energy#:~:text=In.

[8] "Renewable energy market update Outlook for 2020 and 2021," *IEA*, 2020. https://www.iea.org/reports/renewable-energy-market-update/technology-summaries#abstract.

[9] "Spar Cap and Shear Web Bonding Inspection Solution for Wind Turbine Blades." https://www.olympus-ims.com/es/applications/shear-web-bonding-inspection/.

[10] "Improved Inspection of Composite Wind Turbine Blades with Accessible, Advanced Ultrasonic Phased Array Technology," 2018. https://www.slideshare.net/OlympusIMS/improved-inspection-of-composite-wind-turbine-blades-with-accessible-advanced-ultrasonic-phased-array-technology.

[11] T. T. Thomas, M. M. Narkhede, B. S. Patil, and A. Mogra, "Analysis of Wind Turbine Blade Having i Shaped Spar Using Both Epoxy Fiber and Carbon Fiber Using FEM," *Mater. Today Proc.*, vol. 4, no. 2, pp. 2573–2579, 2017, doi: 10.1016/j.matpr.2017.02.111.

[12] "MANUFACTURING PART CONSULTING." https://partconsulting.com/manufacturing-part-consulting/.

[13] A. S. Ganapathi, S. C. Joshi, and Z. Chen, "Experimental and numerical investigation of process-induced deformations of glass/epoxy wind turbine blade spar cap," *J. Compos. Mater.*, vol. 51, no. 27, pp. 3791–3806, 2017, doi: 10.1177/0021998317693909.

[14] W. P. Limited, "Manufacturing of fibre–polymer composite materials," *Introd. to Aerosp. Mater.*, pp. 303–337, 2012, doi: 10.1533/9780857095152.303.

[15] K. Balasubramanian, M. T. H. Sultan, and N. Rajeswari, *Manufacturing techniques of composites for aerospace applications*. Elsevier Ltd, 2018.

[16] European Pultrusion Technology Association, "World Pultrusion Conference 2018," 2018.

[17] J. Sellier, "The Growth of Carbon Fibre in the Wind Energy Sector," no. October, 2018.

[18] U. D. Prepreg and S. Solution, "SparPreg ™."

[19] S. Li, L. Xu, Z. Ding, L. J. Lee, and H. Engelen, "Experimental and theoretical analysis of pulling force in pultrusion and resin injection pultrusion (RIP) - Part I: Experimental," *J.*

Compos. Mater., vol. 37, no. 2, pp. 163–189, 2003, doi: 10.1106/002199803028676.

[20] S. Li, L. Xu, Z. Ding, L. J. Lee, and H. Engelen, "Experimental and theoretical analysis of pulling force in pultrusion and resin injection pultrusion (RIP) - Part II: Modeling and simulation," *J. Compos. Mater.*, 2003, doi: 10.1177/0021998303037003675.

[21] R. Gorthala, J. A. Roux, J. G. Vaughan, and R. P. Donti, "Comparison of processing parameters for pultruded graphite/epoxy and fiberglass/epoxy: a heat transfer and curing model," *J. Reinf. Plast. Compos.*, vol. 13, no. 4, pp. 288–300, 1994, doi: 10.1177/073168449401300401.

[22] R. Gorthala, J. A. Roux, and J. G. Vaughan, "Resin Flow, Cure and Heat Transfer Analysis for Pultrusion Process," *J. Compos. Mater.*, vol. 28, no. 6, pp. 486–506, 1994, doi: 10.1177/002199839402800601.

[23] S. M. Moschiar, M. M. Reboredo, J. M. Kenny, and A. Vázquez, "Analysis of pultrusion processing of composites of unsaturated polyester resin with glass fibers," *Polym. Compos.*, vol. 17, no. 3, pp. 478–485, 1996, doi: 10.1002/pc.10636.

[24] S. M. Moschiar, M. M. Reboredo, H. Larrondo, and A. Vazquez, "Pultrusion of epoxy matrix composites: Pulling force model and thermal stress analysis," *Polym. Compos.*, vol. 17, no. 6, pp. 850–858, 1996, doi: 10.1002/pc.10678.

[25] D. Srinivasagupta, J. L. Kardos, and B. Joseph, "Analysis of pull-force in injected pultrusion," *J. Adv. Mater.*, vol. 38, no. 1, pp. 39–46, 2006.

[26] D. Srinivasagupta, S. Potaraju, J. L. Kardos, and B. Joseph, "Steady state and dynamic analysis of a bench-scale injected pultrusion process," *Compos. Part A Appl. Sci. Manuf.*, vol. 34, no. 9, pp. 835–846, 2003, doi: 10.1016/S1359-835X(03)00182-9.

[27] I. Baran, P. Carlone, J. H. Hattel, G. S. Palazzo, and R. Akkerman, "The effect of product size on the pulling force in pultrusion," *Key Eng. Mater.*, vol. 611–612, pp. 1763–1770, 2014, doi: 10.4028/www.scientific.net/KEM.611-612.1763.

[28] P. Carlone, I. Baran, J. H. Hattel, and G. S. Palazzo, "Computational approaches for modeling the multiphysics in pultrusion process," *Adv. Mech. Eng.*, vol. 2013, 2013, doi: 10.1155/2013/301875.

[29] L. Xu, "INTEGRATED ANALYSIS OF LIQUID COMPOSITE MOLDING (LCM) PROCESSES," The Ohio State University, 2004.

[30] H. L. Price and S. G. Cupschalk, "Pulling Force and Its Variation in Composite Materials Pultrusion.," *Adv. Chem. Ser.*, pp. 301–322, 1984, doi: 10.1021/ba-1984-0206.ch018.

[31] W. I. L. Dae-Hwan Kim, Poong-Gyu Han, Geun-Ha Jin, "kim1997.pdf," *J. Compos. Mater.*, vol. 31, no. 20, pp. 2105–2122, doi: https://doi.org/10.1177/002199839703102005.

[32] R. Menezes Bezerra, "Modelling and Simulation of the Closed Injection Pultrusion Process," p. 151, 2017, [Online]. Available: https://publikationen.bibliothek.kit.edu/1000079057.

[33] P. Carlone and G. S. Palazzo, "Computational modeling of the pulling force in a conventional pultrusion process," *Adv. Mater. Res.*, vol. 772, pp. 399–406, 2013, doi: 10.4028/www.scientific.net/AMR.772.399.

[34] I. Baran, I. Straumit, O. Shishkina, and S. V. Lomov, "X-ray computed tomography characterization of manufacturing induced defects in a glass/polyester pultruded profile," *Compos. Struct.*, vol. 195, no. December 2017, pp. 74–82, 2018, doi: 10.1016/j.compstruct.2018.04.030.

[35] M. S. Irfan *et al.*, "A modified pultrusion process," *J. Compos. Mater.*, vol. 51, no. 13, pp. 1925–1941, 2017, doi: 10.1177/0021998316666653.

[36] M. A. Suhot and A. R. Chambers, “The effects of voids on the flexural properties and failure mechanisms of carbon/epoxy composites,” *J. Teknol.*, vol. 71, no. 2, pp. 151–157, 2014, doi: 10.11113/jt.v71.3736.

[37] M. Mehdikhani, L. Gorbatikh, I. Verpoest, and S. V. Lomov, “Voids in fiber-reinforced polymer composites: A review on their formation, characteristics, and effects on mechanical performance,” *J. Compos. Mater.*, vol. 53, no. 12, pp. 1579–1669, 2019, doi: 10.1177/0021998318772152.

[38] B. Jackson, “SENVOL GRANTED $100K TO EASE ADDITIVE MANUFACTURING MATERIALS CHARACTERIZATION,” *Kunststoff Technik Leoben*. https://3dprintingindustry.com/news/senvol-granted-100k-to-ease-additive-manufacturing-materials-characterization-138758/.

[39] Tencom Ltd, “Deciding Between Pultruded Fiberglass and Pultruded Carbon Fiber.” https://www.tencom.com/blog/pultruded-carbon-fiber-vs-fiberglass.

[40] Fibremax Ltd, “ARAMID FIBER CHARACTERISTICS.” http://www.aramid.eu/characteristics.html.

[41] “What’s the Difference Between Kevlar® and Carbon Fiber?” https://markforged.com/resources/blog/kevlar-vs-carbon-fiber.

[42] A. International, “D 7264/D 7264M – 07,” vol. i, pp. 1–11, 2007.

[43] Iso 14125, “Fibre-reinforced plastic composites — Determination of flexural properties,” *Order A J. Theory Ordered Sets Its Appl.*, vol. 1998, no. July 2002, p. 24, 1998, [Online]. Available: https://books.google.com/books?id=JZBNMwEACAAJ&pgis=1.

[44] ASTM International, “Standard Test Methods for Density of Compacted or Sintered Powder Metallurgy (PM) Products Using Archimedes’ Principle,” *Astm B962-13*, vol. i, pp. 1–7, 2013, doi: 10.1520/B0962-17.2.

[45] S. Struck, “Density of ethanol.” https://sciencestruck.com/density-of-ethanol.

[46] S. K. Dey and M. Xanthos, “Glass Fibers,” *Funct. Fill. Plast.*, vol. 21, no. Ref 19, pp. 141–162, 2010, doi: 10.1002/9783527629848.ch7.

[47] Y. Nasonov, A. Safonov, S. Gusev, and I. Akhatov, “Effect of additives on cure kinetics of pultrusion resins,” *Procedia Manuf.*, vol. 47, no. 2019, pp. 920–924, 2020, doi: 10.1016/j.promfg.2020.04.283.

[48] F. Tucci, V. Esperto, F. Rubino, and P. Carlone, “Experimental measurement of the resistant load in injection pultrusion processes,” *Procedia Manuf.*, vol. 47, no. 2019, pp. 148–153, 2020, doi: 10.1016/j.promfg.2020.04.157.

[49] BYK additives and instruments, “BYK-A555 datasheet,” no. 10, 2016, [Online]. Available: https://www.byk.com/en/products/additives-by-name/byk-a-555.

[50] P. D. Sheet, “Trigonox K-90.” https://www.brenntag.com/media/documents/bsi/product_data_sheets/material_science/akzo_nobel_initiators/trigonox_k-90_pds.pdf.

Appendix

A1. Methods used for research

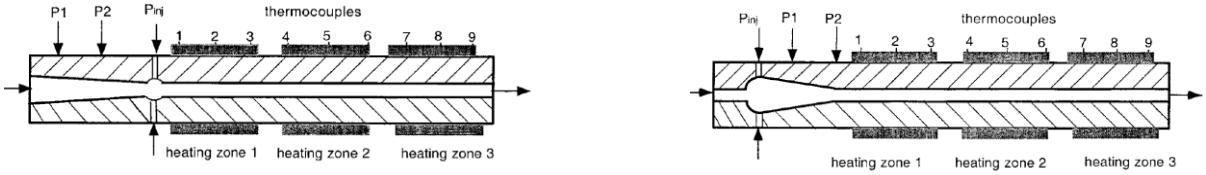

Figure 26: HP die (left) and LP die (right)

Two methods used for the research are given below,

- Mat tracer method – An additional piece of the mat was inserted into the die to measure the PF for different regions. The size of the mat was varied in length and breadth.
  Mats with different dimensions are used for LP and HP die and the mat size for the LP die and the conventional die are the same when the experiments were conducted for the same speed. The length of the conventional die is smaller.
- Short die length method – effect of die length on the PF are noted for 3 different die dimensions - 1.02, 0.686 and 0.457 m. The experiments were performed for the same pulling speed and fibre sheet or mat lay-up. The lay-up was different compared to that used in the mat-tracer method.

A2. Pultrusion line

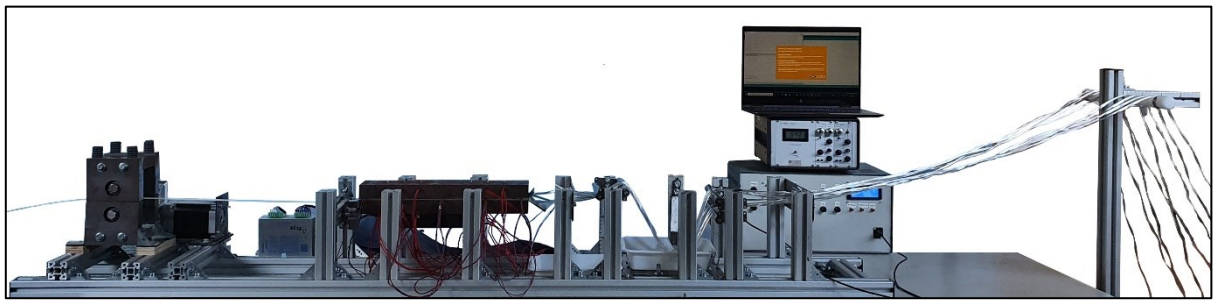

Figure 27: Pultrusion line used for fabrication

B1. Volume fraction calculation:

To calculate the volume fraction of the fibre, it is necessary to know the number of rovings, density of the glass fibre and the resin, cross sectional area and length of the sample, TEX number of the fibre rovings. For this illustration, a sample of 8 rovings were assumed.

Weight of each roving = TEX number * length of the sample
= 0.048 * 60 = 2.88 g

The density of the glass fibres and the density of resin were learnt as is 2.62 g/cm^3 and 1.06 g/cm^3
Volume of the sample = cross sectional area of the sample * length of the sample
= 2 * 10 * 600 = 12 cm^3

For 6 rovings, volume of the fibre is given by,
= mass of 8 fibre rovings / density of glass fibre
= (2.88 * 8) / 2.62
= 8.794 cm^3

Therefore, the fibre volume fraction = volume of the fibre / volume of the sample
= 8.794 / 12
= 73.28 %

Similarly, the FVF for 6,7 and 9 rovings are 54.96%, 64.12 % and 82.44%.

B2. To calculate the maximum number of rovings that can be used for the given profile:

The cross-sectional profile is 2mm x 10mm (Area). The linear density of the fibres used is 4800 TEX.

To theoretically calculate the volume fraction of fibres, we need to know: volume of the fibres in a given volume, the nominal volume of the composite. Assume that the length of the glass fibres taken is 1m.

B2.1. The volume of fibres are calculated as shown below:

Total weight of fibres in 1m (W) is given by,

$$W = N \,.\, Tex\ number \,.\, l \tag{12}$$

Where,
N = *number of rovings*
$Tex\ number$ = *weight of the fibres per unit length* = $4.8\ g/m$
l = *length of the fibres* = $1m$

Therefore, W = (4.8N) g

The total volume of the fibres (V_f) in 1m,

$$V_f = \frac{W}{\rho_f} \tag{13}$$

Where,
ρ_f = *density of fibres* = $2.62\ g/cm^3$
Substituting the values we get, V_f = (1.832N) cm^3

B2.2. The volume of the composite can be found as shown below:

$$V = Area \,.\, L \tag{14}$$

Plugging the above values we find V = 20 cm^3

B2.3. Fibre volume fraction (FVF) is given as,

$$FVF = \frac{V_f}{V} \tag{15}$$

To find the maximum number of rovings that can theoretically be used can be found such that the resin volume fraction > 0 .
Volume fraction of resin = $1 - FVF = 1 - \frac{1.832N}{20} > 0$
Therefore, a maximum of N = 10 rovings can be used for this set-up in theory.

C1. Burn out test

To experimentally verify the results of void content, it is necessary to find out the exact ratio of weight between fibres and resin. The difference in weights for the specimens corresponding to the same sample occurs due to uneven surfaces, irregularities and defects arising due to different cutting techniques and changes in process settings over some time. These anomalies are noted and used as a replacement in the empirical formula (fixed value of %weight fraction of resin and fibre, for all the experiments) used in the calculation of theoretical density. They provide a more apparent and accurate result. The procedure for the test is briefly explained,

The composite specimen is placed inside a non-reactive, heat resistant container and weighed. This is placed inside a furnace which is set to ~600°C. The specimen is burnt so that only the fibres remain in the container. The weight is then measured. The difference in weights would provide the actual weight of the resin. Therefore, the actual weight fraction for resin and fibre can be calculated.

The furnace was kept at the set temperature for nearly 4 hours, but the samples did not undergo burning. Due to instructions from the lab technicians, the samples couldn't be kept overnight. The furnace temperature was increased to around 900°C, but the samples didn't burn. The samples shrink in size, but wherein a solidified state. Efforts were made to find the decomposition/degradation temperature of 4800 TEX E-glass fibres but to no avail. Due to insufficient time, the samples couldn't be examined further by thermogravimetric analysis (TGA) experiments, to find a suitable temperature for the experiments.

The experiments were not reliable and therefore, the results were not used for the calculation.

D1. Average pulling force and temperature values for different runs for 6R

The graphs below depict the average force and SD values separately for pigment and no-pigment case. The blue, orange or yellow and the green line represents the PF for 80, 120 and 159mm/min. The dotted line is one trial (represents the resin mixture + pigment) and the continuous line is another trial (without pigment).

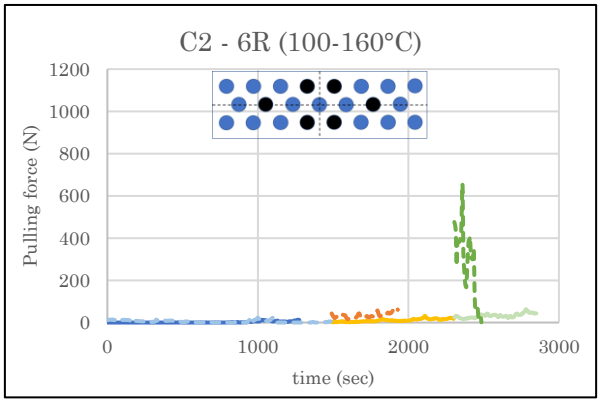

Figure 28: Average pulling force and SD for each run (6R)

		Average inlet and outlet operating temperature (°C)		
Configuration	Run	80 mm/min	120 mm/min	159 mm/min
C2(old resin + no pigment)	1	94.3 – 160.2	93.7 – 160.3	91.9 – 160.1
C2 (new resin + pigment)	1	99 – 154.6	99.9 – 156.4	100.8 – 156.3

Table 7: Average inlet and outlet temperatures for 6R

D2. Average pulling force and temperature values for different runs for 7R

The average temperature measured for each run is tabulated below. The PF for all configurations with 7R, for each run, is shown in the figure. Blue, yellow and green line represents the PF for 80, 120 and 159 mm/min. For C1, light blue, orange and dark green line corresponds to PF value for the trial which was conducted together.

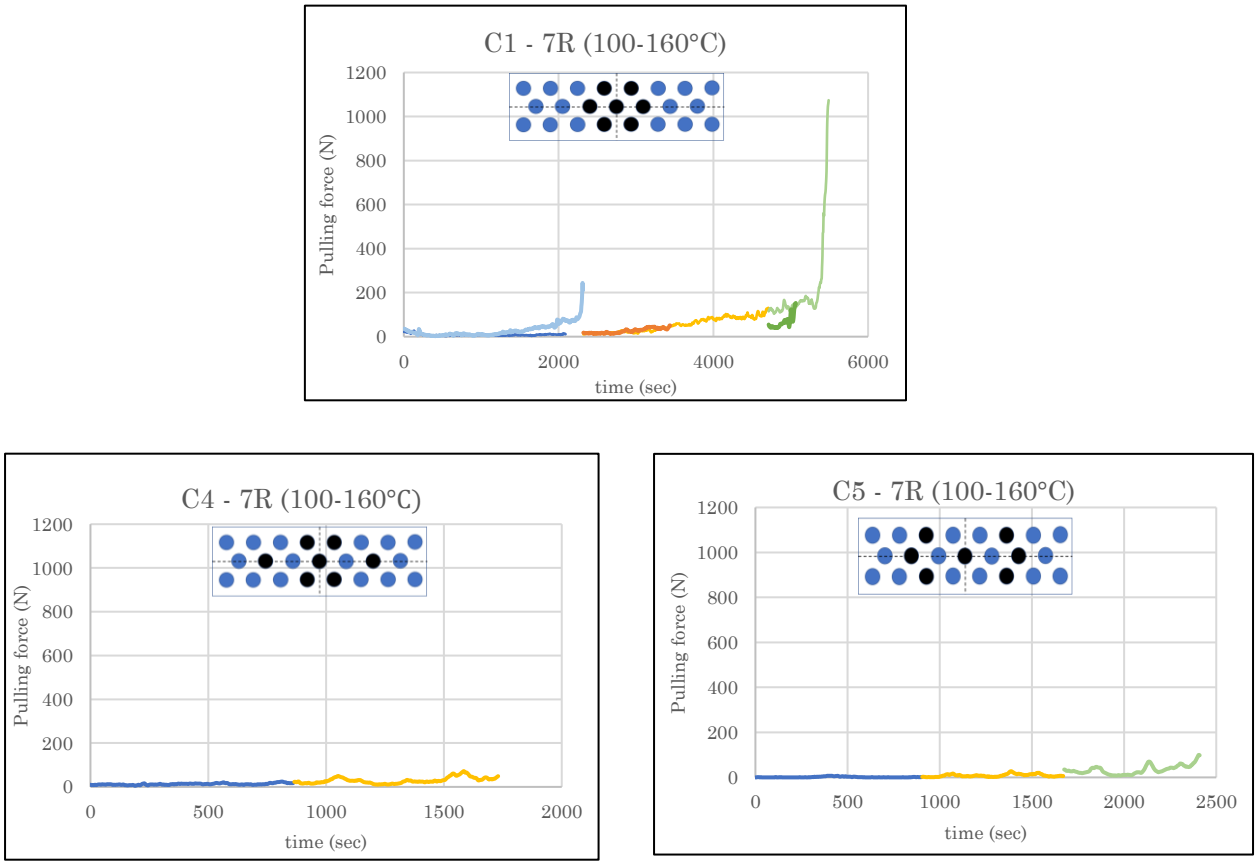

Figure 29: Overall average pulling force and SD for all the runs (7R)

		Average inlet and outlet operating temperature (°C)		
Configuration	Run	80 mm/min	120 mm/min	159 mm/min
C1(old resin + no pigment)	1	95.5 – 153.9	94.4 – 155.1	97.4 – 159.6
	2	95.4 – 157.8	93.9 – 158.2	93.2 – 157.8
C5 (new resin + pigment)	1	101.2 – 155.7	100.5 – 155.7	98.9 – 155.7
C4 (new resin + pigment)	1	98.6 – 153.6	94 – 153.8	–

Table 8: Average inlet and outlet temperature for 7R

D3. Average pulling force and temperature values for different runs for 8R

PF and the average temperatures for different trials are explained below.

D3.1. Configuration C3

Same colours are used for trials that are conducted together. A black dotted line is used to separate the PF for 80, 120 and 159 mm/min. Purple and green dotted lines represent the PF for 120-180°C. The colour code for other lines is seen in the tabulation below.

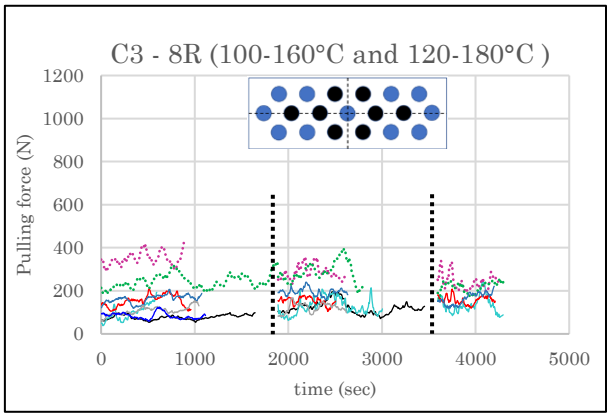

Figure 30: Average pulling force and SD for each run (8R -C3)

		Average inlet and outlet operating temperature (°C)		
Configuration	Run	80 mm/min	120 mm/min	159 mm/min
C3(old resin + no pigment)	1 (black)	100.57 – 156.3	100.8 – 159.8	–
C3 (new resin + pigment) + re-alignment of load cell + (100-160°C)	1 (red)	99.5 – 154.9	97.9 – 155	95.6 – 155.1
	2 (orange)	109.8 – 159.2	107.5 – 159.4	105.4 – 159.3
	3 (cyan)	105.2 – 157.4	105.3 – 159.6	104.2 – 159.5
	4 (brown)	106.8 – 157.7	106.4 – 159.2	–
	5 (yellow)	107.9 – 159.4	–	–
C3 (new resin + pigment) + re-alignment of load cell + (120-180°C)	1 (purple)	119.9 – 176.9	118.7 – 177	116.1 – 177
	2 (green)	116.1 – 175.9	114.7 – 117.5	112.4 – 178.2

Table 9: Average inlet and outlet temperatures for 8R (C3)

D3.2 Configuration C6

The temperatures for the different tests are noted in the table below. A black dotted line separates the PF reading for different PS. The other lines corresponding to a similar test run is marked with the same colour. The colour codes for different test runs are shown in the table below. The speed reduction trial is denoted by red colour in the table. The arrow marks represent the steps used in the process and their corresponding average temperatures.

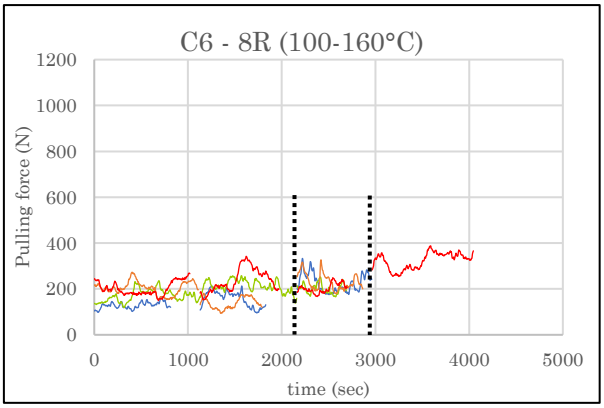

Figure 31: Average pulling force and SD for each run (8R -C6)

		Average inlet and outlet operating temperature (°C)		
Configuration	Run	80 mm/min	120 mm/min	159 mm/min
C6(new resin + pigment)	1 (blue)	99.6 – 155.1	97 – 155.3	94.7 – 155.3
	2 (green)	98.2 – 157.1	96.9 – 157	95.5 – 157.1
C6 (new resin + pigment) + re-alignment of load cell	1 (orange)	108.4 – 152.2	104.4 – 148.9	99.8 – 147.2
	2 (red) (pink and red)	108.6 – 158.1 →	107.2 – 158 →	105.2 – 158.1
		107.8 – 158.1 ←	105.6 – 158.1 (?) ←	

Table 10: Average inlet and outlet temperatures for 8R (C6)

D3.3. Configuration C7 and C8

The average and SD values for different runs are as shown below. Blue, green and orange lines represent the PF for different line speeds.

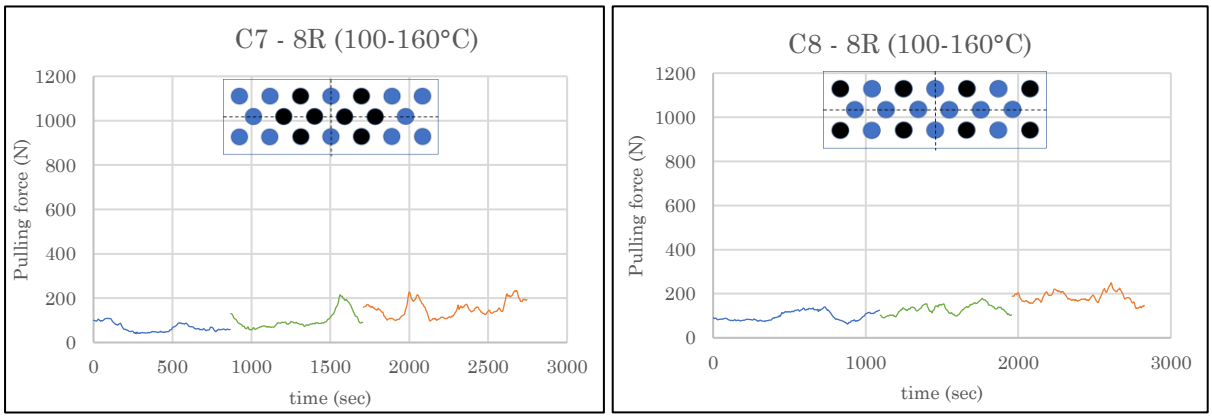

Figure 32: Average pulling force and SD for each run (8R - C7 and C8)

		Average inlet and outlet operating temperature (°C)		
Configuration	Run	80 mm/min	120 mm/min	159 mm/min
C7(new resin + pigment)	1	99.1 – 157.2	96.4 – 157.1	94.4 – 157
C8 (new resin + pigment)	1	98.7 – 155.4	97.2 – 155.6	98.6 – 155.5

Table 11: Average inlet and outlet temperatures for 8R (C7 and C8)

E1. Predicted zone length based on a study

Configuration	Run	Type	Regions or zones of the die (mm)			
			Compression zone	Viscous drag	Gel point	Detachment
C2 (6R)	1 (159 mm/min)	old resin + no pigment	0 – 29	29 – 164	164 – 180	180
C5 (7R)	1 (159 mm/min)	new resin + pigment	0 – 58	58 – 134	134 – 195	195
C3 (8R)	2 (120-180°C @ 159 mm/min) – red and maroon dotted line	new resin + pigment + load cell adjustment	0 – 70	(?)	(?)	(?)
			0 – 51	(?)	(?)	396
	2 (100-160°C @ 159 mm/min) – yellow and pink		0 – 38	(?)	(?)	(?)
			0 – 54	(?)	(?)	389
	1 (100-160°C @ 120 mm/min) – light blue		0 – 23	(?)	(?)	381
	1 (100-160°C @ 80 mm/min) – dark blue		0 – 20	(?)	(?)	340
C6 (8R)	2 – light and dark green	new resin + pigment	0 – 97	97 – 265	265 – (?)	(?)
			(?)	(?) – 275	275 – (?)	(?)
	1 (80 mm/min) - cyan	new resin + pigment + load cell adjustment	0 – 70	70 – 354	354 – (?)	(?)
C7 and C8 (8R)	1 (159 mm/min)	new resin + pigment	0 – 17	17 – 154	154 – 246	246
			0 – 19	19 – 202	202 – 264	264

Table 12: Prediction of zone lengths based on different LFF tests

The different zones are predicted by comparing the PF curves and the plateau's in the graph. The question marks in *Table 12* mean that the values couldn't be predicted due to discrepancies in the graph's peaks (high's and low's).

1. Compression zone prediction:

Based on the research [48], the compression region is predicted not until the material crosses the straight section of the die. It must be noted that the cross-section of the composite is circular and there is no tapered region in the die. A resin injection die is used with a polyester resin system. Therefore, the initial comparisons with respect to the experiments carried out in this research made may not be accurate and comply with the actual behaviour of the resin used, since the

underlying mechanisms are different. The prediction of compression zone is made such that the forces after that point drops from a higher value. This assumption is made based on a paper [48].

2. Gel zone and viscous drag region prediction:

According to [48], when the PF nearly drops to zero, the degree of cure starts increasing. This is represented by the second gradient drop in the graph. Therefore, after this point, the gelation starts and it can be considered as a gel point. This value cannot be easily identified from the graphs obtained for the experiments conducted in this study, due to several slopes in the graph. The prediction of these values is shown in *Table 12*. Viscous drag is taken as a value in between the two zones.

F1. Void content process setting using image analysis

The values of filters used for analysing the images are tabulated below.

Configuration and speed in mm/min for each specimen	median filter (threshold)	Void area fraction	Kuwahara filter sampling width (threshold)	Void area fraction
C7 – 80	17mp (105)	1.488%	35 (98)	1.84%
C7 – 120	17mp (100)	0.527%	35 (97)	0.752%
C7 – 160	23mp (86)	1.008%	35 (58)	1.066%
C8 – 80	15mp (111)	0.908%	21 (107)	1.115%
C8 – 120	15mp (87)	0.649%	21 (72)	0.932%
C8 – 160	15mp (72)	0.728%	35 (64)	0.738%
C6 – 80	23mp (117)	4.086%	35 (91)	4.696%
C6 – 80	23mp (93)	1.794%	35 (87)	2.259%
C6 – 80	23mp (57)	1.346%	35 (92)	1.715%
C6 – 120	23mp (96)	1.077%	35 (87)	1.335%
C6 – 120	23mp (126)	1.583%	35 (94)	1.683%
C6 – 120	23mp (95)	0.282%	35 (88)	0.422 %
C6 – 120	23mp (106)	0.322%	35 (87)	0.449%
C6 – 160	23mp (85)	0.08%	35 (55)	0.216%
C6 – 160	23mp (104)	0.075%	35 (74)	0.128%
C6 – 160	23mp (112)	0.154%	35 (63)	0.181%
C3 – 80	23mp (85)	1.483 %	35 (66)	1.894%
C3 – 80	23mp (89)	1.278%	35 (106)	1.906%
C3 – 80	23mp (104)	0.91%	35 (87)	1.052%
C3 – 80	23mp (750	1.17%	35 (58)	1.544%
C3 – 120	23mp (129)	0.218%	35 (73)	0.282%
C3 – 120	23mp (99)	0.969%	35 (72)	1.161 %
C3 – 120	23mp (106)	0.29%	35 (61)	0.319%
C3 – 160	23mp (99)	0.148%	35 (47)	0.15%
C3 – 160	23mp (98)	0.119%	35 (90)	0.227%
C3 – 160	23mp (137)	0.087%	35 (120)	0.139%
C3 – 160	23mp (90)	0.098%	35 (75)	0.162%

Table 13: Void content using Image-J analysis for micrographs

A sample photo of the microscopic image processing is shown below. A similar filtering process is done for all the samples.

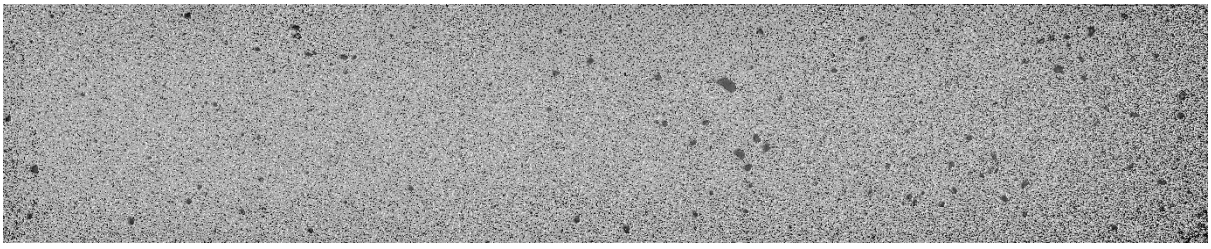

Figure 33: Microscopic image of a specimen

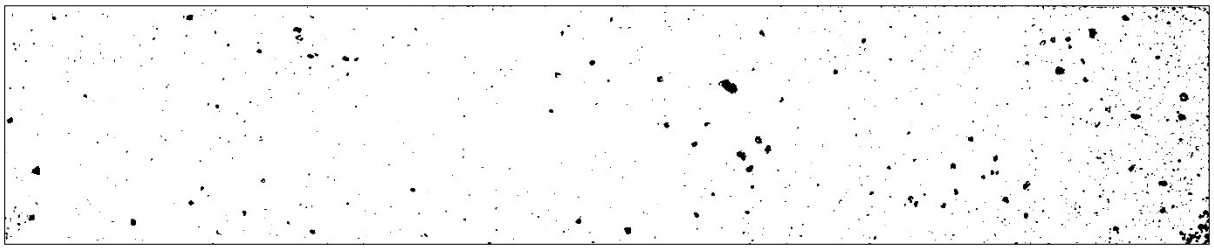

Figure 34: Processed image after applying the median filter

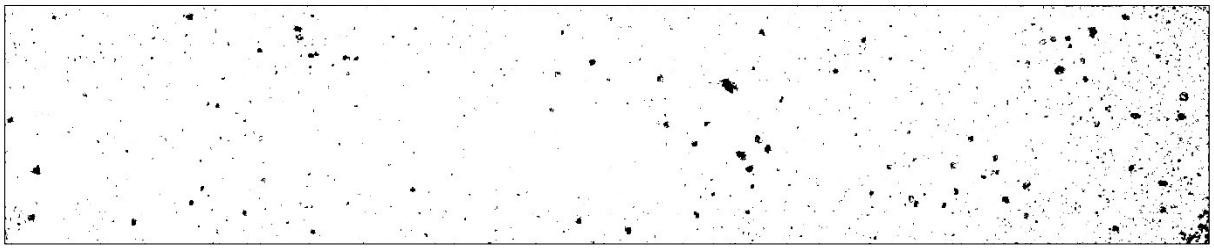

Figure 35: Processed image after applying the Kuwahara filter

F2. Void content values for achimedes principle test

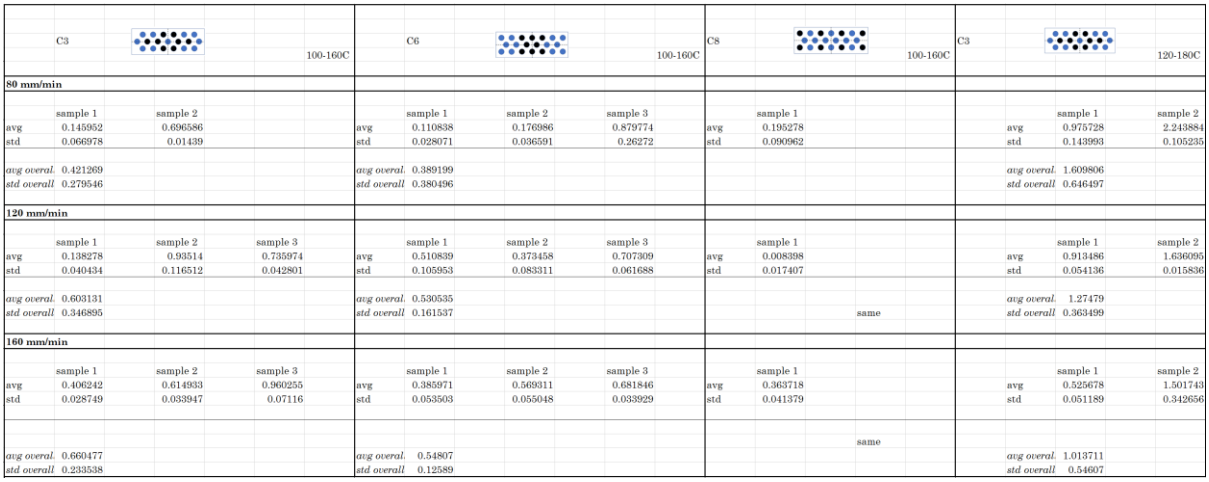

C3			100-160C
80 mm/min			
	sample 1	sample 2	
avg	0.145952	0.696586	
std	0.066978	0.01439	
avg overal.	0.421269		
std overall	0.279546		
120 mm/min			
	sample 1	sample 2	sample 3
avg	0.138278	0.93514	0.735974
std	0.040434	0.116512	0.042801
avg overal.	0.603131		
std overall	0.346895		
160 mm/min			
	sample 1	sample 2	sample 3
avg	0.406242	0.614933	0.960255
std	0.028749	0.033947	0.07116
avg overal.	0.660477		
std overall	0.233538		

C6				100-160C
	sample 1	sample 2	sample 3	
avg	0.110838	0.176986	0.879774	
std	0.028071	0.036591	0.26272	
avg overal.	0.389199			
std overall	0.380496			
	sample 1	sample 2	sample 3	
avg	0.510839	0.373458	0.707309	
std	0.105953	0.083311	0.061688	
avg overal.	0.530535			
std overall	0.161537			
	sample 1	sample 2	sample 3	
avg	0.385971	0.569311	0.681846	
std	0.053503	0.055048	0.033929	
avg overal.	0.54807			
std overall	0.12589			

C8			100-160C
	sample 1		
avg	0.195278		
std	0.090962		
	sample 1		
avg	0.008398		
std	0.017407		
		same	
	sample 1		
avg	0.363718		
std	0.041379		
		same	

C3			120-180C
	sample 1	sample 2	
avg	0.975728	2.243884	
std	0.143993	0.105235	
avg overal.	1.609806		
std overall	0.646497		
	sample 1	sample 2	
avg	0.913486	1.636095	
std	0.054136	0.015836	
avg overal.	1.27479		
std overall	0.363499		
	sample 1	sample 2	
avg	0.525678	1.501743	
std	0.051189	0.342656	
avg overal.	1.013711		
std overall	0.54607		

Figure 36: Void content based on Archimedes principle test

G1. Flexural test results and details

In certain scenarios, the flexure test was conducted such that the bottom surface of the composite during fabrication, is placed facing the top roller. The specimen for each sample set following this criteria is represented as scenario 1 in the table. For scenario 2, the top surface of the composite during production is placed upwards (facing the top roller). The overall average values for each combination is computed using the average values taken for each specimen corresponding to all the samples. The details of the scenarios and the values for each test are presented in the figure below. The number of specimens taken for each combination is marked in the parentheses in *Figure 37*.

80 mm/min - Sample B					120 mm/min - Sample A					160 mm/min - Sample C				
	Average	Std	Average	Std		Average	Std	Average	Std		Average	Std	Average	Std
bottom(1-5)	57159.26	369.34216	996.96364	16.965672	bottom(1-5)	58110.261	357.72759	1037.3	25.850184	bottom(1-4)	57959.977	485.83358	975.68858	18.439628
top(6-10)	55557.143	1017.7372	867.69336	231.89568	top(6-8)	57501.005	578.61452	1011.6035	17.25446	top(5-9)	58150.09	237.56958	1045.44	23.609879
overall	56358.201	1108.0595	932.3285	176.66188	overall	57881.79	540.85751	1027.6638	26.154319	overall	58065.595	381.02951	1014.4394	40.768865
	modulus		strength			modulus		strength			modulus		strength	
80 mm/min - Sample F					120 mm/min - Sample E					160 mm/min - Sample D				
	Average	Std	Average	Std		Average	Std	Average	Std		Average	Std	Average	Std
bottom(2,4,6,8,9)	55219.037	558.75083	903.65306	40.305336	bottom(2-6)=1-5	55945.13	426.86118	953.66374	14.312962	bottom(1-5)	56888.833	202.58657	949.48606	34.31268
top(3,5,7,10)	55748.578	867.39135	896.04683	32.308929	top(7-10)=6-9	55845.454	671.32503	884.06	34.609676	top(6-10)	57466.993	470.043	956.93	7.0340669
overall	55454.389	759.65089	900.27251	37.158272	overall	55900.83	551.34583	922.72823	42.923622	overall	57177.913	463.20404	953.20979	25.045662
	modulus		strength			modulus		strength			modulus		strength	
80 mm/min - Sample G					120 mm/min - Sample H					160 mm/min - Sample I				
	Average	Std	Average	Std		Average	Std	Average	Std		Average	Std	Average	Std
bottom(1,3,5,8)	59098.989	498.10243	1122.65	12.150823	bottom(1,3,5,7)	59434.753	245.36416	1053.4305	37.541212	bottom(2,4,6,8)	59581.884	176.74803	1055	19.161811
top(2,4,6,7)	59006.618	1023.0293	1053.8043	55.530977	top(2,4,6)	59870.972	38.72492	1020.8	10.910545	top(1,3,5,7)	59392.809	385.7999	1,027.03	4.9073287
overall	59052.804	805.90358	1088.2271	52.920698	overall	59621.704	285.73696	1039.446	33.423201	overall	59487.346	314.6078	1041.0125	19.780763
	modulus		strength			modulus		strength			modulus		strength	
80 mm/min - Sample J					120 mm/min - Sample K					160 mm/min - Sample L				
	Average	Std	Average	Std		Average	Std	Average	Std		Average	Std	Average	Std
bottom(1,3,6,8)	59059.624	738.41688	1142.725	49.874211	bottom(1,3,5,7)	59029.131	787.22336	1116.725	50.266409	bottom(1,3,5,7)	60192.517	481.15333	1142.85	21.193218
top(2,4,5,7)	59069.34	634.5529	1124.45	51.862776	top(2,4,6,8)	58883.782	740.80532	1109.725	50.96947	top(2,4,6,8)	60571.46	86.233289	1139.675	39.53134
overall	59064.482	688.46353	1133.5875	51.692225	overall	58956.457	767.81387	1113.225	50.740017	overall	60381.988	394.17242	1141.2625	31.756257
	modulus		strength			modulus		strength			modulus		strength	
80 mm/min - Sample M					120 mm/min - Sample N					160 mm/min - Sample O				
	Average	Std	Average	Std		Average	Std	Average	Std		Average	Std	Average	Std
bottom(1,3,5,7)	57524.054	367.97046	999.70598	19.130077	bottom(1,3,5,7)	57994.205	463.65853	1011.6288	61.405437	bottom(1,3,5,7)	58186.841	457.85267	1029.2435	62.102586
top(2,4,6,8)	57646.504	1098.2533	975.62308	33.427442	top(2,4,6,8)	57724.542	307.78885	983.79	43.97554	top(2,4,6,8)	57588.965	1012.8742	978.88	65.030571
overall	57585.279	821.2976	987.66453	29.777062	overall	57859.373	415.97616	997.71011	55.190287	overall	57887.903	840.9135	1004.0621	68.388288
	modulus		strength			modulus		strength			modulus		strength	
80 mm/min - Sample P					120 mm/min - Sample Q					160 mm/min - Sample R				
	Average	Std	Average	Std		Average	Std	Average	Std		Average	Std	Average	Std
bottom(1,3,5,7)	58500.322	667.99524	1226.025	34.940333	bottom(1,3,5,7)	59654.487	787.82161	1154.95	47.112339	bottom(1,3,5,7)	58140.251	1484.3755	1095.0281	69.479626
top(2,4,6,8)	58530.426	680.96484	1205.225	39.74842	top(2,4,6,8)	59159.506	589.74399	1141.1	39.31749	top(2,4,6,8)	58251.552	377.6799	1095.1	51.561856
overall	58515.374	674.67914	1215.625	38.839952	overall	59407	738.5675	1148.025	43.93944	overall	58195.902	1084.483	1095.064	61.18025
	modulus		strength			modulus		strength			modulus		strength	
80 mm/min - Sample S					120 mm/min - Sample T					160 mm/min - Sample U				
	Average	Std	Average	Std		Average	Std	Average	Std		Average	Std	Average	Std
bottom(1,3,5,7)	59475.161	186.53518	1146.725	24.820292	bottom(1,3,5,7)	59651.759	509.01443	1067.825	14.588073	bottom(1,3,5,7)	59854.759	686.29661	1107.95	16.21581
top(2,4,6,8)	59056.713	1041.0935	1165.15	53.559616	top(2,4,6,8)	59363.062	489.77247	489.77	60.461419	top(2,4,6,8)	59499.351	726.5064	1065.5	39.217534
overall	59265.937	776.60161	1155.9375	42.745875	overall	59507	519.92576	1058.4606	44.965423	overall	59677.055	728.6879	1086.725	36.755739
	modulus		strength			modulus		strength			modulus		strength	
80 mm/min - Sample V					120 mm/min - Sample W					160 mm/min - Sample X				
	Average	Std	Average	Std		Average	Std	Average	Std		Average	Std	Average	Std
bottom(1,3,5,7)	60259.025	907.21191	1147.3	6.8040429	bottom(1,3,5,7)	59264.517	490.90082	1081.3304	53.478186	bottom(1,3,5,7)	59844.257	366.75014	1089.5	15.740394
top(2,4,6,8)	59767.598	719.38063	1081.55	22.488942	top(2,4,6,8)	59749.96	264.44907	1,061.30	28.857321	top(2,4,6,8)	59110.705	1249.6038	1031.45	28.223439
overall	60013.311	854.77848	1114.425	36.834622	overall	59507	463.00362	1071.3152	44.120683	overall	59425.084	1040.0558	1056.3286	37.237336
	modulus		strength			modulus		strength			modulus modified		strength modified	
80 mm/min - Sample Y					120 mm/min - Sample Z					160 mm/min - Sample ALPHA				
	Average	Std	Average	Std		Average	Std	Average	Std		Average	Std	Average	Std
bottom(1,3,5,7)	58235.392	1499.3013	1068.075	18.441309	bottom(1,3,5,7)	60240.116	333.02997	1123.55	21.294189	bottom(1,2,3,4)	58789.495	400.62319	1101	17.361884
top(2,4,6,8)	59540.459	550.63775	1097.7	15.134893	top(2,4,6,8)	59666.999	521.03527	1083.625	32.936634	top(5,6,7,8,9)	58786.335	824.77067	1050.166	45.149114
overall	58887.926	1304.3592	1082.8875	22.449579	overall	59954	522.78978	1103.5875	34.170654	overall	58787.739	670.26124	1072.7589	43.640445
	modulus		strength			modulus		strength			modulus modified		strength modified	

Figure 37: Flexural strength and modulus for each process combination

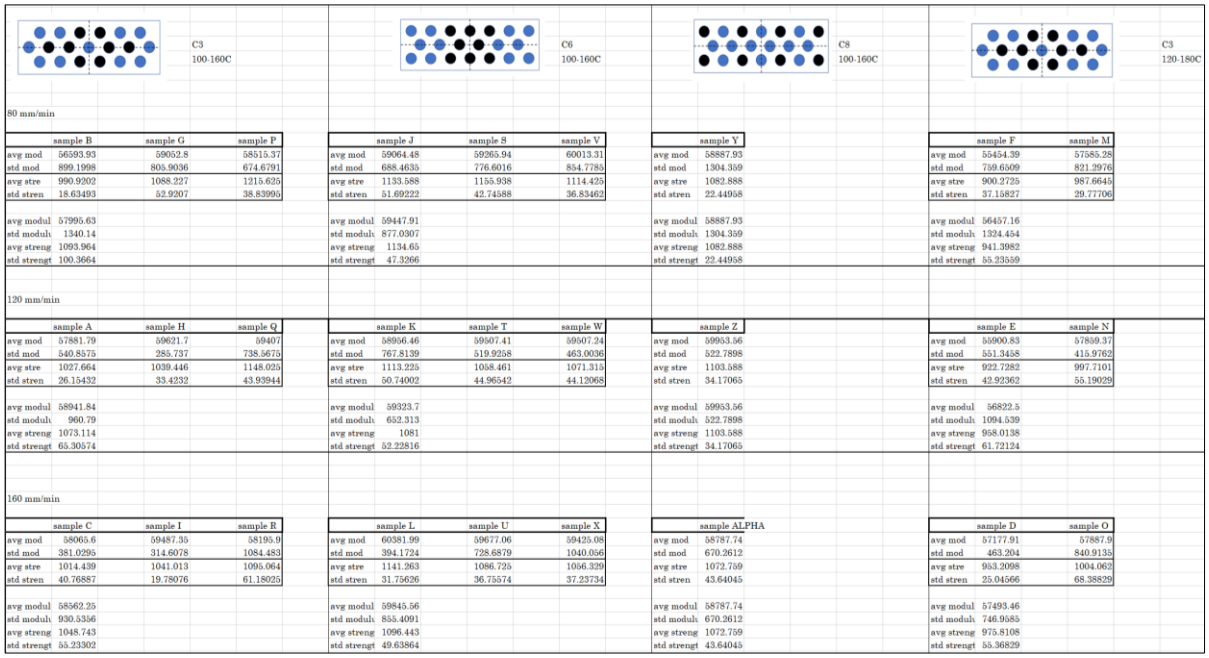

C3 100-160C

80 mm/min

	sample B	sample G	sample P
avg mod	56593.93	59052.8	58515.37
std mod	899.1998	805.9036	674.6791
avg stre	990.9202	1088.227	1215.625
std stren	18.63493	52.9207	38.83995
avg modul	57995.63		
std moduli	1340.14		
avg streng	1093.964		
std strengt	100.3664		

120 mm/min

	sample A	sample H	sample Q
avg mod	57881.79	59621.7	59407
std mod	540.8575	285.737	738.5675
avg stre	1027.664	1039.446	1148.025
std stren	26.15432	33.4232	43.93944
avg modul	58941.84		
std moduli	960.79		
avg streng	1073.114		
std strengt	63.30574		

160 mm/min

	sample C	sample I	sample R
avg mod	58065.6	59487.35	58195.9
std mod	381.0295	314.6078	1084.483
avg stre	1014.439	1041.013	1095.064
std stren	40.76887	19.78076	61.18025
avg modul	58562.25		
std moduli	930.5356		
avg streng	1048.743		
std strengt	55.23302		

C6 100-160C

	sample J	sample S	sample V
avg mod	59064.48	59265.94	60013.31
std mod	688.4635	776.6016	894.7785
avg stre	1133.588	1155.938	1114.425
std stren	51.69222	42.74588	36.83462
avg modul	59447.91		
std moduli	877.0307		
avg streng	1134.65		
std strengt	47.3266		

	sample K	sample T	sample W
avg mod	58956.46	59507.41	59507.24
std mod	767.8139	519.9258	463.0036
avg stre	1113.225	1058.461	1071.315
std stren	50.74002	44.96542	44.12068
avg modul	59323.7		
std moduli	652.313		
avg streng	1081		
std strengt	52.22816		

	sample L	sample U	sample X
avg mod	60381.99	59677.06	59425.08
std mod	394.1724	728.6879	1040.056
avg stre	1141.263	1086.725	1056.329
std stren	31.75626	36.75574	37.23734
avg modul	59845.56		
std moduli	855.4091		
avg streng	1096.443		
std strengt	49.63864		

C8 100-160C

	sample Y
avg mod	58887.93
std mod	1304.359
avg stre	1082.888
std stren	22.44958
avg modul	58887.93
std moduli	1304.359
avg streng	1082.888
std strengt	22.44958

	sample Z
avg mod	59953.56
std mod	522.7898
avg stre	1103.588
std stren	34.17065
avg modul	59953.56
std moduli	522.7898
avg streng	1103.588
std strengt	34.17065

	sample ALPHA
avg mod	58787.74
std mod	670.2612
avg stre	1072.759
std stren	43.64045
avg modul	58787.74
std moduli	670.2612
avg streng	1072.759
std strengt	43.64045

C5 120-180C

	sample F	sample M
avg mod	55454.39	57585.28
std mod	759.6509	821.2976
avg stre	900.2725	987.6645
std stren	37.15827	29.77706
avg modul	56457.16	
std moduli	1324.454	
avg streng	941.3982	
std strengt	55.23559	

	sample E	sample N
avg mod	55900.83	57859.37
std mod	551.3458	415.9762
avg stre	922.7282	997.7101
std stren	42.92362	55.19029
avg modul	56822.5	
std moduli	1094.539	
avg streng	958.0138	
std strengt	61.72124	

	sample D	sample O
avg mod	57177.91	57887.9
std mod	463.204	840.9135
avg stre	953.2098	1004.062
std stren	25.04566	68.38829
avg modul	57493.46	
std moduli	746.9585	
avg streng	975.8108	
std strengt	55.36829	

Figure 38: Average modulus and strength for each process setting

G2. Failure mode

The different failure modes are described in [43] and they are tensile fracture of fibre (1), tensile fracture of the outermost layer (2), compressive fracture (3), tensile and interlaminar fracture (4), compressive and interlaminar fracture (5), and interlaminar shear fracture(6). The failure modes for the different samples (refer *Figure 39*) are tabulated in *Table 14*. The mode of damage reported for each sample is based on the failure mode that occurs most frequently for all the specimens tested.

Sample	Failure mode
B, E, G, J, K, P, X, ALPHA	1
A, C, D, F, H, I	4, 1
L	2, 1
M, N, O	3, 1
Q, R, S, T, Z	2, 4
U, V, Y	2

Table 14: Failure mode types

An image of a failure mode is shown below.

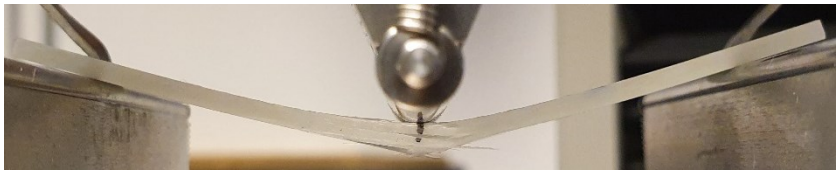

Figure 39: Failure mode for a sample

G3. Thickness and width of the specimen for different samples

The thickness and width for different specimens are shown below. It can be seen that the variation for different specimens is not significant. The averages are represented by yellow, blue and green colour in *Figure 40* and *Figure 42*, and the deviations are represented as brown and blue for 80, 120 and 159 mm/min respectively. Ten specimens per sample were used to find the average thickness and width. A percentage difference between the maximum and minimum value with respect to the average for different speeds and configurations are shown below.

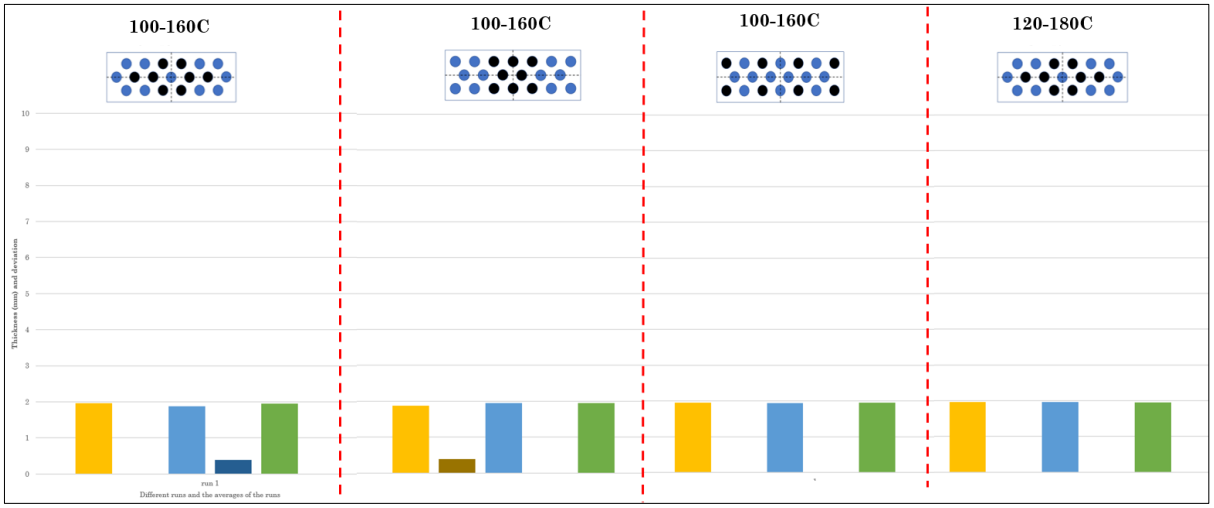

Figure 40: Average and standard deviation for thickness of the composite

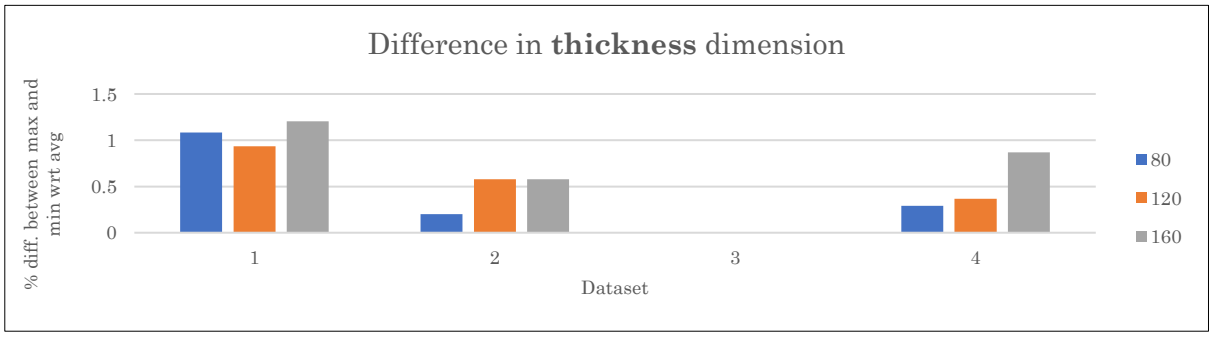

Figure 41: Variation in percentage with respect to mean value of thickness

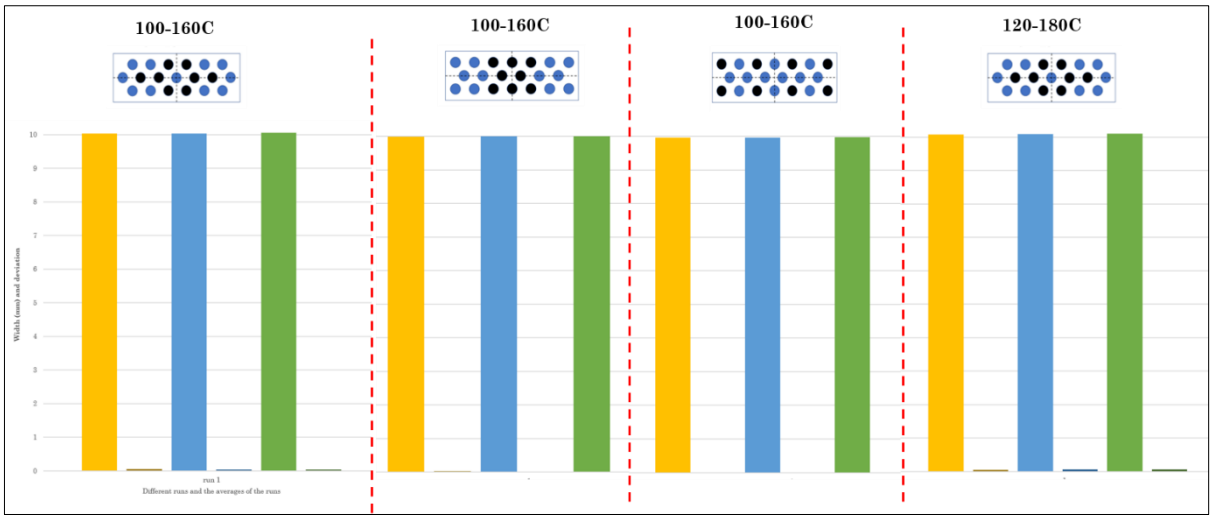

Figure 42: Average and standard deviation for the width of the composite

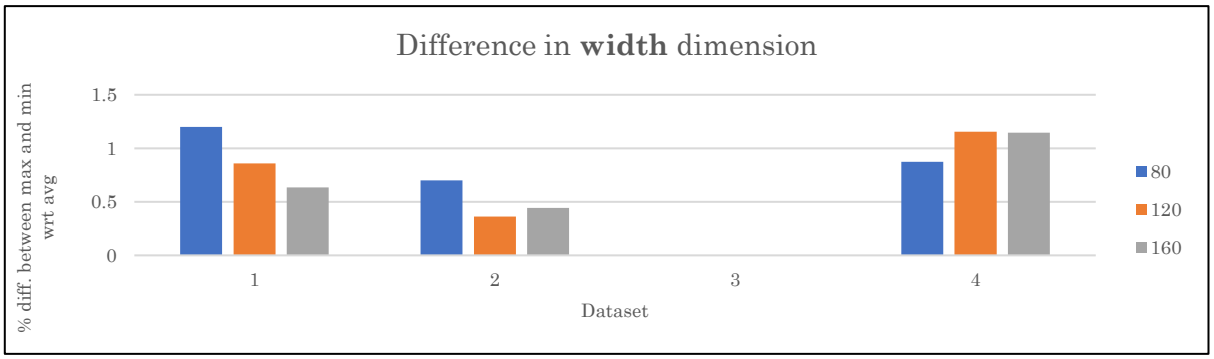

Figure 43: Variation in percentage with respect to the mean value of the width

No specific trend was observed for variation of width and thickness.